

Interface stability in granular open filters in unidirectional flows

Investigating the required minimum filter layer thickness for stable geometrical open filters in unidirectional flows.

Report type: MSc Thesis
Author: R. Joustra
Date: April 2013

Graduation committee: Dr. J.J. Warmink (*University of Twente*)
Dr. Ir. C.M. Dohmen-Janssen (*University of Twente*)
Ir. B. de Sonnevile (*Deltares*)
Ir. H.J. Verheij (*Deltares*)
Ir. K. Dorst (*Rijkswaterstaat*)



Summary

A single-grading stable geometrical open filter is a measure of granular material to protect a bed or construction against scour and erosion. A stable geometrical open filter must have a sufficiently large filter diameter to prevent the shear failure (Chiew, 1995) and a sufficiently large relative layer thickness to prevent transport of bed material through the pores of the filter (winnowing failure (Chiew, 1995)). This thesis focuses on the interface stability in a unidirectional current, e.g. prevention of the transport of bed material through the pores of the filter. The design formula of Hoffmans (2012) can be applied to calculate the minimum required layer thickness to prevent winnowing. This formula is based on the philosophy of simultaneous erosion of the filter material and the bed material, e.g. filter material and bed material are eroded at the same external load conditions. Load damping coefficient α_d within the formula of Hoffmans (2012) is the parameter which describes turbulent kinetic energy damping by the filter. The value for α_d should be increased when the minimum filter layer thickness is insufficient to prevent winnowing.

Van de Sande (2012) recently modified the formula and concluded that the formula is valid for uniform flow conditions. Theoretically the formula is also valid for non-uniform flow (e.g. conditions with additional turbulence) (Hoffmans, 2012), however this has not yet been confirmed with laboratory experiments. Firstly, indicatory results by Van de Sande (2012) show that bed mobility increases for conditions with additional turbulence (non-uniform flow). Secondly, a few results of laboratory tests by Van Velzen (2012) indicated a probable validity of flow with a cylindrical pier (non-uniform flow). Thirdly, Wörman (1989) developed a similar design formula for the layer thickness of geometrical open filters in flows with a cylindrical pier. The similarity of the design formula of Wörman (1989) and Hoffmans (2012) is the design philosophy of simultaneous erosion of filter and bed material. The main difference is that Wörman found a linear relation between the filter and bed grain characteristics and the minimum filter layer thickness, while Hoffmans (2012) described that relation with a logarithmic function. The formula of Wörman is based on experiments of flow at a cylindrical pier and is only tested for small layer thicknesses ($D_f < 0.1$ m) and low flow velocities ($\bar{u} < 0.5$ m/s).

Recently, a database became available with experiments performed by Joustra (2012) and conducted at the research institute Deltares. The test data give the possibility to test the validity of the by Van de Sande (2012) modified version of the formula of Hoffmans (2012) for (1) uniform flow, and for non-uniform flow conditions in cases of (2) sill-induced additional turbulence and (3) flow with a cylindrical pier. In addition, the database provides the possibility of testing the validity of the formula of Wörman (1989) for flow velocities over 0.5 m/s and layer thicknesses over 0.1 m at the cylindrical pier. The aim of this thesis is:

To test the validity of the design formula of Hoffmans (2012) for flows with sill-induced additional turbulence, and flows with a cylindrical pier and to test the validity of the design formula of Wörman (1989) for flow velocities over 0.5 m/s and filter layer thicknesses over 0.1 m at flows with cylindrical piers.

First, the tests conducted by Joustra (2012) are redistributed into flow categories (1) uniform flow, (2) flows with sill-induced additional turbulence and (3) flows with a cylindrical pier. Second, the filter material instability and bed material instability are classified separately. This separate classification is determined for each test with visual observation using underwater camera images and processed videos. Third, the separate classification is combined into a general classification. In addition, the bed material instability classification is verified with 3D Stereo photography images for conditions (1) and (2). The simplified ($\alpha_d = 0.86$) and full version ($\alpha_d = 0.82$) of the formula of Hoffmans (2012) are compared with the general classification for respectively flow condition (1), (2) and (3). The formula of Wörman (1989) is compared with the general classification for tests with condition (3). Finally, results based on data of Joustra (2012) are compared with previous validation results (Van de Sande, 2012 and Van Velzen, 2012) based on data of Van Velzen (2012) for flow condition (3).

First, the data of Joustra (2012) with condition of uniform flow are in agreement with the formula of Hoffmans (2012) with the load damping coefficient $\alpha_d = 0.82$ for the full version and $\alpha_d = 0.86$ for the simplified version. This result is based on one single test that could be classified and selected for validation and an expected classification of three additional tests when the flow velocity would have been further increased. Second, the data of Joustra (2012) with flows with sill-induced additional turbulence suggest to increase the load damping coefficient $\alpha_d = 0.82$ for the full version and the $\alpha_d = 0.86$ for the simplified version of the formula of Hoffmans (2012). A rough estimate of the new load damping coefficient for both versions of the formula and flows with sill-induced additional turbulence is probably within the range $1.2 < \alpha_d < 2.5$, but additional research is highly recommended due to the uncertainty in results and scarcity of tests. Third, data of Joustra (2012) for flows with a cylindrical pier suggest to increase the load damping coefficient $\alpha_d = 0.82$ for the full version and the $\alpha_d = 0.86$ for the simplified version of the formula of Hoffmans (2012). A new estimate of α_d for flows with a cylindrical pier is probably within the range $2.4 < \alpha_d < 3.7$. Fourth, data of Joustra (2012) for flows with a cylindrical pier suggest also that the formula of Wörman estimates the minimum required layer thickness reasonably well for average flow velocities over 0.5 m/s and layer thicknesses over 0.1 m, but the gradient (or coefficient 0.16 [-]) of the linear formula of Wörman (1989) should be changed to a gradient probably in the range between 0.22 [-] and 0.33 [-] to be in agreement with test data of Joustra (2012). Fifth, the results for the formula of Hoffmans (2012) and Wörman (1989) based on data of Joustra (2012) are not in agreement with the conclusions from the previous validation by Van Velzen (2012) and Van de Sande (2012), which are based on data of Van Velzen (2012). A probable cause is that the classification of combined filter and bed instability as applied by Van Velzen (2012) and Van de Sande (2012) is not in agreement with the design philosophy (simultaneous erosion) of both design formulas, i.e. filter, bed or both should be instable to compare a test with the both design formulas.

Finally, it is recommended to optimize the load damping coefficient for uniform flows, highly recommended to test the validity of the roughly estimated range of the load damping coefficient α_d for flows with sill-induced additional turbulence and recommended to determine the characteristic load damping in the filter for flows with a cylindrical pier. For design practice it is recommended to apply the safe upper limit of the load damping coefficient $\alpha_d = 0.86$ as proposed by Van de Sande (2012) for uniform flow, an $\alpha_d = 2.5$ for flows with sill-induced turbulence could be applied after additional validation and for flows with a cylindrical pier the formula of Wörman (1989) with a gradient of 0.33 should be preferred above the formula of Hoffmans (2012) with $\alpha_d = 3.7$.



Preface

This thesis is the final step in finishing my master Civil Engineering & Management at the University of Twente. Also it is my last achievement as a student, thereby the end of my student days. The research was carried out at Deltares. This report describes a test of the validity of design formulas for a stable geometrical open filter with data of laboratory experiments. During the research I learned a lot about physical modeling, analyzing and processing measurement data, writing a scientific report and much more. These and the findings described in this report would not have been possible without the help and support from people who I would like to thank.

First of all, I am very grateful for the advice and feedback I received from my supervising committee Jord, Ben, Henk, Marjolein and Kees. Ben owes my gratitude for introducing me to physical modeling, to the data processing software and the useful discussions about the results. I would also like to thank Henk, a renowned expert in the scientific area of scour and filters, for always being critical on the report, results and conclusions. Kees owes my gratitude for sharing his knowledge on design practice and pointing out the unclear parts within the thesis. Marjolein owes my gratitude for her kind motivational e-mails at the start of this research, always being able to listen and making time for providing feedback on the report and short term meetings in her busy schedule. Last of the committee, but definitely not least: Jord. I would like to thank Jord for all the support he gave during this research. His feedback was extensive, well written, positive as well as critical. Jord pushed me to critically evaluate and discuss scientific papers, assumptions, the results, etc.

Next I would like to thank the organization Deltares and their employees. Deltares gave me the opportunity to conduct experiments in their research facilities for which I was looking for to experience during my master curriculum. Deltares did let me work with their state-of-the-art data processing scripts. From these scripts I learned a lot about the possibilities of the software Matlab.

Last but not least, I would like to thank my family, colleagues, friends and the students who supported and motivated me at difficult times. My special thanks goes to Wouter Knobben. Wouter provided me with very useful comments on my report, which he even e-mailed at times when most people are normally sleeping. Furthermore, I would like to thank Heit, Mem, Doede, Redmer and Sophie for giving support, having patience and having trust in me, which gave me the energy and confidence to conduct and finish this research.

I hope you will enjoy reading this report!

Rinse Joustra

Delft, 1st of April 2013.

Table of contents

SUMMARY	3
PREFACE	5
TABLE OF CONTENTS	6
LIST OF SYMBOLS	7
1 INTRODUCTION	9
1.1 BACKGROUND.....	9
1.2 PROBLEM SUMMARY	16
1.3 RESEARCH AIM.....	17
1.4 RESEARCH QUESTIONS	17
1.5 OUTLINE OF THESIS	17
2 THEORETICAL FRAMEWORK	18
2.1 FLOW MECHANISMS	18
2.2 INCIPIENT MOTION	20
2.3 DESIGN FORMULA OF HOFFMANS (2012)	21
2.4 DESIGN FORMULA OF WÖRMAN (1989).....	22
3 LABORATORY EXPERIMENTS	23
3.1 TEST SET-UP	23
3.2 TEST PROGRAM	25
3.3 DATA	27
3.4 FLOW CONDITIONS	33
4 METHOD	37
4.1 SUMMARY OF METHOD.....	37
4.2 CLASSIFICATION OF INSTABILITY	37
4.3 VERIFICATION OF BED INSTABILITY	39
4.4 VALIDATION OF DESIGN FORMULAS	40
5 RESULTS	42
5.1 CLASSIFICATION OF INSTABILITY	42
5.2 HOFFMANS (2012) FOR UNIFORM FLOWS.....	51
5.3 HOFFMANS (2012) FOR FLOWS WITH SILL-INDUCED ADDITIONAL TURBULENCE	54
5.4 HOFFMANS (2012) FOR FLOWS WITH A CYLINDRICAL PIER.....	57
5.5 WÖRMAN (1989) FOR FLOWS WITH A CYLINDRICAL PIER	57
5.6 COMPARISON BETWEEN DATA OF VAN VELZEN (2012) AND JOUSTRA (2012).....	57
6 DISCUSSION	60
6.1 REFLECTION ON FLOW CONDITIONS AND FILTER GRAIN SIZE	60
6.2 REFLECTION ON CHOICE CLASSIFICATION OF STABILITY	60
6.3 DESIGN OF D_f/D_{F50} FOR UNIFORM FLOW.....	62
6.4 DESIGN OF D_f/D_{F50} FOR FLOWS WITH SILL-INDUCED ADDITIONAL TURBULENCE.....	62
6.5 DESIGN OF D_f/D_{F50} FOR FLOWS WITH A CYLINDRICAL PIER	64
6.6 IMPLICATIONS OF RESULTS AND PHYSICAL MECHANISMS.....	66
7 CONCLUSION AND RECOMMENDATION	68
7.1 CONCLUSIONS	68
7.2 RECOMMENDATIONS	70
REFERENCES	71
APPENDICES	72
1. FIVE FAILURE MECHANISMS	72
2. PREVIOUS VALIDATION RESULTS.....	74
3. SIEVE CURVES OF FILTER MATERIAL.....	76
4. SIEVE CURVE OF BED MATERIAL.....	77
5. FLOW CONDITION IN FRONT OF PIER	78
6. SPATIAL VARIATION IN MEASURED BED STABILITY	81

List of symbols

Regular symbols

B	Width	m
C	Roughness coefficient of Chézy	$m^{1/2}/s$
C_{12}	Diameter of test section 2	m
d_{50}	Diameter of grain size where respectively 50% of the grading is smaller than this grain size. 'f' denotes filter grading. 'b' denotes bed grading	m
d_{15}	Diameter of grain size where respectively 15% of the grading is smaller than this grain size. 'f' denotes filter grading. 'b' denotes bed grading	m
d_{85}	Diameter of grain size where respectively 85% of the grading is smaller than this grain size. 'f' denotes filter grading. 'b' denotes bed grading	m
d_n	Nominal grain diameter	m
D_f	Filter layer thicknesses	m
D_f/d_{f50}	Relative layer thickness	[-]
D_{sill}	Height of sill	m
D_{pier}	Diameter of pier	m
g	Gravitational constant	m/s^2
h_w	Water depth	m
k_f	Local turbulence energy in filter layer	m^2/s^2
k_b	Bed turbulent kinetic energy	m^2/s^2
K	Correction factor	[-]
L_d	Damping depth representing load penetration	m
L	Length	m
n_f	Porosity of the filter	[-]
r_0, r_u	Relative turbulent intensity	[-]
Re_D	Pier Reynolds number	[-]
t	Time	s
\bar{u}, u_0, U_0	Depth average flow velocity	m/s
u_{cr}	Critical (depth average) flow velocity for incipient motion e.g. 'f' denotes filter grains, 'b' denotes bed grains	m/s
u_{RMS}, RMS	Root mean square values. e.g. of velocity u	$m^{(1/2)}/s^{(1/2)}$
u_*	Bed shear velocity	m/s
ν	Kinematic viscosity	m^2/s
V_g	Degree of wide-grading	[-]
V_{gf}, V_{gb}	$1 - d_{15}/d_{50}$ = coefficient for non-uniformity of filter material or bed material	[-]
w	velocity component in vertical direction	m/s
x,y,z	Longitudinal, transverse and vertical coordinate	m
Xr	Reattachment point	m
Zf	Filter-outer flow interface	m
ΔZ_f	Filter-outer flow interface difference	m

Greek symbols

α_d	Load damping coefficient. 's.v.', 'f.v.', denotes α_d for simplified and full version of formula of Hoffmans (2012) respectively.	[-]
$\alpha_{d,Hoffmans}$	Alternative value for the load damping coefficient as derived by Hoffmans (2012)	[-]
$\alpha_{d,Lower\ limit}$	Lower limit of range for new estimate of α_d	[-]
$\alpha_{d,Sande}$	Safe upper for the load damping coefficient as determined by Van de Sande (2012) 's.v.', 'f.v.', denotes α_d for simplified and full version of formula of Hoffmans (2012) respectively.	[-]
$\alpha_{d,Sande,lower\ limit}$	α_d for the lower limit of the area of simultaneous erosion	[-]
$\alpha_{d,Upper\ limit}$	Upper limit of range for new estimate of α_d	[-]
Δ_f, Δ_b	The weight of respectively the filter and base material relative to the density of the water.	[-]
γ	Factor for allowable transport	[-]
$\eta_{c,k}$	Characteristic relative strength	[-]
η_{load}	Relative load	[-]
μ	Median filter difference	mm
ρ_{filter}	Density of the filter grading	kg/m ³
ρ_{bed}	Density of the bed grading	kg/m ³
τ	Shear stress	N/m ²
τ_c	Critical shear stress	N/m ²
$\tau_{c,f,k}$	Mean characteristic strength of the filter layer	N/m ²
$\tau_{c,bf,k}$	Mean characteristic strength of the base layer at the filter-bed interface	N/m ²
Ψ	Shields mobility parameter	[-]
Ψ_{cf}, Ψ_{cb}	Critical mobility parameter for filter grain, bed grain respectively	[-]

1 Introduction

1.1 Background

Scour represents one of the most critical threats to water infrastructure in rivers, coastal and offshore environments throughout the world. The presence of a hydraulic structure changes the local flow pattern. The local change in flow pattern can result in a local increase in sediment transport capacity, which causes local erosion called scour (Sumer & Fredsoe, 2002). For example, in the United States alone, 60% of 1000 bridge failures were due to the mechanism of scour (Briaud et al., 1999). Other hydraulic structures subjected to scour are for example: pipelines, abutments (i.e. bridge approach to river embankment), spur dikes (e.g. groynes), breakwaters, power plants, offshore oil platforms and wind farms. Therefore, investigating scour is a crucial aspect in the design of any hydraulic structure (Verheij & Hoffmans, 1997). Scour can either be accepted and designed for (e.g. a deeper pier foundation) or a measure against scour at the structure can be constructed. One of the measures is granular scour protection or riprap. It has the advantage of being a sustainable, robust, easy to repair and self healing measure (Verheij, Hoffmans, den Adel, Akkerman, & Giri, 2010). Two subcategories are the traditional geometrical closed filters and geometrical open filters.

This research focuses on the subcategory stable geometrical open filter and the design formulas for calculation of the minimum required layer thickness. In the remainder of this chapter, first the types of filters are explained, next the design guideline as described by Rijkswaterstaat is described. Furthermore, two design formulas for the minimum required layer thickness are described. Finally, the uniform and non-uniform flow conditions are briefly described.

Granular filters types

Traditional geometrical closed filters (figure 1-1) require construction of multiple layers of different diameter material (i.e. armour layer and one, or possibly several filter layers), such that it is impossible for the bed material to be transported, as the pores of the filter are too small (Verheij et al., 2010). The filter layer prevents transport of the bed material. The armour layer prevents erosion of filter material. However, the first difficulty with geometrical closed filters is the complex construction (and time-consuming) process of these multiple layers. The second difficulty is the likelihood of the loss of (fine filter layer) material by the local flow velocities during construction.

In contrast, a geometrical open filter (figure 1-2) combines the function of the armour layer and filter layer in a single grading. The result is that grains of the layer are larger than the filter layer of a geometrical closed filter and reduce the two difficulties during construction. A geometrical open filter is, therefore a more cost-effective granular protection against scour. This research focuses on geometrical open filters.

Geometrical open filters can be divided into two sub-categories: (1) stable geometrical open filter and (2) instable geometrical open filters. A stable geometrical open filter is a filter where the bed material is physically able to be transported through the pores of the granular protection, but the hydraulic load on the bed material is too small –because of the damping of the hydraulic load – and therefore prevents that the bed material transport is transported out of the filter. For an instable geometrical open filter the bed material is transported due to a hydraulic load above a certain hydraulic load threshold.

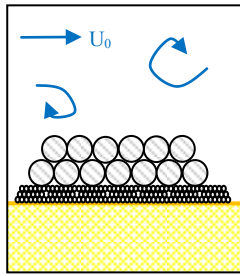


Figure 1-1: Geometrical closed filter. An armour layer covers the filter layer. Two grading system.

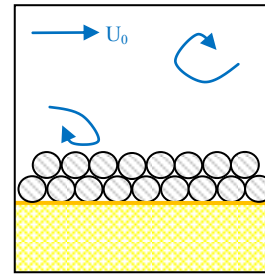


Figure 1-2: Geometrical open filter. Single grading system. This figure shows 2 layers of filter stones.

Design guideline in the Netherlands

A summary of the general design guideline (Franken et al., 1995) for a geometrical open and closed filter in the Netherlands is visualized in figure 1-3. The main focus of this thesis is the step of determination of the interface stability. The first step is to determine design requirements and the hydrodynamic conditions in the outer flow. Next the type of protection is chosen, which in the context of this research is an geometrical open filter. The basic principle of designing a geometrical open filter is based on the consideration that the combination hydraulic load and duration does not exceed the design value for resistance or strength (CIRIA, CUR, CETMEF, 2007). Furthermore, the spatial extent of the protection is determined based on the scour area. Next, the top layer (which in single grading geometrical open filter is the same as the filter layer) is designed and it is checked whether it is stable for the given flow velocity and turbulence. External stability is defined as when the top layer grading is not mobile. This step is essential for the understanding of how a flow condition is incorporated in the design formulas for the required layer thickness. Shear failure is the failure mechanism that describes an undesirable situation of stones mobility (Chiew, 1995). The stable (nominal) grain size d_n [m] is calculated with for example the widely applied formula of Shields for uniform flow. This formula is rewritten (equation 1.1) with correction factors K [-] for specific non-uniform flow conditions (for horizontal bed) (Franken et al., 1995). $K = 1$ in uniform flow.

$$d_n = \frac{(K * u_c)^2}{\Psi_c * \Delta * C^2} \quad (1.1)$$

In equation 1.1., the grain size d_n depends on the critical depth averaged flow velocity u_c [m/s] the correction factor of non-uniformity K (depends on the specific non-uniform flow condition), the critical mobility parameter Ψ_c ($\Psi_c = 0.03$ for initial phase of mobility and $\Psi_c = 0.055$ for the phase of general transport of bed material), the density of the filter stone relative to the water density Δ [-] and the roughness coefficient of Chezy C [$m^{1/2}/s$].

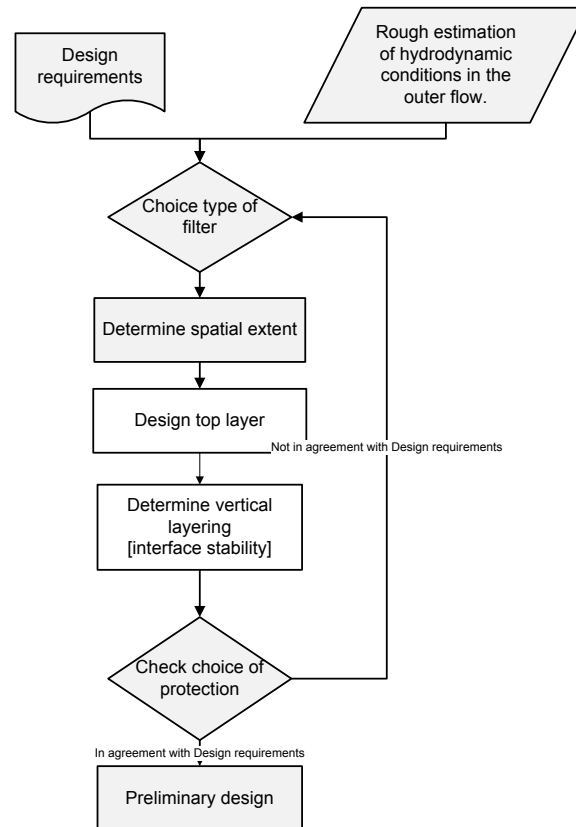


Figure 1-3: A modified version of guideline. Original is a guideline described by Rijkswaterstaat (Franken et al., 1995).

Interface stability

The next step is assuring interface stability or stability of the bed material beneath the filter. If the designed layer dimensions are insufficient to prevent the bed material from transport through the pores, then the failure mechanism winnowing occurs (figure 1-5) (Chiew, 1995). If the geometrical open filter design is in agreement with the design requirements, than a preliminary design can be made (figure 1-3). In addition, shear failure, winnowing failure and 3 other failure mechanisms (not within the scope of this thesis) are described in appendix 1.

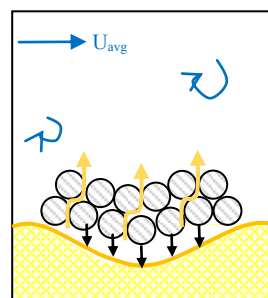


Figure 1-4: Winnowing induced failure. The filter layer thickness is insufficient to damp the hydraulic load on the bed material. The underlying bed material is transported through the filter layer pores. This transport of bed material causes failure and filter layer settlement.

Design formulas for interface stability

In order to assure interface stability in a geometrical open filter, several formulas were developed in the past (e.g. De Graauw et al., 1984, Klein Breteler in 1989 (Verheij et al., 2010), Wörman, 1989, Bakker et al., 1994 and Hoffmans, 2012).

A first approach calculates the filter grain size d_{f15} (15% of the grading is smaller than the grain size d_{f15}) for the filter layer-grading with a minimum layer thickness of two to three times the median grain size d_{f50} in uniform flow (De Graauw et al., 1984, Klein Breteler in 1989 (Verheij et al., 2010), Bakker et al., 1994). If the filter layer-grading is insufficiently external stable, than a second (or more) filter-layer grading is designed on top of the first filter-layer-grading.

A second approach includes the layer thickness D_f which results in a smaller number of filter-layer-grading's. The smaller number of filter-layer-gradings is more practical within the construction process. The focus is on the second approach. Two formulas for this second approach are the formula of Hoffmans (2012) and Wörman (1989). Hoffmans (2012) derived a formula on a theoretical basis that was validated with a limited number of tests. Wörman (1989) developed a formula based on experiments for non-uniform flow condition: flow with a cylindrical pier. Both the formula of Wörman and Hoffmans apply the design philosophy of simultaneous erosion of filter and bed material. The applicability of the formula of Hoffmans (2012) for both uniform flow (Van de Sande, 2012) and theoretically for non-uniform flow conditions (Hoffmans, 2012), is an advantage above other present design formulas and the main focus of this thesis. The formula of Wörman (1989) is based on experiments for the non-uniform flow, flow with a cylindrical pier. The formula of Wörman is also within the scope of this research as a reference formula for flow with a cylindrical pier. Figure 1-5 visualizes respectively the linear or logarithmic relation between the relative grain size d_{f50}/d_{b50} and the relative layer thickness D_f/d_{f50} of the formula of Wörman and Hoffmans (2012).

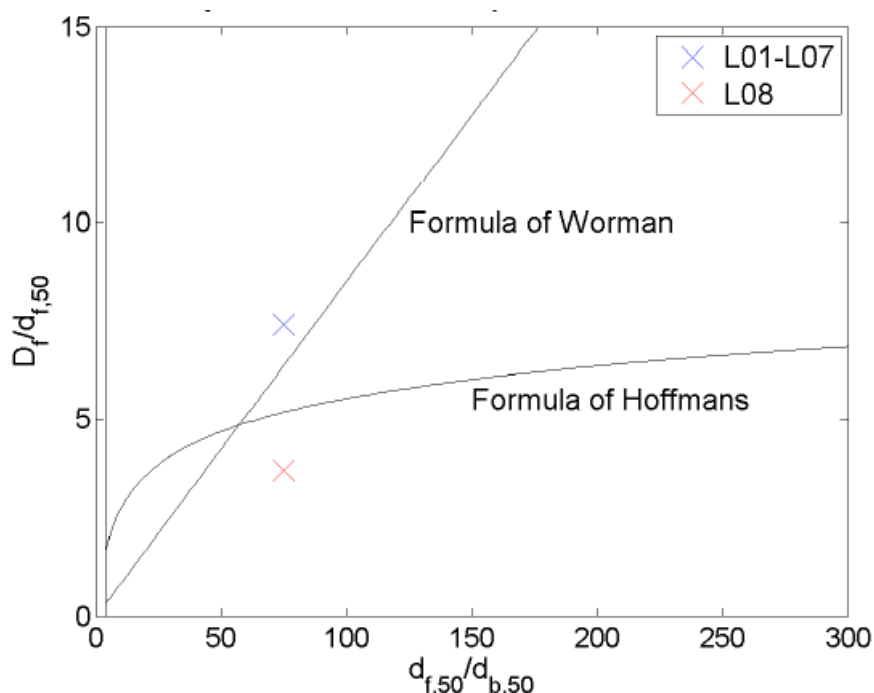


Figure 1-5: The simplified version of the formula of Hoffmans (eq. 1.3 with $\alpha_d = 1.2$) and Wörman (eq. 1.4) (Van Velzen, 2012). Positions above both curves suggest that filter moves first, i.e. thickness is *sufficient* to prevent bed material transport through the pores (winnowing). Positions below the curves indicate bed moves first or simultaneous erosion of filter and bed, i.e. the layer thickness is *insufficient* to prevent winnowing.

Design formula of Hoffmans (2012)

Hoffmans (2012) described two versions of the formula: (1) full version formula, (2) simplified formula. These full (equation 1.2) and simplified version (equation 1.3) include the suggested modifications by Van de Sande (2012) (change the relative layer thickness from D_f/d_{f15} to D_f/d_{f50}) and a new version specific value for load damping coefficient α_d , (e.g. full version with $\alpha_{d,f.v.}$ simplified version with $\alpha_{d,s.v.}$). Load damping coefficient α_d is the parameter which describes turbulent kinetic energy damping by the filter.

The formula of Hoffmans (2012) relates the required layer thickness D_f to the filter and bed material characteristics and is valid for uniform flow conditions (Van de Sande, 2012). The design load conditions are indirectly incorporated in the median filter diameter d_{f50} , because the filter diameter is calculated with for example equation 1.1 (e.g. and the flow velocity \bar{u}). In non-uniform flow conditions, e.g. additional turbulent conditions, the flow velocity and turbulence are indirectly incorporated in the larger required external stable filter grain diameter. A larger filter grain size d_{f50} directly results in a larger relative layer thickness (equation 1.2, 1.3 and figure 1-5).

$$\frac{D_f}{d_{f50}} = \alpha_{d,f.v.} * \ln \left(\frac{\Delta_f}{\Delta_b} * \frac{d_{f50}}{d_{b50}} * \frac{\Psi_{cf}}{\Psi_{cb}} * \frac{(1 - \gamma V_{Gf})}{(1 - \gamma V_{Gb})} \right) \quad (1.2)$$

$$\frac{D_f}{d_{f50}} = \alpha_{d,s.v.} * \ln \left(\frac{d_{f50}}{d_{b50}} \right) \quad (1.3)$$

Where:

- D_f = filter layer thickness [m]
- d_{f15}, d_{f50} = grain diameter of filter or base material where respectively 15% or 50% of the mixture smaller is than this base or filter material grain size [m]
- $\alpha_{d,f.v.}, \alpha_{d,s.v.}$ = a coefficient representing load penetration or load damping in a granular filter [-]
- Δ_f, Δ_b = the weight of respectively the filter and base material relative to the density of the water [-]
- Ψ_{cf}, Ψ_{cb} = the critical shields mobility parameter for filter material or bed material [-]
- V_{Gf}, V_{Gb} = $1 - d_{15}/d_{50}$ = coefficient for non - uniformity of filter material or bed material [-]
- γ = factor for allowable transport (= 0.623 [-])

Equation 1.3 is a rewritten after equation 1.2 with the assumptions (1 to 4) for the filter and bed characteristics.

$$(1) \frac{d_{f50}}{d_{f15}} \approx 1.25; \quad (2): \frac{\Delta_f}{\Delta_b} = 1; \quad (3) \frac{\Psi_{cf}}{\Psi_{cb}} = 1; \quad (4): \frac{(\gamma V_{Gf})}{(\gamma V_{Gb})} = 1;$$

The values for $\alpha_{d,f.v.}$ and $\alpha_{d,s.v.}$ are described by table 1-1. Within the formula, α_d determines the steepness of the curve (figure 1-5). The value for α_d should be increased when the minimum filter layer thickness is insufficient to prevent winnowing.

Hoffmans (2012) determined the value of α_d based on damping of flow velocity fluctuations inside the filter pores (use of data from Klar (2005). Van de Sande (2012) found a better fit with his test experiments and proposed a new $\alpha_{d,Sande}$ ($\alpha_{d,Sande,safe}$) for both versions of the formula (equation 1.2 and 1.3). In addition, Van de Sande proposed a α_d for the lower limit of the band of simultaneous erosion of 0.28 for the full version of the formula and 0.27 for the simplified version of the formula.

Table 1-1: α_d values with additional safety for simplified version (s.v.) and full versions (f.v.) of the formula of Hoffmans (2012).

Author [year]	$\alpha_{d,f.v.}$ [-]	$\alpha_{d,s.v.}$ [-]
Van der Sande [2012]	0.82	0.86
Hoffmans [2012]	1.2	1.2

Next to uniform flow conditions, in practice also locations of non-uniform flow can require scour protection (e.g. behind sluices, weirs, at bridge piers etc.). Figure 1-6 visualizes the flow conditions: (1) uniform flow, (2) flow with sill-induced turbulence and (3) flow with a cylindrical pier conditions. Flow condition (2) and (3) are conditions of non-uniform flow. Flow condition (1), (2) and (3) are often encountered as locations for which a geometrical open filter can be applied as a measure against scour. Conditions of uniform flow (1) are where the degree of turbulence and flow velocity profile are ‘uniform’ or normal in the flow direction, where bed level lowering is not desired. A condition of sill-induced additional turbulence (2) is where the fluctuations in the flow velocity are higher than uniform flow; also known as a backwards facing step. The local fluctuations induce an enhanced load (compared with uniform flow), where the highest load occurs near the reattachment point (red stones in figure 1-6). A cylindrical pier (e.g. bridge pier) (3) induces a three-dimensional flow field near the pier, which also enhances the local loads (Whitehouse, 1998).

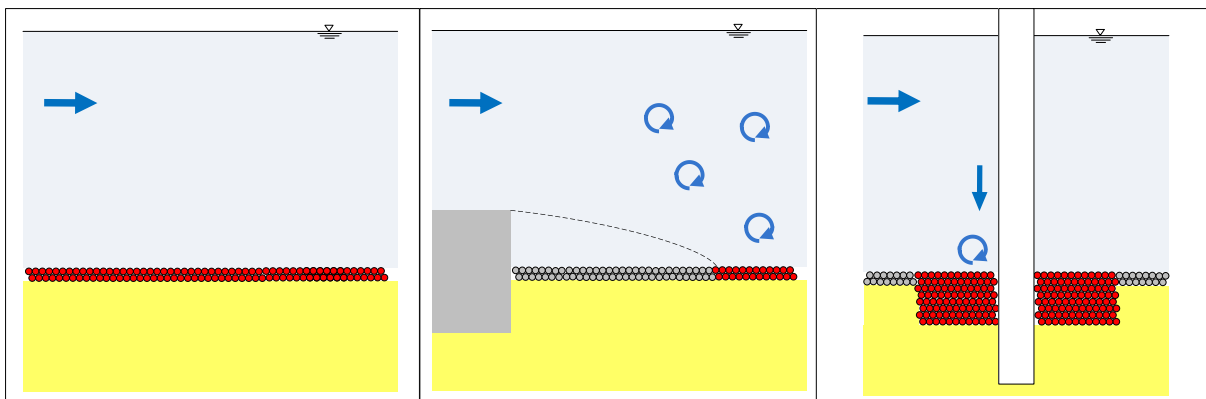


Figure 1-6: Very schematic visualization of the unidirectional flow conditions. Left image shows uniform flow. Middle image shows additional turbulence (behind the reattachment point, at the red stones). Right image shows cylindrical pier (down flow and forward bound vortex), not shown is the enhanced flow near the pier due to flow contraction and the vortex shedding downstream of the pier. Chapter 2 describes the flow processes in more detail.

Hoffmans (2012) stated that the formula is theoretically valid for both uniform and non-uniform flow conditions. However, Hoffmans (2012) only described the validity for non-uniform flow conditions in a general way.

A first remark is that Van de Sande (2012) showed that flows with sill-induced additional turbulence increases bed mobility (test T06b) and flows with a rectangular or circular pier (T06c) also increases the bed mobility. Both tests were conducted with fixed filter material (glued). Increased turbulence levels induced by piers or sills on the flow also increase the filter mobility. Additional turbulence is already incorporated in the calculation of the d_{f50} (equation 1.1, factor K), i.e. a larger filter grain size is calculated and thus results in a larger relative layer thickness D_f/d_{f50} (equation 1.2, equation 1.3). The unknown filter mobility in additional turbulent conditions is required to determine if the calculation of the larger filter grain size results in a sufficient relative layer thickness. Therefore, Van de Sande (2012) could not test the validity of $\alpha_{d,Sande}$ in the formula of Hoffmans (2012) with his experiments for both type non-uniform flow.

A second remark is that, although it was not the primary purpose of her thesis, Van Velzen (2012) did test the validity of the formula of Hoffmans (2012) and Wörman (1989) for conditions with a cylindrical pier. Van Velzen (2012) applied two values of the relative layer thicknesses (3.7 [-] (marker L08) and 7.4 [-] (marker L01-L07)), classified only bed instability (winnowing/no winnowing) and applied a stable filter grain size to prevent shear failure. Results show an agreement between the data (marker L01-L07 and marker L08) and the formula of Hoffmans (2012) with $\alpha_{d,Hoffmans}$ (figure 1-5) for non-disturbed depth average flow velocities of $\bar{u} = 0.34$ m/s. Hence, data are also in agreement with the formula of Hoffmans (2012) and $\alpha_{d,Sande}$ (Van de Sande, 2012) (appendix 2). However, at the moment only a single marker (L01-L07) confirms the validity of the formula of Hoffmans (2012) for flows with a cylindrical pier.

The formula of Hoffmans (2012) is not yet tested for conditions with sill-induced turbulence and confirmed with one single marker (and relative layer thickness). More tests are required to confirm the conclusion of data of Van Velzen (2012).

Design formula of Wörman (1989)

A comparable formula based on the same concept of simultaneous erosion which proved valid for cylindrical (bridge) piers is the formula of Wörman (1989). Within the context of this research of unknown validity of Hoffmans (2012) for piers, the formula of Wörman (1989) provides an interesting comparison. The Wörman formula relates filter, bed grain size and porosity linearly with the layer thickness D_f , while Hoffman's formula relates the filter and bed characteristics to the layer thickness D_f with a logarithmic relation. Like the formula of Hoffmans (2012), load conditions (e.g. flow velocity) are incorporated in the filter grain size d_{f50} . Equation 1.4 describes the rewritten formula (Hoffmans, 2012) with the assumptions of porosity $n_f = 0.4$ [-], $d_{85} = 1.25 * d_{50}$ and $d_{85} = (1/1.25) * d_{50}$.

$$\frac{D_f}{d_{f50}} = 0.0853 * \left(\frac{d_{f50}}{d_{b50}} \right) \quad (1.4)$$

Where:

D_f = granular filter layer thickness [m]
 d_{f50}, d_{b50} = diameter of filter or base grain size where respectively 50% of the filter layer mixture is smaller than this base or filter material grain size [m]

The formula is explicitly described to be valid for $0 < d_{b85}/d_{f15} < 0.1$ and test conditions similar to the test conditions applied by Wörman (1989). It is derived from a stability criterion that includes the depth average flow velocity \bar{u} [m/s] for cylindrical piers. The derivation to the design formula includes the assumption that the local flow velocity u is two times the depth average flow velocity \bar{u} , which includes safety. Although Wörman (1989) describes the design formula does not include additional safety.

The test program consisted of depth average flow velocities of $0.22 < \bar{u} < 0.53$ [m/s]. In addition, the water depth h_w varied between 0.30 and 0.40 m and the tested layer thicknesses D_f are between 10 and 100 mm. The pier diameters applied are $D_{\text{pier}} = 0.15$ m and $D_{\text{pier}} = 0.28$ m.

New data

Recently, a database became available with experiments by Joustra (2012) conducted at the research institute Deltares. The database consists of water level, flow, filter surface height, filter pore-pressure measurements and camera images. The parameters layer thickness D_f , grain size d_{f50} and flow conditions are varied. The flow conditions are: (1) uniform flow, (2) flows with sill-induced additional turbulence and (3) flow with a cylindrical pier.

1.2 Problem summary

The design formula for geometrical open filters of Hoffmans (2012) is not sufficiently validated for the non-uniform flow conditions: (1) sill-induced additional turbulence and (2) flow with a cylindrical pier. In addition, recently, a database became available with experiments performed by Joustra (2012), conducted at the research institute Deltares. The systematically varied flow conditions, layer thicknesses and filter grain sizes give the opportunity to validate the design formulas for uniform flow and non-uniform flow (e.g. sill induced additional turbulence or flow with a cylindrical pier).

The simplified and full versions of the formula of Hoffmans (2012) with respectively $\alpha_{d,Sande,s.v.} = 0.86$ and $\alpha_{d,Sande,f.v} = 0.82$ are in of agreement with the uniform flow data of Van de Sande (2012) and e.g. Van Huijstee & Verheij (1991) as described by Van de Sande (2012). Additional tests with uniform flow might support this previous validation result and would be useful because that would test the modification of α_d made by Van de Sande (2012).

In addition, the full and simplified versions of the formula with these α_d 's are theoretically expected to be in line with sill-induced additional turbulent conditions (e.g. downstream of a backwards facing step), because the layer thickness D_f increases as a result of the increase of the filter diameter d_{f50} . At the moment it is unknown if including additional turbulence within the calculation of d_{f50} results in a sufficiently stable relative layer thickness to prevent filter settlement (or the failure mechanism winnowing). However, first indicative measurements of sediment transport by Van de Sande (2012) show that the bed mobility is affected by the additional turbulent conditions (sill and pier induced). As the bed mobility increases due to the presence of a sill (Van de Sande, 2012), this could suggest that a higher α_d for sill-induced additional turbulence conditions should be applied.

Although Hoffmans (2012) suggests that the formula is valid for conditions of non-uniform flow, the results of comparison between data of Van Velzen(2012) and the formula are yet insufficient (one value relative layer thickness and relative grain size) to confirm the validity of the formula for flows with a cylindrical pier. Therefore, due to the limited data, additional validation for flows with a cylindrical pier is necessary to test the applicability of the formula for this type of non-uniform flow.

The Wörman (1989) formula is also based on simultaneous mobility of both geometrical open filter grains and bed grains, but this formula is based on tests with a cylindrical pier for flow conditions ($0.22 < \bar{u} < 0.5\text{m/s}$) and layer thickness D_f between 1 and 10 cm. The formula is not yet tested for higher flow conditions and larger filter layer thicknesses.

1.3 Research aim

The research aim of this thesis contributes to knowledge on how the minimum filter layer thickness required for a stable granular open filter is designed for uniform and non-uniform flows. The aim of this thesis is:

To test the validity of the design formula of Hoffmans (2012) for flows with sill-induced additional turbulence, and flows with a cylindrical pier and to test the validity of the design formula of Wörman (1989) for flow velocities over 0.5 m/s and filter layer thicknesses over 0.1 m at flows with cylindrical piers.

1.4 Research questions

The research aim is divided into 5 research questions. Research question 1-4 comes from the test of the validity of the design formula of Hoffmans (2012). More specifically, research question 1 follows from the availability of uniform flow data within the database. Research question 5 describes the test of validity of Wörman.

- 1) *How do the data compare to previous validation of the load damping coefficient α_d (Van de Sande, 2012) for uniform flow?*
- 2) *What is the effect of sill-induced additional turbulence on the load damping coefficient α_d ?*
- 3) *What is the effect of flows with a cylindrical pier on the load damping coefficient α_d ?*
- 4) *How do the data of flows with a cylindrical pier and flow velocities over 0.5 m/s compare to the design formula of Wörman (1989)?*
- 5) *How do the data compare to the previous validation of the formula of Hoffmans (2012) and the formula of Wörman (1989) based on data of Van Velzen (2012) for flows with a cylindrical pier?*

Load damping coefficient α_d is defined as $\alpha_{d,Sande,f.v.}$ for the full version of the formula (equation 1.2) and defined as $\alpha_{d,Sande,s.v.}$ for the simplified version of the formula (equation 1.3). In addition, the data is defined as the dataset of lab experiments conducted by Joustra (2012). The flow velocity is defined as the undisturbed depth average flow velocity \bar{u} [m/s].

1.5 Outline of thesis

Firstly, the theoretical framework (chapter 2) and laboratory experiments by Joustra (2012) (chapter 3) are described. Secondly, the research method to find the answers to questions 1-5 is described in chapter 4. The results of this thesis are described in chapter 5, and discussed in chapter 6. The conclusions and recommendations are described in chapter 7.

2 Theoretical framework

This chapter describes a brief summary of the theory about the flow processes relevant for the three research flow conditions (section 2.1), the theory about the incipient of motion and visual observation of mobility (section 2.2), and a more detailed description of the design formula of Hoffmans (2012) (section 2.3) and Wörman (1989) (section 2.4).

2.1 Flow mechanisms

Uniform and non-uniform flow

The mean and the fluctuating forces are both important in the mobility of the grains. The mean forces originate from the average shear stresses induced on the grains by the average flow velocities. Mclean et al., in 1994, Kleinhans & Van Rijn, in 2002 and Smeedle & Nelson, in 2003 (Hofland, 2005) “stated that: “Turbulence fluctuations of velocity and pressure are a key factor in the entrainment of bed material, as the mean forces alone are often not large enough to displace the particles”. The origin of the fluctuating forces can be the vortices shed from the stones upstream, the turbulence that originates from the difference in flow velocity in the outer flow or from the vortices that are shed from the stone itself, as suggested by Kalinkse in 1947 (Hofland, 2005). The velocity profile is logarithmic shaped and the theoretical magnitude of turbulence expressed as the depth average relative turbulence intensity r_0 for uniform flow lies typically between $r_0 = 0.042$ [-] (for smooth, wide channels) and $r_0 = 0.126$ [-] (for small rough channels) (Hoffmans, 2012).

Turbulence fluctuations can also be the result of a hydraulic structure, e.g. a backward facing step or a bridge pier. These latter conditions are classified as non-uniform flow, because there is a spatial variation in flow (e.g. water level, flow velocity and/or flow direction). The following sections describe the processes that are relevant for this thesis because the data of Joustra (2012) contains data of sill-induced additional turbulence and flows with a cylindrical pier.

‘Sill-induced additional turbulence’ or ‘backwards facing step’

The backward facing step is a classical situation of a condition with increased turbulent fluctuations. An example of the practical situation is an outflow structures (e.g. sluices, near power plants or at the Dutch Eastern Scheldt storm surge barrier). Figure 2-1 visualizes a sill (or backwards facing step) that influences the flow conditions behind a backwards facing step.

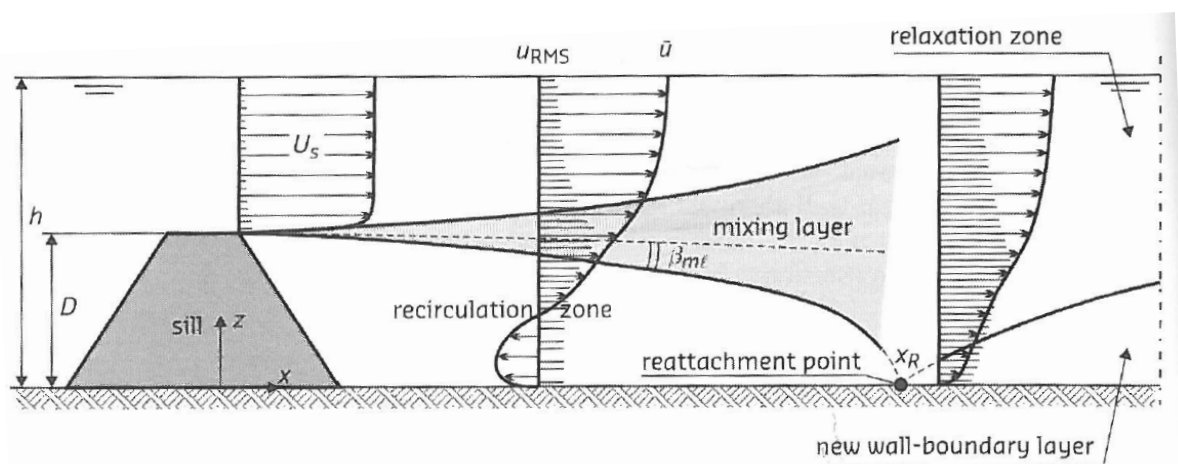


Figure 2-1: Flow velocity profile, zones and reattachment point behind a sill (e.g. backwards facing step). (Hoffmans, 2012).

Behind the sill in the recirculation zone an eddy develops. Between the recirculation zone and the flow with higher flow velocities above the sill, a mixing layer develops where turbulence is generated. The upper flow reattaches at the reattachment point X_R and forms a new boundary layer. At the reattachment point, the

velocities near the bed are nearly zero, but the damage to the unprotected bed is nearly maximal near the reattachment point (Hofland, 2005). This is because of the high levels of turbulence. In 1987 Nakagawa & Nezu (Hofland, 2005) found that the reattachment point is located further downstream for lower Reynolds numbers and for higher Froude numbers. Lower Reynolds numbers describe a less turbulent regime or more laminar flow regime. Higher Froude numbers are governed by increasing the depth average horizontal velocities or decreasing the water level) and describe a regime more towards supercritical flow. Schiereck (1995) described that the reattachment point is located at a distance downstream of 5-7 times the height of the sill. The location where the vertical and horizontal forces are strong enough for filter mobility is at the location between 10 and 20 times the height of the Sill according to Rajaratnam and Subramanya in 1968, Xingkui and Fontijn in 1992 and the experiments of Umland in 1982 (Hoffmans, 2012). The flow recovers to the equilibrium conditions when the turbulent boundary layer thickness equals the water depth, and occurs after 20-50 times the water depth (Hoffmans, 2012).

Furthermore, the relative turbulent intensity r_0 as function of x downstream of the sill ($x > 6 * D_{sill}$) can be calculated with the equation 2.1 as described by Hoffmans (2012):

$$r_0(x) = \sqrt{0.0225 \left(1 - \frac{D_{sill}}{h_w}\right)^{-2} \left(\frac{x - 6 * D_{sill}}{6.67 * h_w} + 1\right)^{-1.08} + \left(1.2 * \frac{u_*}{U_0}\right)^2} \quad (2.1)$$

Flow with a cylindrical pier

Another typical situation, next to uniform flow and the sill-induced additional turbulence is a condition with a cylindrical pier (e.g. bridge piers). Sumer and Fredsoe (2002) state the following relevant physical mechanisms (figure 2-2) that are responsible for scour near a pier; (1) Horse shoe vortices, (2) Lee wake vortices, (3) streamline contraction, (4) Down flow. The dominant feature in the scour process is the Horse shoe vortex (Breusers et al., 1977). Nielsen, Sumer, Fredsoe & Christensen (2010) observed that the horse-shoe vortex enters pores between the grains (figure 2-3) and suggest that this is the most important flow process regard to transport of sediment and sinking (i.e. bed instability) of the granular scour protection. In addition, Schiereck (1995) describes the down flow as a jet perpendicular to the surface of the granular material.

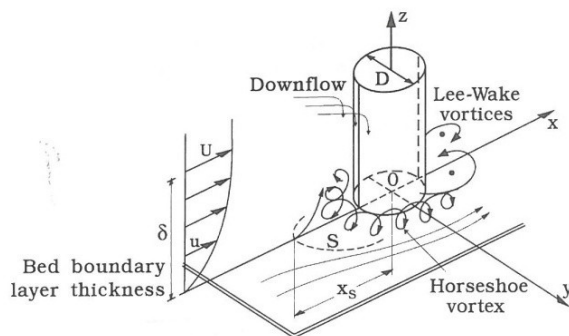


Figure 2-2: Physical mechanism causing scour in the vicinity of an unprotected pier in steady current (Sumer and Fredsoe, 2002).

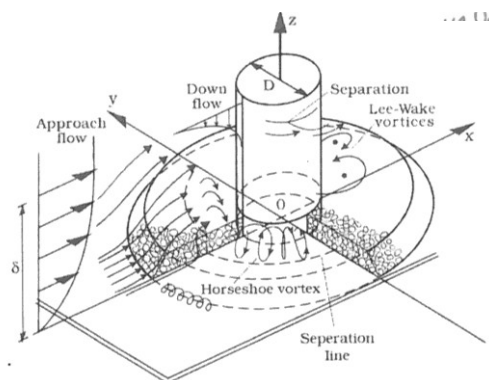


Figure 2-3: Flow pattern around a cylindrical pier Nielsen et al. (2010).

The flow field can be described as follows (figure 2-2 and figure 2-3): the approaching flow reaches the obstacle and an adverse pressure gradient develops at the upstream front of the pier due to the velocity gradient in the logarithmic vertical flow profile. The flow velocities are the highest near the surface and the lowest near the bed, due to friction. The flow decelerates the most at the surface level (high pressure at water surface, Bernoulli's law) and decelerates less at the bottom (low pressure at bottom, Bernoulli's law), both due to the presence of the pier in the flow. This vertical pressure difference causes a down flow to

develop. As a result of the down flow and the strong adverse pressure gradient in the turbulent boundary layer, a forward bound vortex develops near the bed. The flow field near the side of the pier, forces the forward bound vortex to wrap around the pier, resulting in the horseshoe vortex. The forward bound vortex (located in front of the pier) and the horse shoe vortex (wrapping around the pier) are the most important mechanisms controlling scour of sediment around the base of the cylinder (Whitehouse,1998). Without a incoming boundary layer and a sufficiently strong adverse pressure gradient, the horse shoe vortex is not generated (Sumer and Fredsoe, 2002).

Lee wake vortices form behind the pier, when the pier boundary layer flow cannot follow the pier perimeter. Whitehouse (1998) describes: *“The lee wake vortex is formed by rolling up and separation of the unstable shear layers generated around the structure and gives rise to eddies being shed downstream in a periodic fashion”*. The formation of these eddies or lee wake vortices depends strongly on the pier Reynolds number Re_D (2.2) and pier geometry. The pier Reynolds number is related to the non-disturbed depth average velocity \bar{u} , Pier diameter D and viscosity ν . Small Reynolds number result in no lee wake vortices (as the flow can follow the perimeter of the pier). If the Re_D increases, lee wake vortices are formed. When the Re_D is sufficiently high, vortex shedding occurs (cut-off of lee wake vortices) (Sumer and Fredsoe, 2002). Sumer and Fredsoe (2002) described equation 2.2:

$$Re_d = \frac{\bar{u} * D}{\nu} \quad (2.2)$$

The stream line contraction occurs due to the resistance caused by the obstacle and follows from the continuity restrictions. The same discharge passes a smaller area, so flow velocities must increase. This is visualized in small distances in the streamline at the side edges of the pier in figure 2-2 and figure 2-3.

2.2 Incipient motion

(Critical) Shields mobility parameter

According to the widely used sediment mobility theory of Shields(1936), the degree of sediment mobility depends on the shear stress, the difference in density between sediment and fluid, the particle diameter, the kinematic viscosity and the gravitational acceleration (Yang, 2003). When the shear stress τ (~related to u^2) and the shield mobility parameter Ψ exceed the sediments critical value τ_c or Ψ_c , the grains are transported. The degree of transport under uniform flow is determined by the grain size specific Ψ_c .

The stability of one grain diameter in a homogeneous bed under uniform flow conditions is characterized by the critical shield mobility parameter. In non-uniform flow, direction and magnitude of the flow differs from uniform flow. The effect of non-uniform flow can be incorporated in a in a factor K that is multiplied with the depth average flow velocity u_{cr} (equation 1.1). Factor K is determined for specific condition and will result in a higher or lower representative depth average flow velocity (Schierreck, 1995).

The shields shear stress theory is based on a homogeneous bed material. In practice both filter- and bed material are never completely uniform. In highly non-uniform grading (or wide grading) the processes of armoring can take place. The larger grains prevent the smaller grains from incipient of motion. Armoring increases strength of the bed material (Hoffmans,2012).

Visual observation of transport

Breusers (1977) described seven phases for visual observation of transport (Verheij et al., 2010). These classes are described by figure 2-4. Phase 6 describes the critical mobility as defined by Shields in 1936. Figure 2-4 therefore shows that transport of a grain can also occur locally below the critical value of mobility. For example, in general the filter grains of geometrical open filter have a diameter of d_{150} larger than 2 mm (specific grain size $D^*>30$) and Ψ_c between than 0.030 (phase 1) and often 0.055 (phase 6). According to Breusers (977), in that case phase 6 of permanent particle movement is observed at all locations. For engineering purposes, this is often not desirable. Therefore, Ψ_c is chosen often equal to phase 1 of particle movement and represents occasional particle movement at some locations. The phases of Breusers (1977) are relevant for this report in classification of the data of Joustra (2012).

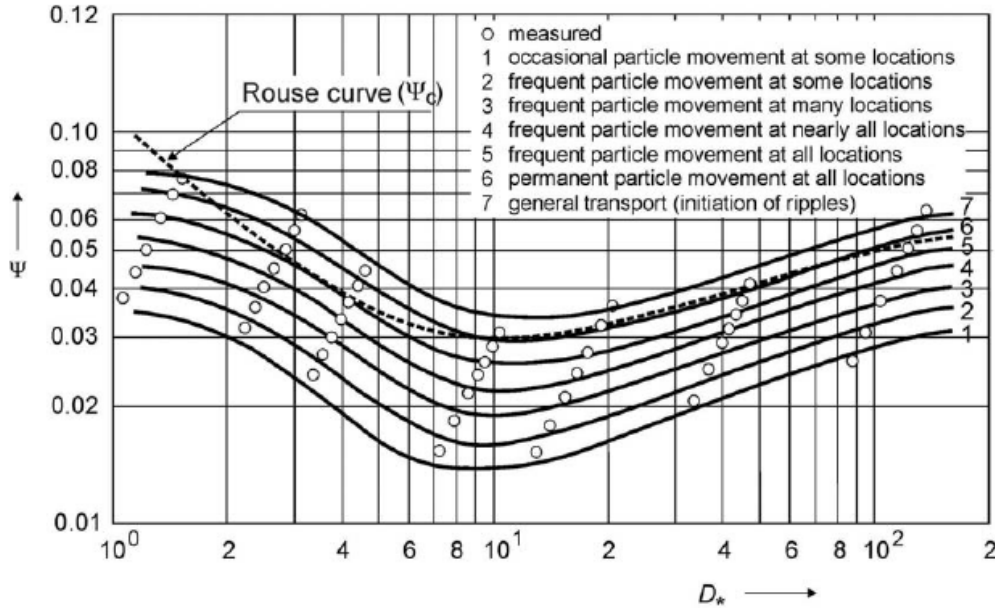


Figure 2-4: Seven phases of transport as described by Breusers in 1977 (Verheij et al., 2010) $D^* = d_{50}(\Delta_{\text{grain}} * g/v^2)$.

2.3 Design formula of Hoffmans (2012)

Chapter 1 already described the simplified and full version of the formula. This section describes the theory behind the formula of Hoffmans (2012). The philosophy of simultaneous erosion is described by the characteristic relative strength $\eta_{c,k}$ [-]. For geometrical open filter this is incorporated within equation 2.3 (Bakker in 1994 and Grass in 1970 (Hoffmans, 2012)). $\tau_{c,bf,k}$ represents the mean characteristic strength of the base layer at the filter-bed interface. $\tau_{c,f,k}$ represents the mean characteristic strength of the filter layer. The other parameters are described in section 1.1.

$$\eta_{c,k} = \frac{\tau_{c,bf,k}}{\tau_{c,f,k}} = \frac{d_{b50} \Delta_b \psi_{c,b} (1 - \gamma V_{Gb})}{d_{f50} \Delta_f \psi_{c,f} (1 - \gamma V_{Gf})} \quad (2.3)$$

The load damping is not yet taken into account in equation 2.2. Hoffmans (2012) applied the turbulent kinetic energy coefficient k_f (equation 2.4) as the measure for the damping of the loads in the geometrical open filter.

$$k_f(z) = \frac{3}{2} * u_{RMS,p}^2(z) \quad (2.4)$$

The relative load at a certain depth in the filter is described by η_{load} (equation 2.5). Hoffmans (2012) described that the relative load at the filter-bed interface is independent of the flow velocity as observations showed that $k_f(z)$ increases with increase in k_b (equation 2.4). This means that the damping depth L_d only depends on the load damping coefficient α_d and the grain size d_{f15} . Thus in a general way, the increased turbulence in the outer flow (i.e. sill-induced, pier induced) is theoretically incorporated into the formula of Hoffmans (2012). Hoffmans (2012) calibrated α_d based on damping of flow fluctuations inside the filter pores (figure 2.5). The velocity fluctuations were measured by Klar (2005) under uniform flow conditions. The relative load at the filter-bed interface is described by equation 2.6. $z = 0$ m is at the filter-outer flow interface and $z = -D_f$ is at the bed-filter interface.

$$\eta_{load}(z) = \frac{k_f(z)}{k_b} \approx e^{\frac{z}{L_d}} \quad (2.5)$$

$$\eta_{load}(-D_f) \approx e^{\left(\frac{-D_f}{\alpha_d * d_{f15}}\right)} \quad (2.6)$$

Combining equation 2.3 and 2.6 resulted in the original design formula with a relative layer thickness of D_f/d_{f15} (equation 1.2). Van de Sande (2012) proposed a new α_d , and a relative layer thickness D_f/d_{f50}

(equation 1.2). Change of D_f/d_{f15} to D_f/d_{f50} is based on a few wide filter grading experiments (Van de Sande, 2012). However, at the moment the formula is not yet tested for non-uniform flow conditions. The non-uniform flow of a cylindrical pier is in a general way described by increased turbulence, but validation is recommended (Van de Sande, 2012, Hoffmans, 2012).

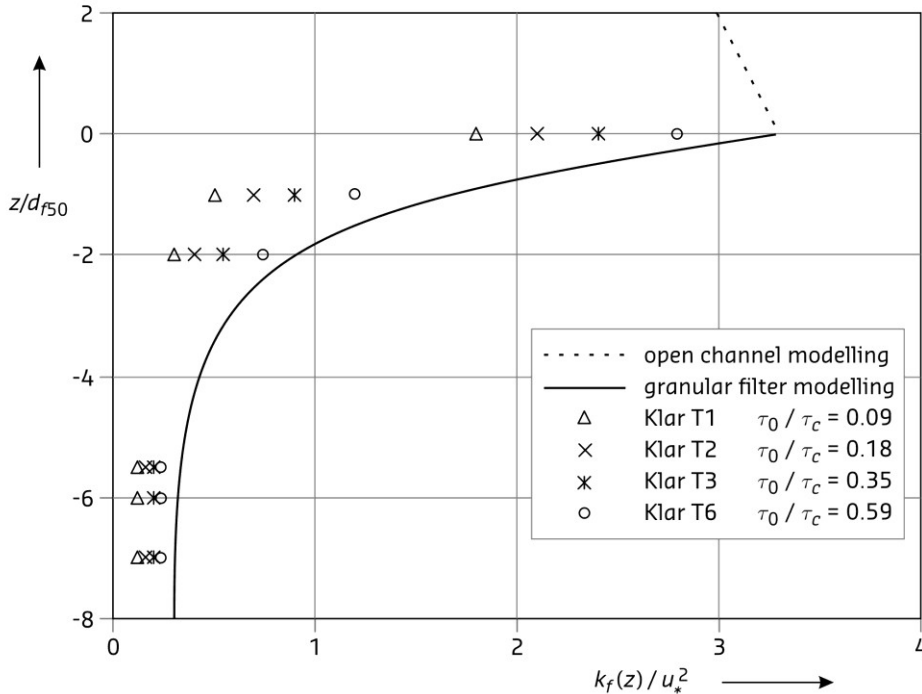


Figure 2-5: Exponential decrease in turbulent kinetic energy with depth z (Hoffman,2012)

2.4 Design formula of Wörman (1989)

Wörman (1989) derived his formula (equation 2.8) based on a fitted empirical gradient (i.e. 0.16), Wörman (1989) stability criteria (equation 2.7), experiments with a cylindrical pier, the Isbash formula from 1935 (Breusers,1977) and a description for the local flow velocity of twice the depth average flow velocity (Worman, 1989). Because the formula is based on piers, the horse shoe vortex is directly incorporated into the formula. In addition, Wörman (1989) stated that: “The governing dimensionless parameters describe suitable thickness of riprap layer, grain size of the riprap material, grain size of base material and mean flow velocity”. As described in section 1.1 the formula thus differs mainly from the formula of Hoffmans (2012) by the linear relation between these parameters and the thickness (Hoffmans ,2012). Hoffmans (2012) found a logarithmic relation. Explanation of parameters in equation 2.7 and 2.8 are described in section 1.1.

$$\frac{\bar{u}}{g * D_f} \approx 6 * \left(\frac{d_{b85}}{d_{f15}} \right) \quad (2.7)$$

$$\frac{D_f}{d_{f15}} = 0.16 * \left(\frac{n_f}{(1 - n_f)} * \frac{\Delta_f}{\Delta_b} * \frac{d_{f85}}{d_{b85}} \right) \quad (2.8)$$

3 Laboratory experiments

3.1 Test set-up

Laboratory experiments were part of the KPP ('Kennis Primaire Processen') research project and were executed between the 23rd of July and the 17th of August. The aim of the experiments was to populate a database for research into the relation between transport of bed material through the filter and into the flow, filter and bed characteristics for different flow conditions: these conditions being (1) uniform flow, (2) sill-induced additional turbulence and (3) conditions with a cylindrical pier. An additional aim was to populate the database with measurements of pressure signals and signal fluctuations within the filter. These pressure signals are outside the scope of this thesis.

The laboratory experiments are executed in the Atlantic Basin at Deltares. The set-up of the basin is visualized in figure 3-1 and 3-2.

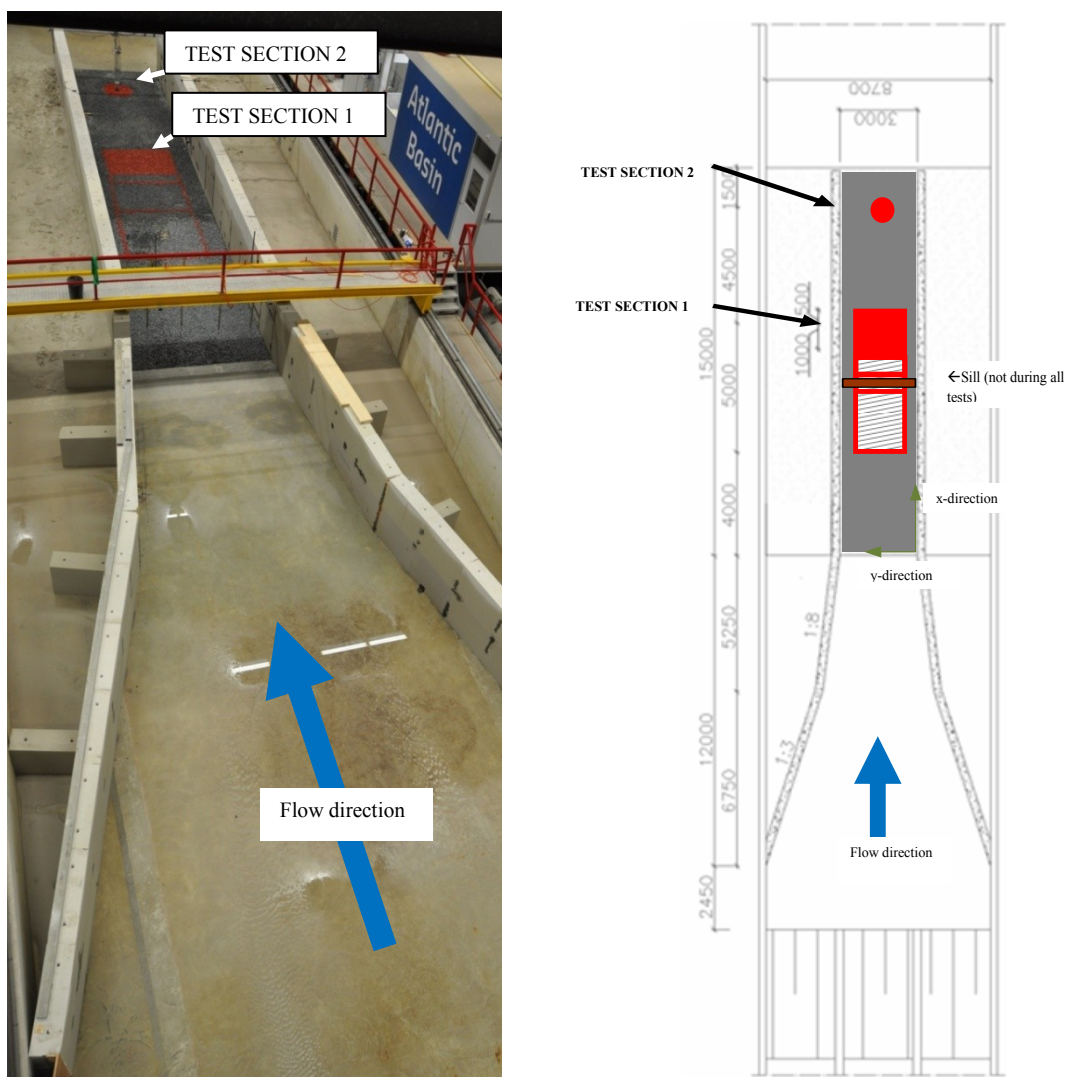


Figure 3-1: Set-up of laboratory experiments in top view photo (left) and schematized view on the test sections (right). The blue arrows mark the flow direction. The striped area within the red lines shows the area where granular material covers the bed material. Only the red filled areas are the test sections.

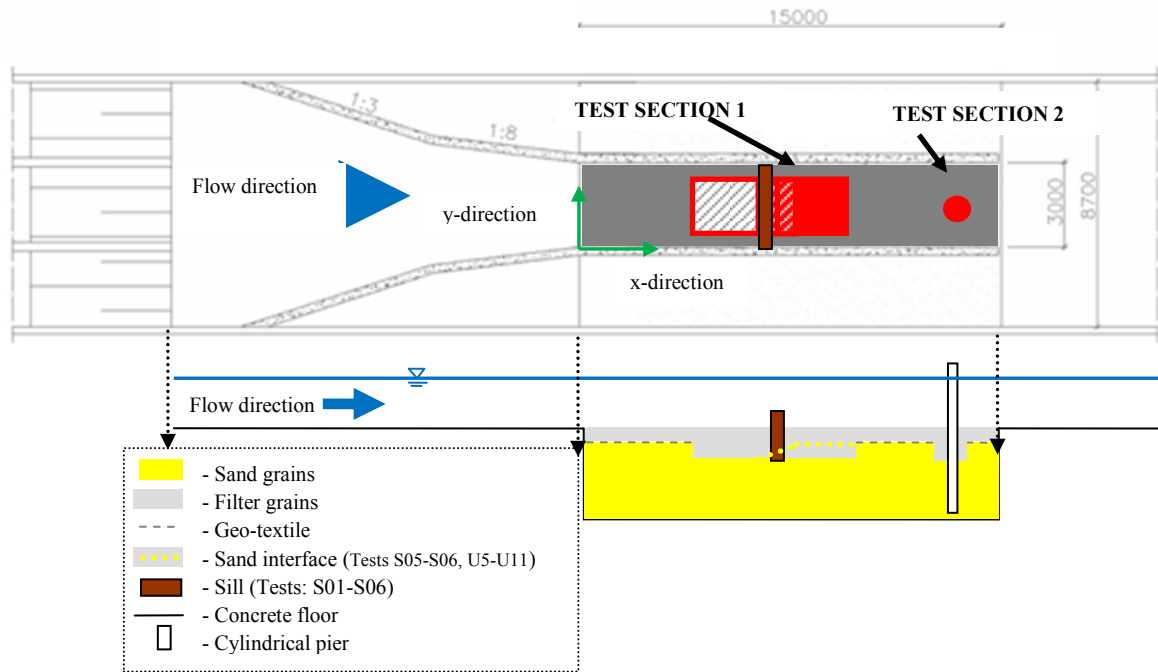


Figure 3-2: Top view and cross sectional view.

Test section 1 and test section 2

A part of the total Atlantic basin floor area is covered with concrete and a part is covered with fine sand ($d_{b50} = 0.165 \text{ mm}$). The basin is narrowed by construction of two walls. The (grey) zone of increased flow velocities and contains sand is defined as ‘the testable area’ (shown in figure 3-2). The testable area has a length of 15 meters and width of 3 meters.

Within the testable area, two test sections are distinguished; (Test section 1; T1) flat bed, for conditions with and without additional turbulence, and (Test section 2: T2) flat bed with circular pier ($D_{\text{pier}} = 0.15 \text{ m}$).

Test section 1 is used for two aims, that are achieved by application of two phases within the test series. Within the first phase, the damping of average velocity induced pressure and velocity fluctuation induced pressure within the filter is measured for different grain sizes and turbulent intensities. The second phase aims to measure the degree of filter settlement. The filter stones cover the bed material (sand, $d_{b50} = 0.16\text{mm}$). The dimensions of this test section (red in figure 3-1) are length $L = 2.0\text{m}$ and width $B = 2.0\text{m}$. The thickness of filter layer was increased by keeping the filter top level equal to the surrounding area (figure 3-1), lowering the bed level (by removal of bed material) and filling this volume with filter material. Two type of flow conditions are tested in this test section: (1) uniform flow conditions and (2) additional turbulence flow. The additional turbulence is generated with a sill. Figure 3-3 visualizes the wooden sill and its location in front of test section 1. The wooden T-shaped sill with a height of 0.2 m (measured from the topside of the filter) is placed at 2.0 m in front of the pressure sensors.



Figure 3-3: Wooden sill in front of test section 1.

A delineated (perimeter marked with red lines in figure 3-1) area is designed in front of this test section. This area is defined as the ‘filter flow adaptation area’. The function is to provide an adaption length for infiltration of the flow into the filter layer. Here filter stones cover the bed

material (sand). The dimensions are $L = 3.5$ m and $B = 2.0$ m. In addition, a slope (1:10) at a distance of 0.5 m of the left side of test section 1 is constructed in the preparation of some tests (U05-U11 and S05-S06).

Test section 2 is used to measure the degree measure of filter settlement, down flow velocity and flow contraction effect on velocity at a cylindrical pier. The filter stones cover the bed material. The transparent pier has a diameter of $D_{\text{pier}} = 0.15$ m. The diameter of the test section 2 is approximately $C_{12} \approx 0.83$ m. This corresponds to the representative bed protection $C_{12} \approx 6 * D$ by Whitehouse (1998). The thickness of the filter layer was increased by keeping the filter top level equal to the surrounding area (figure 3-2), lowering the bed level (by removal of bed material) and filling this volume with filter material.

The remaining area surrounding both test sections (gray in figure 3-1) contains bed material covered with geo-textile. The geo-textile is covered with stones of similar size as the test sections to fixate the location of the geo-textile. Geo-textile prevents having to reconstruct the filter top layer surrounding the test sections after each test.

Test parameters

The flow conditions only contain a current (no waves). The parameters that are varied during the test program are the layer thickness D_f [mm], filter grain size d_{f50} [mm], average flow velocity \bar{u} [m/s] and flow conditions consisting of (1) uniform flow, (2) additional turbulence and (3) with cylindrical pier. The three flow velocities that were tested are; 0.5 m/s, 1.0 m/s and 1.5 m/s. The water level was kept at 1.0 m for $\bar{u} = 0.5$ m/s and $\bar{u} = 1.0$ m/s. To achieve the average flow velocity 1.5 m/s, water levels were decreased to $h_w = 0.67$ m, because of limited discharge capacity. The test duration was 1.5 hours per test.

Two filter gradations are tested. The first gradation has a median filter diameter $d_{f50} = 27.0$ mm, the second a filter diameter of $d_{f50} = 20.0$ mm. The associated relative grain size diameter (d_{f50}/d_{b50}) is respectively 146 [-] and 109 [-]. The first filter grain diameter has a $d_{f15} = 22$ mm and $d_{f85} = 40$ mm. The second filter grain diameter has a $d_{f15} = 16$ mm and $d_{f85} = 22$ mm. The open filter grain diameters are selected to be 'just' external stable with phase 1 ($\Psi_c = 0.03$) using equation 1.1 (Schierreck, 1995). The sieve curves are described by appendix 3 and 4. The test parameters per test are described in section 3.2 Test program.

3.2 Test program

Table 3-1 describes the test program and the values for each test parameter during the test. The ID of the database, or Test ID (e.g. 1a) is redefined in this thesis to the Report ID to distinguish the flow conditions and the flow velocity. The ID stands for the (Report or Test) number. The U, S and P in front of the number represent respectively flow condition uniform flow, sill-induced additional turbulence and cylindrical pier. Furthermore, table 3-1 contains the absolute filter layer thickness D_f , filter and bed material grain sizes (both absolute and relative) and the degree of wide-grading by V_g . Data of the density of the bed and filter material is not available, therefore the density of both filter and bed material is assumed 2650 kg/m^3 . A coupled test is for example test T01 ('T01a+T01b'), or an uneven Report ID combined with the following 'even' number. The flow velocity is increased from T01a to T01b.

Section 3.1 described that test section 1 is positioned upstream of test section 2. When a sill was applied in front of test section 1, a higher degree of velocity fluctuations is measured in vertical velocity signal in front of the cylindrical pier (section 3.4) than in tests without a sill. Therefore, the increased turbulent intensity in the flow is described within table 4-1 by 'likely'.

Table 3-1: Overview of test parameters. The colours green, orange and blue represent the flow conditions uniform flow, flow with sill-induced additional turbulence and flows with a cylindrical pier, respectively. $\bar{U} = U_0$. $H_w = 1.0$ m for $\bar{u} = 0.5$ m/s and $\bar{u} = 1.0$ m/s. $H_w = 0.67$ m for $\bar{u} = 1.5$ m/s.

Report ID	Test ID	Add.Turbulence	Pier	\bar{u} [m/s]	D_f [mm]	d_{b50} [mm]	d_{f50} [mm]	$V_{g,bed}$ [-]	$V_{g,filter}$ [-]	D_f/d_{f50} [-]	d_{f50}/d_{b50} [-]
U1	T01a	No	No	0.5	200	0.165	24.1	0.23	0.14	8.3	146.1
U2	T01b	No	No	1.0	200	0.165	24.1	0.23	0.14	8.3	146.1
U3	T04a	No	No	0.5	200	0.165	18.0	0.23	0.14	11.1	109.1
U4	T04b	No	No	1.0	200	0.165	18.0	0.23	0.14	11.1	109.1
U5	T05a	No	No	0.5	50	0.165	18.0	0.23	0.14	2.8	109.1
U6	T05b	No	No	1.0	50	0.165	18.0	0.23	0.14	2.8	109.1
U7	T06a	No	No	0.5	100	0.165	18.0	0.23	0.14	5.6	109.1
U8	T06b	No	No	1.0	100	0.165	18.0	0.23	0.14	5.6	109.1
U9	T08a	No	No	0.5	25	0.165	18.0	0.23	0.14	1.4	109.1
U10	T08b	No	No	1.0	25	0.165	18.0	0.23	0.14	1.4	109.1
U11	T08c	No	No	1.5	25	0.165	18.0	0.23	0.14	1.4	109.1
S1	T02a	Yes	No	0.5	200	0.165	24.1	0.23	0.14	8.3	146.1
S2	T02b	Yes	No	1.0	200	0.165	24.1	0.23	0.14	8.3	146.1
S3	T03a	Yes	No	0.5	200	0.165	18.0	0.23	0.14	11.1	109.1
S4	T03b	Yes	No	1.0	200	0.165	18.0	0.23	0.14	11.1	109.1
S5	T07a	Yes	No	0.5	100	0.165	18.0	0.23	0.14	5.6	109.1
S6	T07b	Yes	No	1.0	100	0.165	18.0	0.23	0.14	5.6	109.1
P1	T01a	No	Yes	0.5	150	0.165	24.1	0.23	0.14	6.2	146.1
P2	T01b	No	Yes	1.0	150	0.165	24.1	0.23	0.14	6.2	146.1
P3	T02a	Likely	Yes	0.5	50	0.165	24.1	0.23	0.14	2.1	146.1
P4	T02b	Likely	Yes	1.0	50	0.165	24.1	0.23	0.14	2.1	146.1
P5	T03a	Likely	Yes	0.5	200	0.165	24.1	0.23	0.14	8.3	146.1
P6	T03b	Likely	Yes	1.0	200	0.165	24.1	0.23	0.14	8.3	146.1
P7	T04a	No	Yes	0.5	100	0.165	24.1	0.23	0.14	4.1	146.1
P8	T04b	No	Yes	1.0	100	0.165	24.1	0.23	0.14	4.1	146.1
P9	T05a	No	Yes	0.5	200	0.165	18.0	0.23	0.14	11.1	109.1
P10	T05b	No	Yes	1.0	200	0.165	18.0	0.23	0.14	11.1	109.1
P11	T06a	No	Yes	0.5	100	0.165	18.0	0.23	0.14	5.6	109.1
P12	T06b	No	Yes	1.0	100	0.165	18.0	0.23	0.14	5.6	109.1
P13	T07a	Likely	Yes	0.5	50	0.165	18.0	0.23	0.14	2.8	109.1
P14	T07b	Likely	Yes	1.0	50	0.165	18.0	0.23	0.14	2.8	109.1
P15	T08a	No	Yes	0.5	300	0.165	18.0	0.23	0.14	16.7	109.1
P16	T08b	No	Yes	1.0	300	0.165	18.0	0.23	0.14	16.7	109.1
P17	T08c	No	Yes	1.5	300	0.165	18.0	0.23	0.14	16.7	109.1

3.3 Data

The main data resource for this thesis is a database which resulted from laboratory experiments carried out as part of the KPP research project ('Kennis Primaire Projecten') of Deltares and Rijkswaterstaat (Joustra, 2012). At the start of this research, the database consisted only of un-processed raw data. Section 3.3.1 describes the available data, while section 3.3.2 describes the data processing. Furthermore, validation results as interpreted by Van de Sande (2012) are added to this thesis as a reference. This validation results are based on data of Van Huijstee & Verheij (1991), Bakker in 1960 (Van de Sande, 2012), Van der Sande (2012), Van Velzen (2012) and Wörman (1989). Appendix 2 describes these validation results.

3.3.1 Raw dataset

Four types of data are obtained by the tests: (1) sub-water surface camera images, (2) hydrodynamic data, (3) bathymetry data and (4) pressure data inside the filter layer. The focus of this research is on data types (1), (2) and (3). (4) was recorded in anticipation of further research.

Submerged camera images were made during the tests at test section 1 (position near the wall) and test section 2 (position inside pier).

Furthermore, six EMS flow velocity meters measured the flow velocity in two directions. During the test, four flow sensors measured the flow velocity in the horizontal plane (x- and y-direction) along the width in front of the test sections. These four EMS meters were relocated occasionally (both vertical as horizontal), to measure 1 minute flow velocities at multiple x- and z-positions within the testable area. Furthermore, two additional EMS measured the flow velocities near the cylindrical pier. One EMS measured the vertical and horizontal flow (x- and z- direction) in front of the pier and one EMS measured the horizontal flow at the side of the pier. Also, the water level is measured at the x - location of the pressure sensors (test section 1), near the side-walls.

The bathymetry data consists of raw 3D -stereo-photography (3D-SP) coupled-images and internal camera images. 3D-SP is applied before and after each 'coupled test' (e.g. test ID 'T01'). Processing the 3D-SP data results in spatial information (x, y, z) of the filter-outer flow interface on the time step before and after the coupled test. The bathymetry by 3D-SP is available for before test U5, U7, U9, S5, P1, P3, P5, P7, P9, P11, P13 and P15. In addition, the bathymetry data by 3D-SP is available after test U6, U8, U10, S6, P2, P4, P6, P8, P10, P12, P14 and P16. No 3D-SP data is available for test U1, U2, U3, U4, S1, S2, S3 and S4. The bathymetry data by internal camera imagery is available for before, after and during tests P1 to P17, but outside the scope of this thesis.

3.3.2 Data processing

The raw data (underwater camera images, 3D-SP) as described in section 3.3.1 must be processed, before the data can be applied in the validation of the design formulas. In addition, the flow velocity measurements are processed to describe the flow conditions during the tests (e.g. with flow velocity and turbulent intensity profiles, etc.).

Visual observation to classify filter and bed stability

The camera photos are processed into a movie for each test. The photos and videos are required to classify the filter stability. The processing occurred with video processing software VMACH. Additional information about the test (e.g. test id, flow velocity, etc.) are added to the movie. Furthermore, three images (start; $t = 0$ min, intermediate $t \approx 45$ min and last camera images $t \approx 90$ min) are selected and compared for the visual observation of the bed stability. Figure 3-4 and 3-5 give examples of camera images.



Verification of filter instability in uniform flow and flows with sill-induced additional turbulence

The method 3D Stereo-Photography (3D-SP) is applied to quantify the degree of filter settlement for the conditions of uniform flow and sill-induced additional turbulence. First, the method 3D-SP is used to calculate the bathymetry from a set of photo-pairs made before and after each ‘coupled test’. Within the 3D-SP method, the degree of disparity between two photos (photo pairs) is used as input for the calculation of the filter-outer flow interface level. The larger the distance between a pixel in photo 1 and the same pixel in photo 2, the closer this pixel (point) is to the camera. This is the same principle as two eyes estimating distance. The photo pairs are made at multiple locations around the test section. The data set of photo pairs is the input for the calculation and reconstruction of the bathymetry. Next, the difference in filter-outer flow interface is computed by subtraction of the initial bathymetry from the final bathymetry. A negative value describes a decrease, and could either describe filter settlement (i.e. bed instability), filter instability or both. The filter-outer flow interfaces levels and differences are calculated with Matlab-scripts available at Deltares. The method of stereo-photography is commonly used in consultancy studies at Deltares. The resolution of the grid is 1mm and typical measurement errors in perfect conditions are in the order of 1 mm. Figure 3-6 and figure 3-7 show the equipment of stereo-photography.

Next, data is extracted from a polygon (in this case a rectangular area; visualized in figure 3-8), because the bathymetry data covers a larger area than the test section. The polygon is defined in the middle of test section 1, to exclude the area outside test section 1 that is covered with geo-textile. The statistics that are applied in the verification of filter settlement (measure for bed instability) between the tests are the median and standard deviation of the filter-outer flow interface difference for data within the polygon area.



Figure 3-4: One frame of the video of camera 1. Camera 1 filmed the condition uniform flow and the condition sill-induced additional turbulence. The flow direction is from left to right.

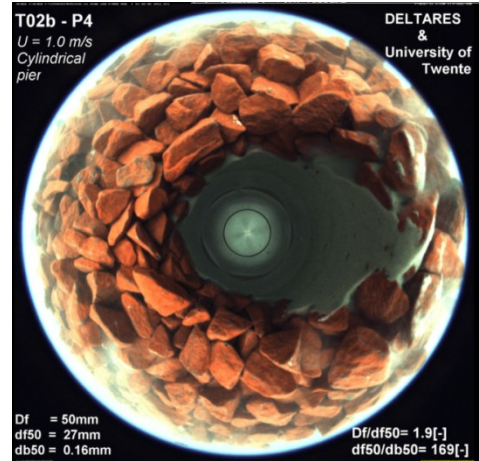


Figure 3-5: One frame of the video of camera 2. Camera 2 filmed the condition with a cylindrical pier. The camera is fixed inside pier, facing downwards. The red filter stones are on top of the white-grey bed material. Flow direction is from left to right.

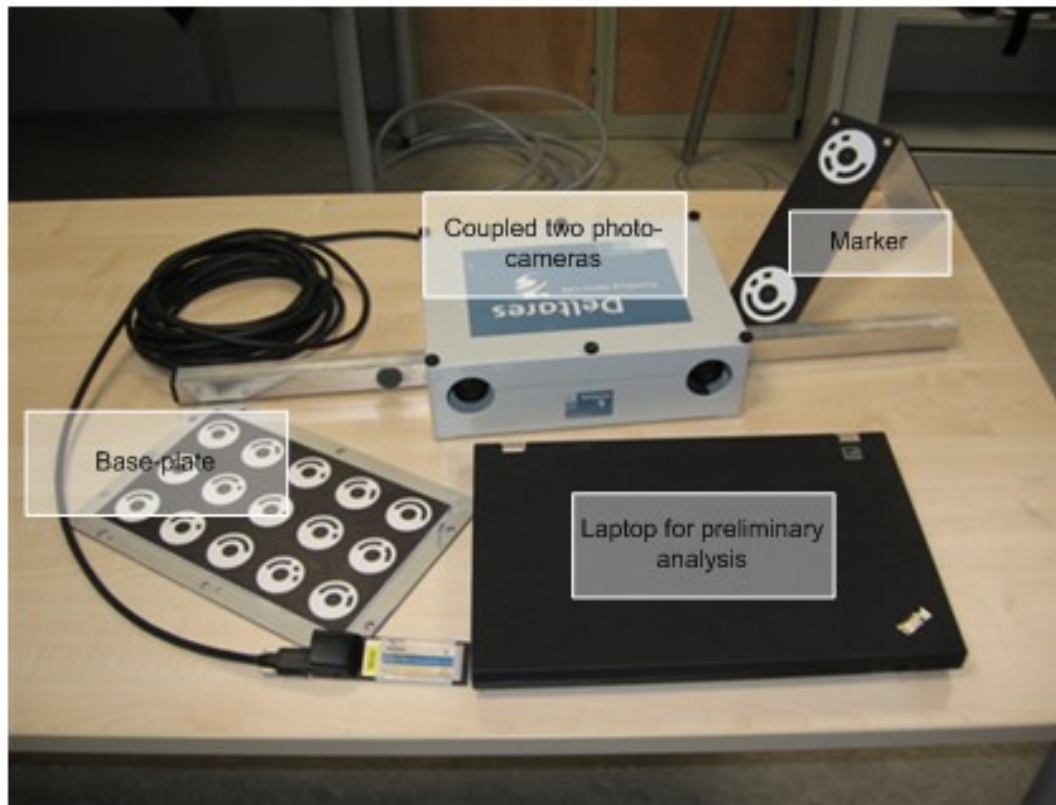


Figure 3-6: Stereo-photography equipment.



Figure 3-7: Stereo photography set. The set contains the camera attached to a laptop (on the table), the markers (around pile) and baseplate (attached to wall).

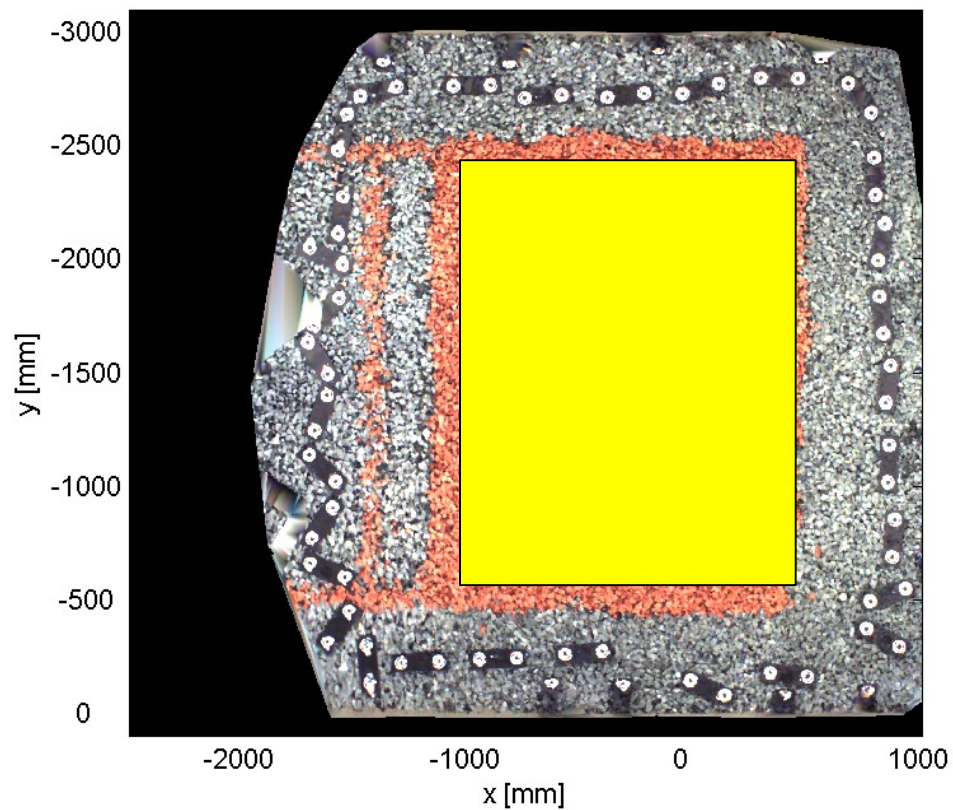


Figure 3-8: Dimensions and location of the polygon (yellow area) in test section 1.

Flow conditions uniform flow and flows with sill-induced additional turbulence

The flow profiles ($u(x, z)$) and turbulent fluctuations profiles (as described by the root-mean-square values RMS (equation 3.1) and the relative turbulent intensities r_u (equation 3.2)) are calculated from the EMS flow velocity data measured at the test section with uniform flow and near the test section with sill-induced additional turbulence. These profiles describe the flow conditions (uniform flow and flows with sill-induced additional turbulence).

The sill in front of the test section is expected to induce additional turbulence in the test section. The increase in turbulence intensity increases the degree of mobility of the filter stones (Schiereck, 1995) and it is expected (based on observations of Van de Sande (2012)) that an increase in turbulent fluctuations increases the degree of bed instability.

Statistics (median u , root-mean-squared (RMS) and relative turbulence intensity r_u) are calculated from the flow velocity data measured at multiple depths downstream of the locations of the sill for the conditions uniform flow and flows with sill-induced additional turbulence, to quantify the effect of the sill on the flow and the investigate the distribution of these statistics over the width of the test section. The location of the flow-, turbulence profiles and EMS are show in figure 3-9 (top view). The cross sections where the flow profiles are measured are visualized by figure 3-11 and 3-12. The data processing software Matlab is used to calculate and visualize the statistics into figures.

Flow condition with a cylindrical pier

Next, the vertical and horizontal velocity raw signals measured in front of the cylindrical pier are processed. This provides insight in occurrence and magnitude of the expected down flow and/or horse shoe vortex in front of the pier. The cross section at test section 2 (with a cylindrical pier) is visualized by figure 3-10.

The median and RMS values calculated from the vertical flow velocity signal describe the degree of the down flow and down flow fluctuations. The statistics are calculated for test P15, P16 and P17 with flow velocities of respectively $\bar{u} = 0.5$ m/s, $\bar{u} = 1.0$ m/s and $\bar{u} = 1.5$ m/s. Test P15, P16 and P17 all have the same relative layer thickness and relative grain size. In addition, these test also have relative no to minor degree of filter-outer flow interface decrease. The statistics are calculated over a 10 minutes time window. The data contains a gradually increasing flow velocity during test P17 between $t = \text{min}$ and $t \approx 35$ min, therefore with a additional buffer of 8 minutes the time window is chosen to be from 41 to 51 minutes.

$$RMS(u(z)) = \sqrt{(\bar{u}_z - u'_z)^2} \quad (3.1)$$

$$r_u(z) = \frac{RMS(u(z))}{\bar{u}} = \frac{\sqrt{(\bar{u}_z - u'_z)^2}}{\bar{u}} \quad (3.2)$$

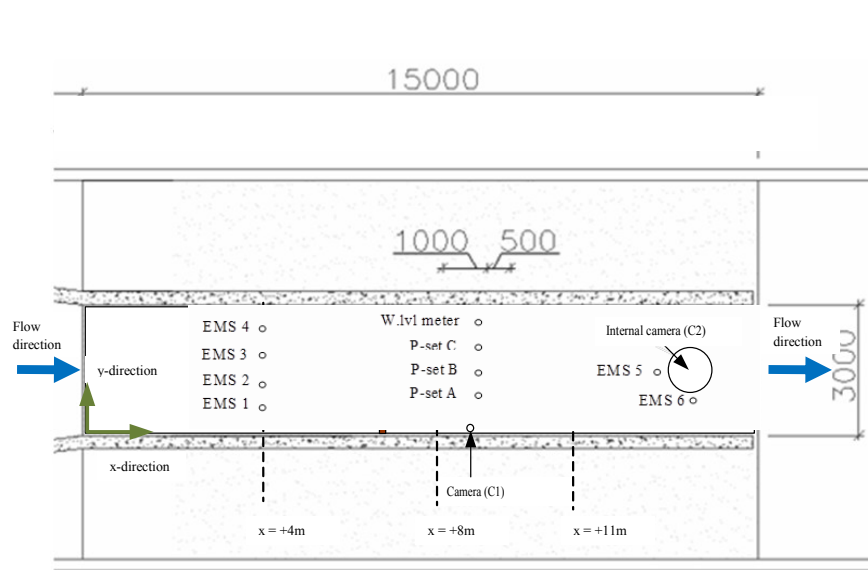


Figure 3-9: Location of flow velocity profile measurements; $x = 4$ m, $x = 8$ m and $x = 11$ m. The distance is described in mm.

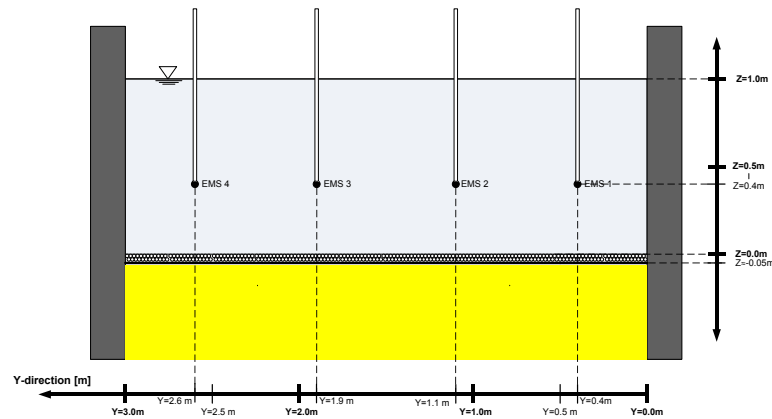


Figure 3-11: The default position and lateral cross-section of the EMS sensors at location $x = 4$ m. This also visualizes the cross-section at location $x = 11$ m.

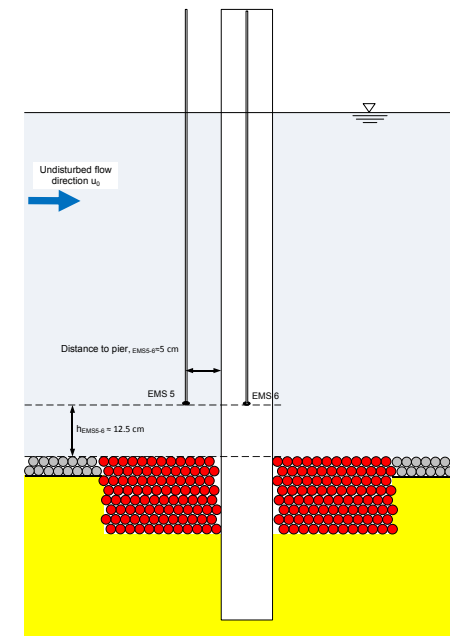


Figure 3-10: Location of EMS 5 and 6 relative to the pier. Right image shows the cross-sectional view of the Pier.

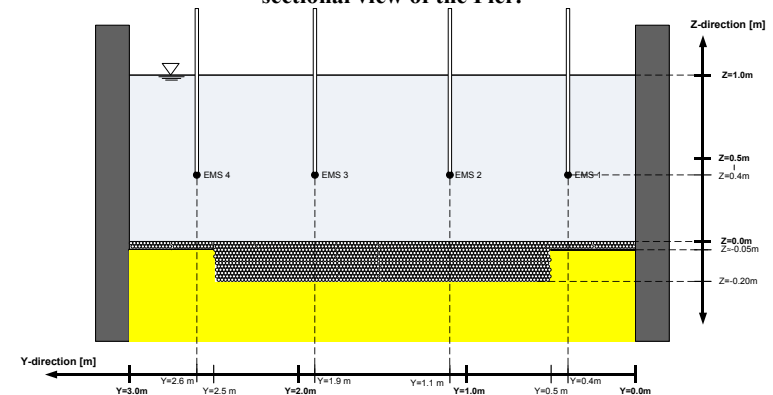


Figure 3-12: Lateral cross-section at $x = +8$ m for test U1-U4 and S1 and S2. Layer thickness was modified for the other tests. The layer thickness during test U5 was 0.10 m.

3.4 Flow conditions

3.4.1 Uniform flow

The flow profiles of the outer flow above test section 1 (uniform flow and sill-induced turbulence) are visualized by figure 3-13 and figure 3-14, respectively. The measured flow profiles at the test section show the expected logarithmic velocity profile over depth. The depth average flow velocities at the test section and 40% of the water depth for the expected $\bar{u} = 0.5$ m/s and $\bar{u} = 1.0$ m/s differs between +4 and +5% from the expected \bar{u} . The theoretical magnitude of turbulence expressed as the depth average relative turbulence intensity r_0 for uniform flow lies typically between $r_0 = 0.042$ [-] (for smooth, wide channels) and $r_0 = 0.126$ [-] (for small rough channels) (Hoffmans, 2012). The test setup results in a theoretical r_0 more towards small rough channels. A rough visual estimation, from figure 3-13 and 3-14, of the depth average turbulent intensity is $r_0 \approx 0.1$ confirms this. The relative turbulent intensity r_u for both flow velocities $\bar{u} = 0.5$ m/s and $\bar{u} = 1.0$ m/s is in the same order of magnitude so the relative turbulent intensity r_0 .

The fluctuations in the flow velocity in the lower 13% of the water column as described by the RMS are doubled from ~ 0.06 m/s to ~ 0.12 m/s for $\bar{u} = 1.0$ m/s compared to $\bar{u} = 0.5$ m/s. This confirms the expectations, since the Reynolds number in open channel flow is linearly proportional to the flow velocity.

However, two EMS (2 and 3) in the middle of the width of the channel show lower measured flow velocities compared with the EMS (1 and 4) at the walls of the channel. This yields for the height of 10 – 60% above the filter-outer flow interface and $\bar{u} = 0.5$ m/s. This non-uniform distribution of flow velocity over width does not occur during the flow velocity $\bar{u} = 1.0$ m/s, and therefore has a limited effect on the classification of bed stability.

The phenomenon of non-uniform distribution of flow is not fully understood, but one hypothesis is described next. The flow velocity distribution over width at $x = 4$ m for $\bar{u} = 0.5$ m/s is observed uniform. Downstream of $x = 4$, the geo-textile beneath the stones is not present and the filter layer thickness increases from $D_f = 50$ mm to $D_f = 200$ mm. The water is infiltrated within this thicker filter, the water level stays the same and therefore the cross-sectional area between $y = 0.5$ m and $y = 2.5$ m increases with the additional voids between the stones. The discharge in flow direction is constant, but the area increases. Because of the law of continuity, the discharge through the filter lowers the discharge above the filter and therefore lowers the flow velocity above the filter. The fact that the flow velocity is not uniform distributed over the width at $x = 4$ m for $\bar{u} = 1.0$ m/s is because the flow contraction as a result of the test section is not yet diffused. Furthermore, this effect is smaller during tests with $\bar{u} = 1.0$ m/s, which can be explained by friction. It is assumed that the friction induced on the flow inside the filter voids are relatively high compared to the friction induced by the top layer of the filter on the outer flow. This results in a distribution of discharge that is more to the area above the filter, than to the flow within the filter pores. However, this hypothesis is not proven.

3.4.2 Sill-induced additional turbulence

The flow velocity profile, turbulent intensity profiles (RMS of $u(z)$ and r_0) are visualized by figure 3-15. The measurement location is 22.5 times the sill height (+4.5 m) downstream of the sill and at 2.5 m downstream of the centre of test section 1. The centre of the test section is located at 10 times the sill height. The theory (section 2.1) expects a positive flow velocity at all depths downstream of the reattachment point. The flow velocity is observed to be positive at all water depths at the measurement location, so the location is clearly downstream of the reattachment point. Schiereck (1995) describes that the reattachment point is located 5-7 times the height of the sill, downstream of the sill. The location where the vertical and horizontal forces are strong enough for filter mobility is at distance between 10 and 20 times the height of the sill, according to Rajaratnam and Subramanya in 1968, Xingkui and Fontijn in 1992 and the experiments of Umland in 1982 (Hoffmans, 2012). So it is expected that test section 1 is at or downstream of the reattachment point.

The presence of the sill did induce additional turbulence in the outer flow (figure 3-14) at all measured water depths at a distance 22.5 times the sill height compared to the uniform flow situation (figure 3-12) with the same flow velocity $\bar{u} = 0.5$ m/s. The depth average relative turbulent intensity is visually approximated $r_0 \approx 0.2$ to 0.25 [-].

Like uniform flow at $\bar{u} = 0.5$ m/s, for the condition of sill-induced additional turbulence, the velocity distribution over width is also not uniform distributed over width. The visual observed classification of instability of the bed and filter that are applied in the validation of the formula of Hoffmans (2012) depend on the observation of flow velocity at $\bar{u} = 1.0$ m/s. It was impossible to measure the flow velocity profiles at 1.0 m/s due to the high oscillatory movement of the equipment. An increase in flow velocity caused a more uniform distribution over width for $\bar{u} = 1.0$ m/s. It is assumed that the same effect occurs at $\bar{u} = 1.0$ m/s for sill-induced additional turbulence.

3.4.3 Cylindrical pier

Figure 3-16 illustrates the flow conditions as measured by the EMS (6) in front of the pier. The flow conditions for $\bar{u} = 0.5$ m/s, $\bar{u} = 1.0$ m/s, $\bar{u} = 1.5$ m/s are represented by the median and RMS of the vertical direction velocity signal w [m/s]. The fixed EMS measured the flow velocities at ~ 13 cm above the bed and 5 cm in front of the pier. In addition, an example for a test where a sill is applied in front of the upstream test section is also shown in figure 3-16.

Figure 3-16 shows that when the depth average flow velocity \bar{u} increases from 0.5 m/s, to 1.0 m/s, to 1.5 m/s, the flow velocity in vertical direction also increases to respectively 0.05 m/s, to 0.10 m/s, to 0.22 m/s. A down flow was present in front of the pier. The down flow velocity is more than linear related to the depth average flow velocity. In addition, figure 3-16 also shows that when \bar{u} increases, the flow fluctuations in the vertical flow velocity also increase. The additional turbulence due to the presence of a sill at test section 1, did also induce additional fluctuations in the down flow, but has only minor effect on the median down flow velocity.

The increase in fluctuations in flow velocity with increased area flow velocity could be the result of the increased turbulence in the outer flow or could be the result of the turbulence generated in by the pier itself, e.g. horse shoe vortex.

The flow velocity signals $u(t)$ and $w(t)$ are described by appendix 5. Not all tests could be applied for the analysis of the down flow, because during some tests the equipment got loose and shifted along the pier edge.



Uniform flow condition

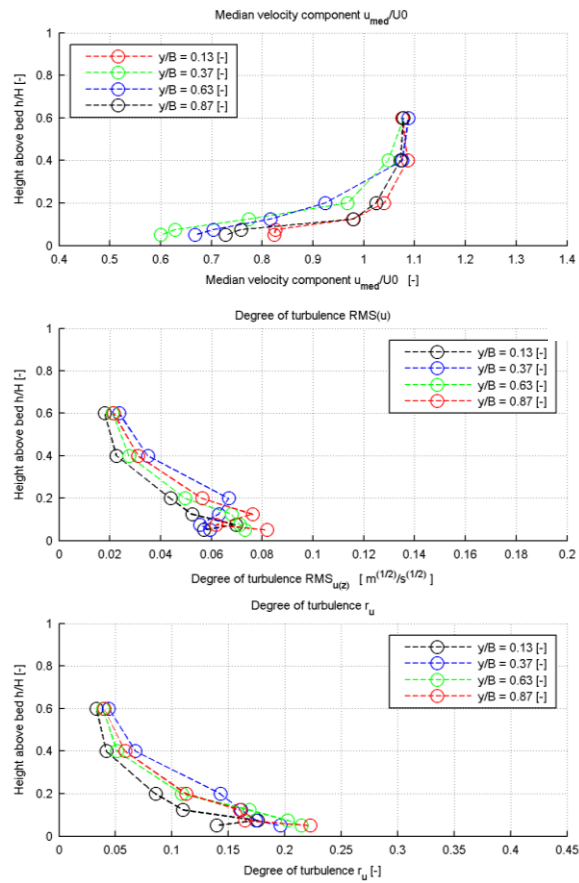


Figure 3-13: Uniform flow condition with $\bar{u} = U_0 \approx 0.5$ m/s. The statistics median flow velocity (above), turbulence intensity as RMS (middle) and relative turbulence intensity r_u (below). Test = U1. Location is $x = 8$ m.

Uniform flow condition

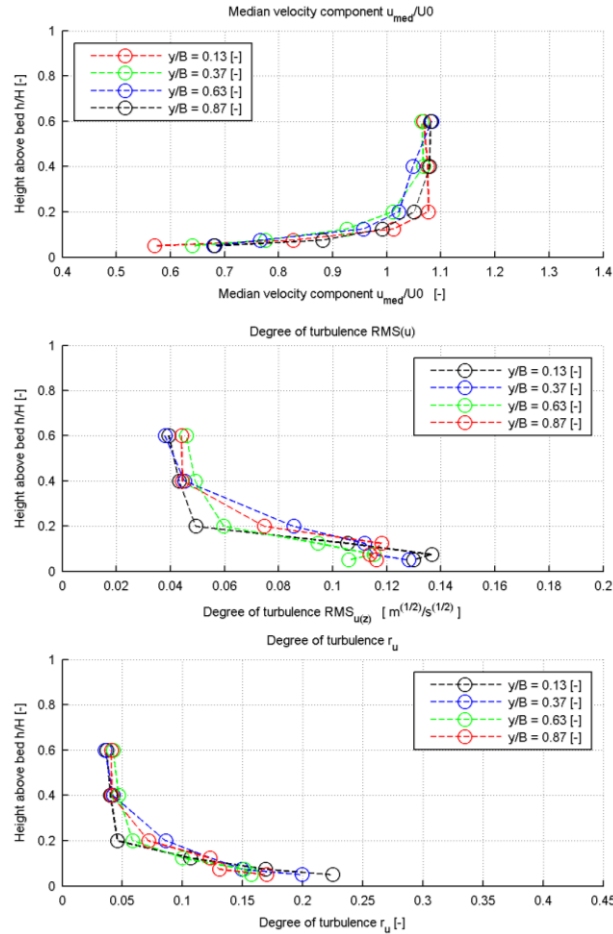


Figure 3-14: Uniform flow conditions with $\bar{u} = U_0 \approx 1.0$ m/s. The statistics median flow velocity (above), turbulence intensity as RMS (middle) and relative turbulence intensity r_u (below). Test U2. Location $x = 8$ m.

Sill-induced additional turbulence condition

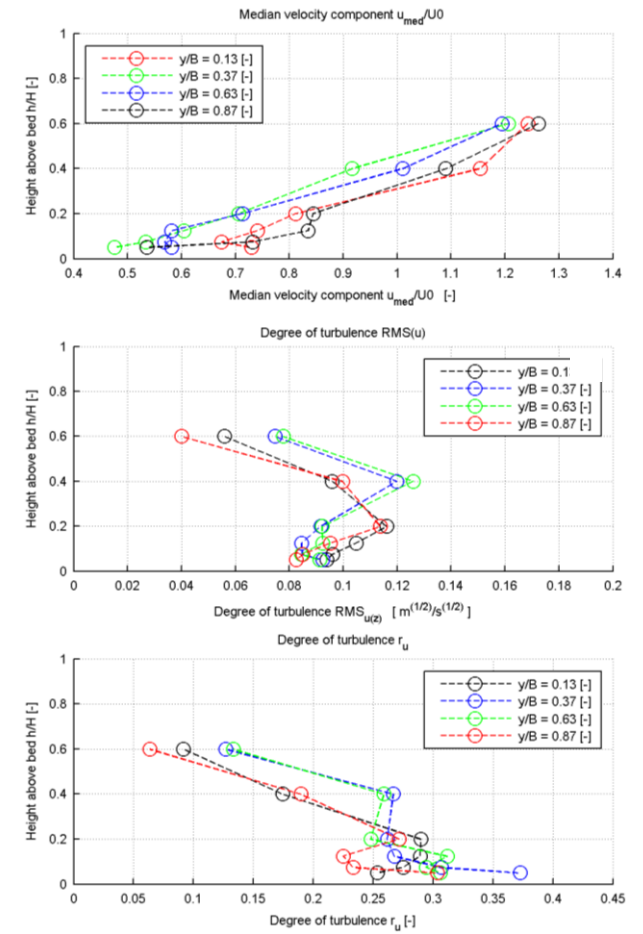


Figure 3-15: Sill-induced additional turbulence with $\bar{u} = U_0 \approx 0.5$ m/s. The statistics median flow velocity (above), turbulence intensity as RMS (middle) and relative turbulence intensity r_u (below). Test = S3. Location is $x = 11$ m.

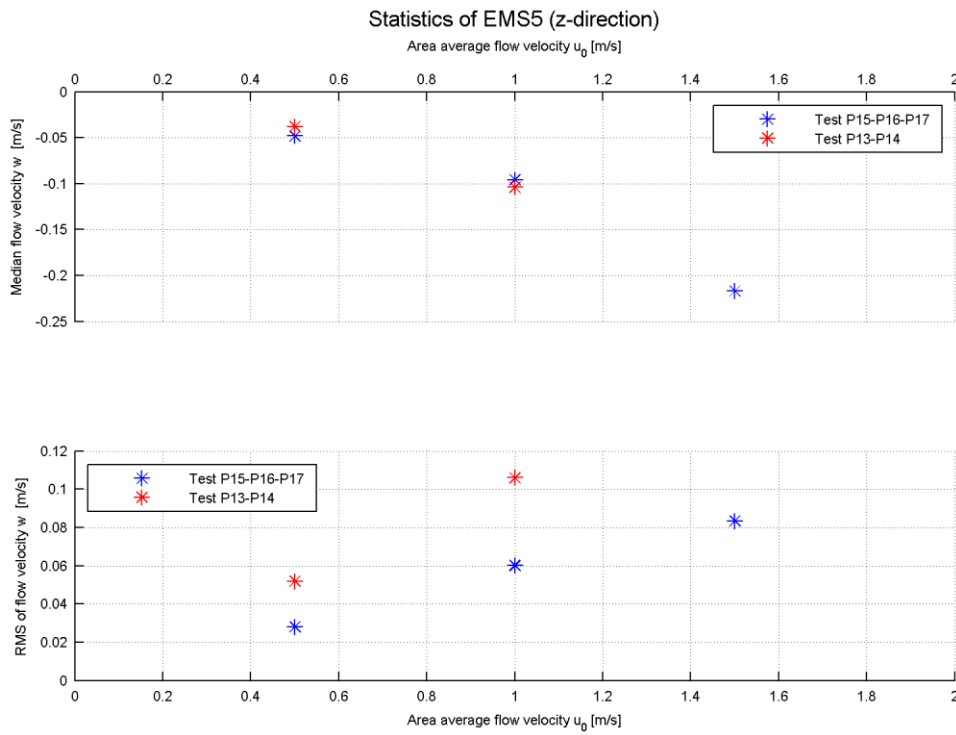


Figure 3-16: Statistics of velocity component in y-direction from 10 minutes EMS signal 5 during test P15-16-17 (without additional turbulence) and test P13-P14 (with additional turbulence). Appendix 5: Flow condition in front of pier for the signals. Z-direction is positive and $z = 0$ m is located at the filter-outer flow interface.

4 Method

4.1 Summary of method

The raw data from experiments conducted by Joustra (2012) are applied to answer research questions 1 to 5. First, the tests are redistributed into flow categories (1) uniform flow (e.g. U1), (2) sill-induced additional turbulence (e.g. S1) and (3) flow with a cylindrical pier (e.g. P1). Second, the filter material instability and bed material instability are classified separately. This separate classification is determined for each test with visual observation using underwater camera images and processed videos. The classification is described in section 4.2. Third, the separate classification is combined into a general classification, which is based on the philosophy of simultaneous erosion. In addition, the bed material instability classification is verified with 3D Stereo photography images for conditions (1) and (2) (section 4.3). Research question 1, 2 and 3 are answered by comparison of the general classification for respectively condition (1), (2) and (3) with the simplified and full version of the formula of Hoffmans (2012) with the $\alpha_{d,Sande}$ (section 4.4). Question 4 is answered by comparison of the general classification for conditions (3) with the formula of Wörman (1989) (section 4.4). Question 5 is answered by evaluation of the classification of data of Van Velzen (2012) and comparison between the validation of both design formulas with data of Van Velzen (2012) and the validation of both design formulas with data of Joustra (2012) (section 4.4).

4.2 Classification of instability

The objective of the formula of Hoffmans (2012) and the formula of Wörman (1989) is to determine the optimum filter layer thickness where the incipient motion of filter and incipient motion of bed material occurs at the same depth average flow condition, i.e. simultaneous erosion. Therefore, the classification of both the filter material instability and the bed material instability is important. The classification (figure 4-1) of the test data to assess the geometrical open filter performance is based on four categories: G.I ‘Only filter material is *instable*’, G.II ‘Both filter and bed material are *instable*’, G.III ‘Only bed material is *instable*’ and G.IV ‘Both filter and bed are *stable*’.

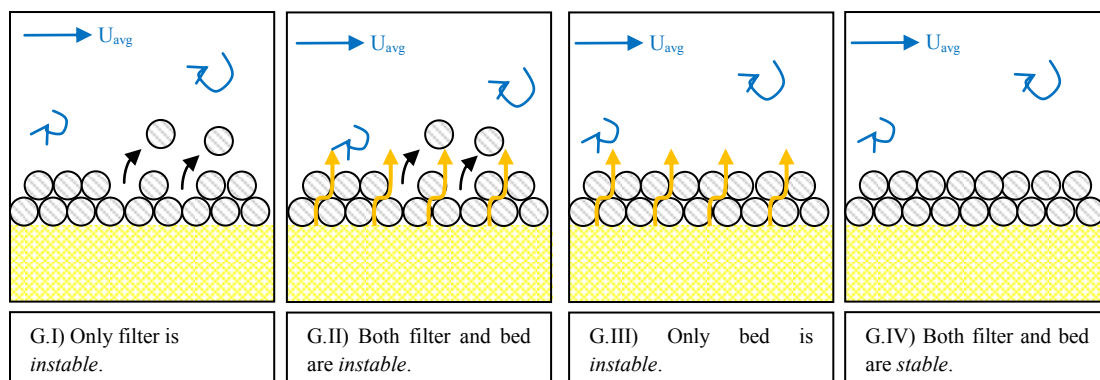


Figure 4-1: General classification of combined filter and bed stability.

Van de Sande (2012) applied the general classification of ‘filter moves first’, ‘simultaneous erosion’ and ‘bed moves first’. In this thesis, the way the general classification is applied, is similar to the general classification as applied by Van de Sande (2012). During the tests of Van de Sande (2012) and Van Huijstee and Verheij (1991) the flow velocity was increased from zero to the condition of instability or maximum flow velocity capacity of the facility, while during the tests of Joustra (2012) the flow velocity was 0.0 m/s, 0.5 m/s or 1.0 m/s. Moreover, the general classification of Van de Sande (2012) could not be applied directly as for example, you cannot ‘see’ based on a single test with constant average flow velocity

that ‘filter moves first’. The reason for not directly applying the general classification by Van de Sande (2012) is caused by the different test set-ups.

First, a general classification is applied to each single test (e.g. P1, P2, P3, U1, U2, S1, S2, etc.). Each single test is part of a coupled test. A coupled test is defined as a test with filter and bed characteristics (e.g. relative layer thickness, relative grain size, relative grading, etc.), but the flow velocity is different. For example, test T01 (P1&P2), T02 (P3&P4), T03 (P5&P6) etc. Next, from each coupled test, one is chosen for application in the validation procedure. This test is the one with the classification of G.I, G.II or G.III and the lowest flow velocity.

The test data applied for the classification of either filter material or bed material are the underwater camera images and processed videos. In other words, the classification of filter and bed (in)stability is based on visual observation. Videos are applied for identification of the filter (in)stability. The first $t = 0$ min, intermediate $t \approx 45$ min and last camera images $t \approx 90$ min are investigated to identify bed (in)stability. Applying discrete time steps for comparison of the images makes bed instability identification easier compared to using videos.

Criteria for filter (in)stability

The classification and critical threshold phase as described by table 4-1 are applied within this thesis for the classification of filter (in)stability. The critical condition for filter instability is similar to the condition applied by Van Huijstee (i.e. F.III), which corresponds to phase 3 of the classification of phase of transport by Breusers (1977) (figure 4-2). Van Huijstee and Verheij (1991) defined phase 3 as $\Psi_c = 0.035$ [-] for grain size $d_{50} > 5$ mm and uniform flows. Also Van Huijstee & Verheij (1991) determined the filter (in)stability based on visual observation.

Table 4-1: Classification of filter stability according to Van Huijstee & Verheij (1991). This classification of filter stability is also applied in this thesis.

Class	Description	Stable/Instable	Remarks
F.I	No movement at all	[Stable]	
F.II	Shaking stones, a single stone rolls	[Stable]	
F.III	Some stones are rolling	[Instable]	Critical condition Breusers (1977) phase 3
F.IV	Movement at all locations	[Instable]	

Van de Sande (2012) determined the critical average flow u_{cr} based on relating the measured transport of filter material by counting the moved stones for subsequent tests and an incremental flow velocity. The phase of transport according to Breusers (1977) (figure 4-2) was taken as the boundary of phase 1 and the boundary of phase 6. However, the laboratory experiment test data of this thesis do not allow a similar method, because moved filter stones were not counted and the flow velocities consisted of two discrete sequential flow steps (0.5 m/s to 1.0 m/s). Therefore, the visual observation of the filter instability is applied.

Criteria for bed (in)stability

Visual observed filter settlement on camera images is chosen as the method for identification of bed material instability. Unfortunately, filter settlement cannot easily be related to the 7 phases of transport of Breusers (1977). Table 4-2 describes the classification that is applied to identify whether the bed material is (in)stable.

Table 4-2: Classification of bed stability.

Class	Description	Remarks Uniform and Sill	Remarks Cylindrical pier	Stable/Instable
B.I	No filter settlement	No filter settlement	No filter settlement	[Stable]
B.II	Minor or small degree of filter settlement.	Local filter settlement	Minor filter settlement	[Instable]
B.III	Major or large degree of settlement	Filter settlement at many locations	Major filter settlement	[Instable]

Three classes are distinguished in table 4-2. Class B.I is determined as stable bed material. Class B.II and Class B.III are both classified as instable. A distinction between class B.II and B.III is made to describe the ‘grey’ area between fully stable filter material and complete filter settlement, resulting from practical issues. For example, the layer thickness is not always exactly as described by the design specifications and spatial variation in layer thickness/grain size distribution/etc. can exist.

Note the difference in classification of the filter settlement between uniform/sill and cylindrical pier. The filter settlement starts (according to the camera images) in the front 180 degrees near the pier, which always results in classification of local filter settlement. Therefore, a distinction between minor and major filter settlement is made to determine the gray area between stable bed material and total bed material instability. The minor and major degree of filter settlement in the case of a cylindrical pier is respectively the maximum visually estimated settlement on $\Delta Z_f < (1/3 * d_{f50})$ and $\Delta Z_f > (1/3 * d_{f50})$. Here, ΔZ_f is the filter settlement at the end of the test. For the condition of sill-induced additional turbulence, a grid is plotted onto the camera images to systematically check each cell on settlement. The latter was necessary due to the high filter mobility during conditions of sill-induced additional turbulence.

Van de Sande (2012) determined the critical average flow u_{cr} based on relating the measured transport of bed material by weighting the transported sediment (winnowed) for subsequent tests and an incremental flow velocity. The laboratory experiments dataset (Joustra, 2012) did not contain any similar transport data related to flow velocity. In addition, the method of Van Huijstee & Verheij (1991) could not be used as camera images at the filter-bed interface are not available within the dataset. Classification for bed instability is different than the classification of bed instability applied by previous validations of the formula of Hoffmans (2012). However, the result of the distinction between stable/instable bed material in this thesis is expected to be similar to previous validation attempts.

4.3 Verification of bed instability

The filter surface level difference is defined as the height of the filter-outer flow interface before the coupled test minus the height of the filter-outer flow interface after the coupled test. The method of 3D stereo-photography (3DSP) is applied to calculate filter surface level. The statistics of the filter surface level differences (median, standard deviation) difference from within the rectangular area inside the test section (polygon) are compared with the visual observed classification of bed instability for the test conditions of uniform flow and flow with sill-induced additional turbulence. In addition, the spatial variation in filter settlement is analyzed to verify if the statistics are representative for the test section.

Section 4.2 described that a coupled test only 3DSP images are available before and after a coupled test. Therefore, no distinction can be made between the separate tests (U1, U2) and only the settlement during the coupled test (e.g. T06) can be verified. In addition, the visual observation could only be verified for the tests for which data of 3DSP is available.

4.4 Validation of design formulas

Design formula of Hoffmans (2012) for uniform flow, sill-induced additional turbulence and flows with a cylindrical pier [Research question 1, 2 and 3]

The full (equation 1.2) and simplified (equation 1.3) version of the design formula of Hoffmans (2012) with $\alpha_{d,Sande}$ are selected for validation. Adjustments proposed by Van de Sande (2012) (described in section 1.1) are included in the simplified and full version of the formula. The full version of the formula includes more information (e.g. relative degree of wide grading, relative density, etc.), but the information is not always known in practice. Therefore, Hoffmans (2012) proposed a simplified version of the formula which requires less information of filter and bed characteristics to calculate the minimum required relative layer thickness.

The method to answer research question 1, 2 and 3 consists of visual comparison between the general classification of the tests (position and colour of the marker) and the full and simplified version of the formula of Hoffmans (2012) with $\alpha_{d,Sande}$ (green curve). Both tests and formulas are visualized in graphs (figure 4-2). In addition, the general classifications are also compared with the design formula of Hoffmans (2012) with the alternative value α_d , i.e. $\alpha_{d,Hoffmans}$ (blue curve). Furthermore, the lower limit of the area of simultaneous erosion of the formula of Hoffmans (2012) with $\alpha_{d,Sande,lowerlimit}$ (red curve) is visualized in graphs as a reference.

Figure 4-2 shows the position of data of Joustra (2012) as markers and the general classification as a marker colour. Additional data with classifications as described by Van de Sande (2012) and adapted to the general classification of this thesis are compared with data of Joustra (2012). The additional data consists of data of Van Huijstee & Verheij (1991), Van de Sande (2012), Bakker (1960) and Van Velzen (2012). The location of the marker is independent of the flow velocity and depends only on the filter and grain characteristics (e.g. relative grain diameter d_{f50}/d_{b50} , the relative layer thickness D_f/d_{f50} , etc.). The colour of the markers visualizes the general classification and therefore is dependent on the flow velocity.

The (green) curve with $\alpha_{d,Sande}$ is the threshold for bed instability and valid for uniform flow. The markers of the class: G.I ‘Only filter is *instable*’ (blue markers) should be located above the green curve in area A. The markers of class: G.II ‘Both filter and bed are *instable*’ (yellow marker) should be located between the green and red curve in area C. The markers of G.III ‘Only bed is *instable*’ (red marker) should be located below the red curve in area D. Area B illustrates the area of ‘only filter is *instable*’ as proposed by Hoffmans (2012) with $\alpha_{d,Hoffmans} = 1.2$.

Chapter 5 describes the classification and comparison between the markers and the curves of both full and simplified version of the formula. Results are described for uniform flow (section 5.2), flows with sill-induced additional turbulence (section 5.3) and flows with a cylindrical pier (section 5.4).

Validation of the design formula of Wörman (1989) for flows with piers [Question 4]

The method of validation of the design formula of Wörman (1989) is similar to the method for validation of the formula of Hoffmans (2012). Data of depth average flow velocities of 0.5 m/s, 1.0 m/s and 1.5 m/s are both available and applied to answer question 4. Figure 4-3 visualizes an example of the formula of Wörman (1989), the unclassified data of Joustra (2012) and data of Van Velzen (2012). The formula of Wörman (1989) is also based on the philosophy of simultaneous erosion, therefore a marker near the curve of the formula should show G.II ‘Both filter and bed are *instable*’ (yellow). In addition, markers above the curve should show G.I ‘Only filter is *instable*’ (blue) and markers below the curve should mark ‘G.III Bed is *instable*’ (red). Section 5.5 describes the result of the validation of the design formula of Wörman (1989).

Data of Van Velzen (2012) [Question 5]

Figure 4-3 shows also the position and observation of data of Van Velzen (2012). Van de Sande (2012) applied the classification of ‘filter moves first’ (white, L01-L07) for the marker above both curves of Hoffmans (2012) and Wörman (1989) and applied the classification of ‘simultaneous erosion’ for the marker at the curve of the formula of Hoffmans (2012) with $\alpha_{d,Sande}$ (green, L08). To answer question 5 the classification of Van de Sande (2012) these markers is compared with the general classification made in this thesis and the original classification of Van Velzen (2012). In addition, the results of the validation by Van de Sande (2012) and Van Velzen (2012) is an agreement between the data of Van Velzen (2012) and the formula of Hoffmans (2012) and the formula of Wörman (1989) for flows with cylindrical piers. This conclusions is compared with the answer to research question 3 and 4.

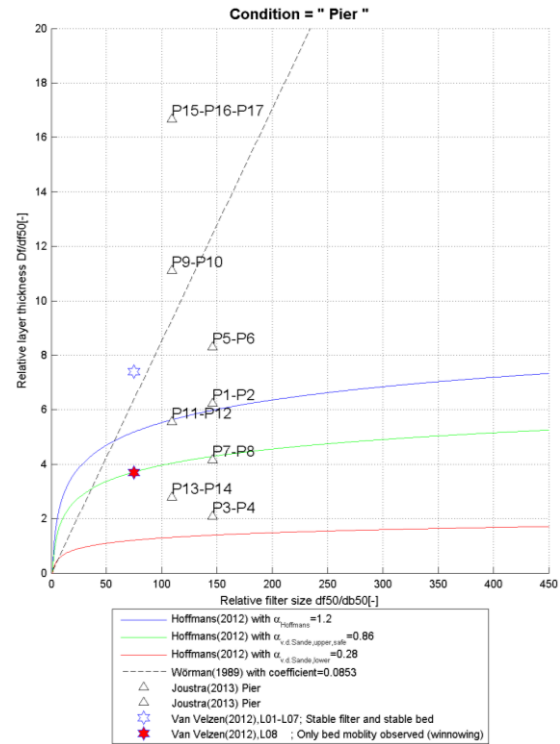
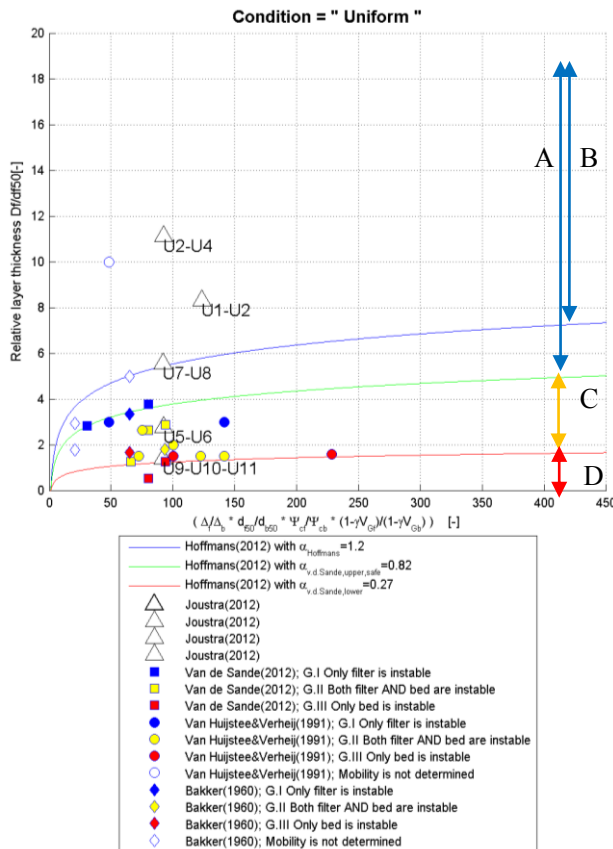


Figure 4-2: Example of graph visualizing data of Joustra (triangular markers) and others. Similar graph is applied in comparison between data and full version of the formula of Hoffmans (2012).

Figure 4-3: Example of graph visualizing data of Joustra (2012), Van Velzen (2012) and the formula of Hoffmans (2012) and the formula of Wörman (1989).

5 Results

5.1 Classification of instability

5.1.1 Visual observation of filter stability and bed stability

In summary, the general classification of combined filter and bed material is based on the separate bed instability and filter instability classifications. As described in section 4.2, the first test (e.g. P2, P3, P6) from a coupled test (e.g. T01, T02, T03, etc.) where either filter or bed instability, or both occurs is selected for validation. For example during flow velocities of $\bar{u} = 0.5$ m/s in test P1 (T01) the general classification is 'G.IV: Both filter and bed are stable'. During flow velocities of $\bar{u} = 1.0$ m/s in test P2 (T01) the general classification is 'G.III: Only bed is unstable'. As both have equal bed and filter characteristics (i.e. coupled test), test P1 is selected for validation. In addition, if during a test with $\bar{u} = 0.5$ m/s already a general classification G.I, G.II, or G.III is determined, than that test is selected for validation.

Results of classifications are described in table 5-1, table 5-2 and table 5-3. These tables describe respectively (1) uniform flow, (2) sill-induced additional turbulence and (3) flows with cylindrical pier. The first column describes the individual test number. The second column describes the coupled test number combined with character 'a', 'b' or 'c' which corresponds to respectively depth average flow velocity $\bar{u} = 0.5$ m/s, $\bar{u} = 1.0$ m/s and $\bar{u} = 1.5$ m/s. The third, fourth and fifth column describe respectively the depth average flow velocity, relative layer thickness and relative grain size. Column six, seven and eight describe filter, bed and general classifications. Column nine shows which tests are selected for the validation. Results of classification of bed instability are visualized in figure 5-1 (uniform flow), figure 5-2 (flow with sill-induced additional turbulence) and in figure 5-3 (flow with cylindrical pier).

1) Uniform flow

Result of classification shows that the critical conditions for filter material (phase 3; $\Psi_c = 0.035[-]$; Van Huijstee & Verheij (1991)) is quite strict. Both filter grain sizes ($d_{f50} = 24.1$ mm & $d_{f50} = 18.0$ mm) were classified stable (i.e. $\Psi < \Psi_{cf}$) for all tests, except test U11 ($\bar{u} = 1.5$ m/s; $d_{f50} = 18.0$ mm).

In addition, only test U9 ($\bar{u} = 0.5$ m/s), U10 ($\bar{u} = 1.0$ m/s) and U11 ($\bar{u} = 1.5$ m/s) with a relative layer thickness D_f/d_{f50} of 1.4 [-] experienced bed instability (i.e. filter settlement). Test U1 to U8 have a relative layer thickness D_f/d_{f50} of 2.8 [-] or higher. In general, a relative layer thickness of at least 2 is applied for filters (Verheij et al, 2010). Coupled test T08 consists of individual tests U9, U10 and U11. U9 or U10 could be selected for validation. The general classification of U9 and U10 are both 'G.III Only bed material is *instable*', therefore selection of either U9 or U10 would not make a difference in the validation. However, the bed (in)stability classification of U9 is B.II: 'Local filter settlement', while the bed (in)stability classification of U10 is B.III: 'Filter settlement at many locations'. Section 5.1.2 will show that the filter surface level difference calculation between before test U9 and after test U10 suggests filter settlement (i.e. bed instability). A higher flow velocity induces more loads on the bed, therefore the highest confidence is in the visual observed bed instability of U10 and U10 is selected for validation.

Finally, there is one additional remark about the filter instability criteria. Tests U1 to U8 are classified as G.II 'Both filter and bed are *stable*'. Table 5-1 describes that the filter stability classification is class F.II for U8, U2 and U4, while class F.III is defined as critical. Figure 5-1 visualizes the degree of bed instability related to flow velocity \bar{u} and relative layer thickness D_f/d_{f50} for conditions of uniform flow. For $\bar{u} = 0.5$ m/s and $\bar{u} = 1.0$ m/s the minimum required relative layer thickness for a stable geometrical open filter is at least 2.8 [-] (table 5-1). The relative layer thickness of tests U2, U8, U4 is at least twice this minimum required layer thickness (i.e. 8.3 [-], 5.6 [-] and 11.1 [-] respectively). It is therefore expected, that at least U2, U8, U4 would be classified as 'Only filter is *instable*' when the flow velocity is increased beyond $\bar{u} = 1.0$ m/s. This expected classification for tests U2, U8 and U4 could therefore also be compared with the formula of Hoffmans (2012).

2) Sill-induced additional turbulence

Results of the classification for sill-induced additional turbulence are described in table 5-2. Results show that filter mobility exceeded the threshold for filter instability during test S2 ($d_{f50} = 24.1$ mm; $\bar{u} = 1.0$ m/s), S4 ($d_{f50} = 24.1$ mm; $\bar{u} = 1.0$ m/s) and S6 ($d_{f50} = 18$ mm; $\bar{u} = 1.0$ m/s). The filter grain sizes and depth average flow velocity are similar to uniform flow tests; therefore additional turbulence did increase the loads on the filter grains. This is expected (e.g. Schiereck, 1995, Hoffmans, 2012, Hofland, 2005).

Classification of bed instability is only possible for test S6. Determination of bed instability is impossible to observe on the photos and videos of test S2 and S4, because of the high filter grain mobility and the high turbidity of the flow. Tests S1 and S3 cannot be used for validation because the bed and filter material were still stable under these test conditions. The problem causing the high turbidity was fixed in test S6. Results of classification of test S6 ($\bar{u} = 1.0$ m/s) is G.II 'Both filter and bed are *instable*'. Only test S6 is therefore selected for validation. Figure 5-2 visualizes degree of bed instability related to flow velocity \bar{u} and relative layer thickness D_f/d_{f50} for flows of sill-induced additional turbulence. The relative layer thickness of test S6 is 5.6 [-]. Comparison between uniform flow (U8) and sill-induced additional turbulence (S6), similar relative grain size and flow velocity shows that bed instability increases for flows with sill-induced additional turbulence (i.e. increase of minimum required layer thickness). This conclusion is in line with the observations of Van de Sande (2012) of increased bed instability in sill-induced additional turbulent conditions. The visual observation of bed instability in filter instability class F.IV is still difficult and uncertain. Although this uncertainty, S6 is the only test with a sill for which bed instability could be classified. Nonetheless, the bed instability classification and thus general classification of S6 handled with care.

Finally, tests S2 & S4 do not have a general classification (due to the combination of high turbidity and high filter mobility). The filter and bed instability of S2 is not determined. However, it is expected that general classification of at least S4 is 'Only filter is *instable*'. Filter classification is F.II (stable) at test S3 ($\bar{u} = 0.5$ m/s) and F.IV (instable) at S4 ($\bar{u} = 1.0$ m/s), and a relative layer thickness of 11.1 [-] in both tests. Bed classification at test S5 ($\bar{u} = 0.5$ m/s) shows B.I (stable) and at test S6 ($\bar{u} = 1.0$ m/s) shows B.II (instable), and a relative layer thickness of 5.6 [-]. The relative layer thickness of S6 is approximately twice the relative layer thickness of S3, with similar depth average flow velocity ($\bar{u} = 1.0$ m/s) and relative grain size ($d_{f50}/d_{b50} = 109.1$ [-]). It is therefore expected, that the classification of S4 is 'Only filter is *instable*'. This expected classification for test S4 could therefore also be compared with the formula of Hoffmans (2012).

3) Flows with cylindrical pier

Results of classification of flows with a cylindrical pier are described in table 5-3. Results show that threshold condition for filter instability is exceeded for most tests with filter grain sizes of $d_{f50} = 18$ mm (except for test P10) and depth average flow velocity $\bar{u} = 1.0$ m/s. In addition, no tests with filter grain size $d_{f50} = 24.1$ mm exceeded the threshold condition. Comparison between tests with a cylindrical pier (P12, P14, P16) and tests under uniform flow conditions (U6, U8, U10) with similar filter grain sizes ($d_{f50} = 18$ mm) and flow velocities ($\bar{u} = 1.0$ m/s) shows that piers increase the filter mobility, which is expected (Shiereck, 1995). Comparison between tests with a cylindrical pier (P12, P14, P16) and flows with sill-induced turbulence (S4, S6) with similar filter grain sizes ($d_{f50} = 18$ mm) and flow velocities ($\bar{u} = 1.0$ m/s) shows less increase in filter mobility than flows with sill-induced additional turbulence compared to uniform flows.

Tests P2, P3, P6, P7, P10, P11, P13 and P17 are selected from their coupled tests for validation of the design formula of Hoffmans (2012) and the design formula of Wörman (1989). Test P17 is classified as G.I 'Only filter is *instable*'. Tests P2, P3, P6, P7, P10, P11 and P13 are classified as 'G.III Only bed is *instable*'. None of the selected tests are classified as 'Both filter and bed are *instable*'. There is one remark on the selection of P17 from the coupled tests T08 (P15-P16-P17). Visual observation of test P16 shows

minor filter settlement (i.e. bed is instable). This observation should result in selection for validation with general classification G.II: ‘Both filter and bed are *instable*’. However, bed instability classification of test P17 shows B.I: ‘No filter settlement’ (bed is stable). A rearrangement of filter stones (layer thickness of $D_f = 300$ mm) might have caused filter settlement during test P16. While the occurrence of bed instability during test P16 is not quite understood, the fact that no filter settlement occurs during P17 gives reason to assume that the filter settlement might be caused by a rearrangement of filter stones. Therefore, P17 is selected for validation instead of P16.

Figure 5-3 visualizes the degree of bed instability related to flow velocity \bar{u} and relative layer thickness D_f/d_{f50} for flows with a cylindrical pier. Results of bed instability classification for flows with pier (P11) compared with flows with sill-induced turbulence (S5) and uniform flow (U7) with similar relative layer thickness ($D_f/d_{f50} = 5.6$ [-]), relative grain size ($d_{f50}/d_{b50} = 109.1$ [-]) and undisturbed depth average flow velocity $\bar{u} = 0.5$ m/s, show that bed mobility increase also increases the bed instability. This observation is in agreement with observations of Van de Sande (2012). In addition, the increase in bed instability for cylindrical piers is likely higher than for sill-induced additional turbulence. In other words, the minimum required relative layer thickness D_f/d_{f50} for flows with piers is thicker than the minimum D_f/d_{f50} for flows with sill-induced additional turbulence, which also exceeds the minimum D_f/d_{f50} for uniform flows.

Table 5-1: Result of observed filter and bed (in)stability for uniform flow.

ReportID	TestID	\bar{u} [m/s]	Df/df50 [-]	df50/db50 [-]	Filter stability classification	Bed stability classification	General classification	Selected for validation [yes/-]
U1	T01a	0.5	8.3	146.1	F.II) Shaking stones	B.I) No filter settlement.	G.IV) Both filter and bed are <i>stable</i> .	-
U2	T01b	1.0	8.3	146.1	F.II) Shaking stones, a single stone rolls	B.I) No filter settlement.	G.IV) Both filter and bed are <i>stable</i> .	-
U3	T04a	0.5	11.1	109.1	F.II) Shaking stones	B.I) No filter settlement.	G.IV) Both filter and bed are <i>stable</i> .	-
U4	T04b	1.0	11.1	109.1	F.II) Shaking stones, a single stone rolls	B.I) No filter settlement.	G.IV) Both filter and bed are <i>stable</i> .	-
U5	T05a	0.5	2.8	109.1	F.II) Shaking stones, a single stone rolls	B.I) No filter settlement.	G.IV) Both filter and bed are <i>stable</i> .	-
U6	T05b	1.0	2.8	109.1	F.II) Shaking stones, a single stone rolls	B.I) No filter settlement.	G.IV) Both filter and bed are <i>stable</i> .	-
U7	T06a	0.5	5.6	109.1	F.I) No movement at all.	B.I) No filter settlement.	G.IV) Both filter and bed are <i>stable</i> .	-
U8	T06b	1.0	5.6	109.1	F.II) Shaking stones, a single stone rolls	B.I) No filter settlement.	G.IV) Both filter and bed are <i>stable</i> .	-
U9	T08a	0.5	1.4	109.1	F.I) No movement at all.	B.II) Local filter settlement.	G.III) Only bed material is <i>instable</i> .	Yes
U10	T08b	1.0	1.4	109.1	F.II) Shaking stones, a single stone rolls	B.III) Filter settlement at many locations.	G.III) Only bed material is <i>instable</i> .	-
U11	T08c	1.5	1.4	109.1	F.IV) Movement at all locations	B.III) Filter settlement at many locations.	G.II) Both filter and bed are <i>instable</i> .	-

Table 5-2: Result of observed filter and bed (in)stability for sill-induced additional turbulence condition.

ReportID	TestID	\bar{u} [m/s]	Df/df50 [-]	df50/db50 [-]	Filter stability classification	Bed stability classification	General classification	Selected for validation [yes/-]
S1	T02a	0.5	8.3	146.1	F.II) Shaking stones, a single stone rolls.	B.I) No filter settlement.	G.IV) Both filter and bed are <i>stable</i> .	-
S2	T02b	1.0	8.3	146.1	F.III) Some stones are rolling.	Unknown.	Unknown. No filter settlement could be observed, due high turbidity and high filter mobility.	-
S3	T03a	0.5	11.1	109.1	F.II) Shaking stones, a single stone rolls.	B.I) No filter settlement.	G.IV) Both filter and bed are <i>stable</i> .	-
S4	T03b	1.0	11.1	109.1	F.IV) Movement at all locations.	Unknown.	Unknown. No filter settlement could be observed, due high turbidity and high filter mobility.	-
S5	T07a	0.5	5.6	109.1	F.II) Shaking stones, a single stone rolls.	B.I) No filter settlement.	G.IV) Both filter and bed are <i>stable</i> .	-
S6	T07b	1.0	5.6	109.1	F.IV) Movement at all locations.	B.II) Local filter settlement.	G.II) Both filter and bed are <i>instable</i> .	Yes



Table 5-3: Result of observed filter and bed (in)stability for flows with a cylindrical pier.

ReportID	TestID	\bar{u} [m/s]	$D_f/df50$ [-]	$df50/db50$ [-]	Filter stability classification	Bed stability classification	General classification	Selected for validation [yes/-]
P1	T01a	0.5	6.2	146.1	F.II) Shaking stones	B.I) No filter settlement.	G.IV) Both filter and bed are <i>stable</i> .	-
P2	T01b	1.0	6.2	146.1	F.II) Shaking stones, a single stone rolls	B.III) Major filter settlement.	G.III) Only bed material is <i>instable</i> .	Yes
P3	T02a	0.5	2.1	146.1	F.I) No movement at all.	B.III) Major filter settlement.	G.III) Only bed material is <i>instable</i> .	Yes
P4	T02b	1.0	2.1	146.1	F.II) Shaking stones, a single stone rolls	B.III) Major filter settlement.	G.III) Only bed material is <i>instable</i> .	-
P5	T03a	0.5	8.3	146.1	F.II) Shaking stones	B.I) No filter settlement.	G.IV) Both filter and bed are <i>stable</i> .	-
P6	T03b	1.0	8.3	146.1	F.II) Shaking stones, a single stone rolls	B.II) Minor filter settlement.	G.III) Only bed material is <i>instable</i> .	Yes
P7	T04a	0.5	4.1	146.1	F.I) No movement at all.	B.II) Minor filter settlement.	G.III) Only bed material is <i>instable</i> .	Yes
P8	T04b	1.0	4.1	146.1	F.II) Shaking stones, a single stone rolls	B.III) Major filter settlement.	G.III) Only bed material is <i>instable</i> .	-
P9	T05a	0.5	11.1	109.1	F.II) Shaking stones	B.I) No filter settlement.	G.IV) Both filter and bed are <i>stable</i> .	-
P10	T05b	1.0	11.1	109.1	F.II) Shaking stones, a single stone rolls	B.II) Minor filter settlement.	G.III) Only bed material is <i>instable</i> .	Yes
P11	T06a	0.5	5.6	109.1	F.I) No movement at all.	B.II) Minor filter settlement.	G.III) Only bed material is <i>instable</i> .	Yes
P12	T06b	1.0	5.6	109.1	F.III) Some stones are rolling.	B.III) Major filter settlement.	G.II) Both filter and bed are <i>instable</i> .	-
P13	T07a	0.5	2.8	109.1	F.II) Shaking stones, a single stone rolls	B.III) Major filter settlement.	G.III) Only bed material is <i>instable</i> .	Yes
P14	T07b	1.0	2.8	109.1	F.III) Some stones are rolling.	B.III) Major filter settlement.	G.II) Both filter and bed are <i>instable</i> .	-
P15	T08a	0.5	16.7	109.1	F.I) No movement at all.	B.I) No filter settlement.	G.IV) Both filter and bed are <i>stable</i> .	-
P16	T08b	1.0	16.7	109.1	F.III) Some stones are rolling.	B.II) Minor filter settlement.	G.II) Both filter and bed are <i>instable</i> .	-
P17	T08c	1.5	16.7	109.1	F.IV) Movement at all locations.	B.I) No filter settlement.	G.I) Only filter is <i>instable</i> .	Yes

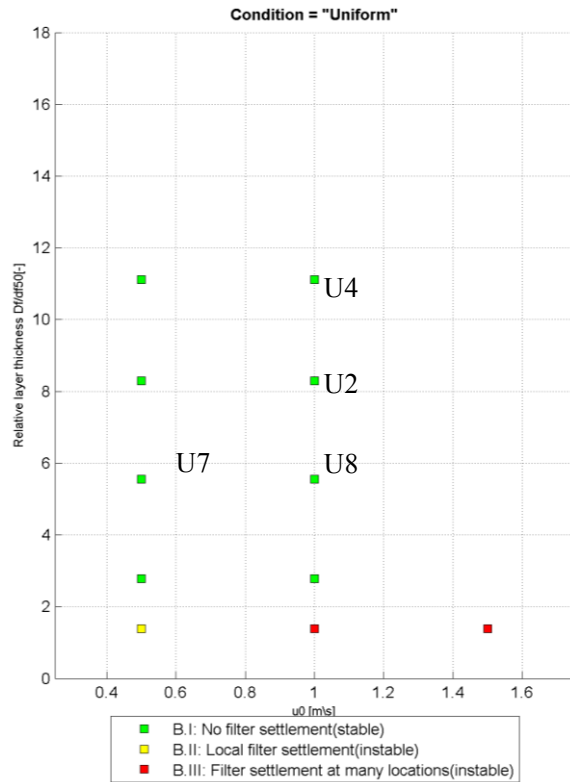


Figure 5-1: Visual observation of bed (in) stability for condition (1) uniform flow.

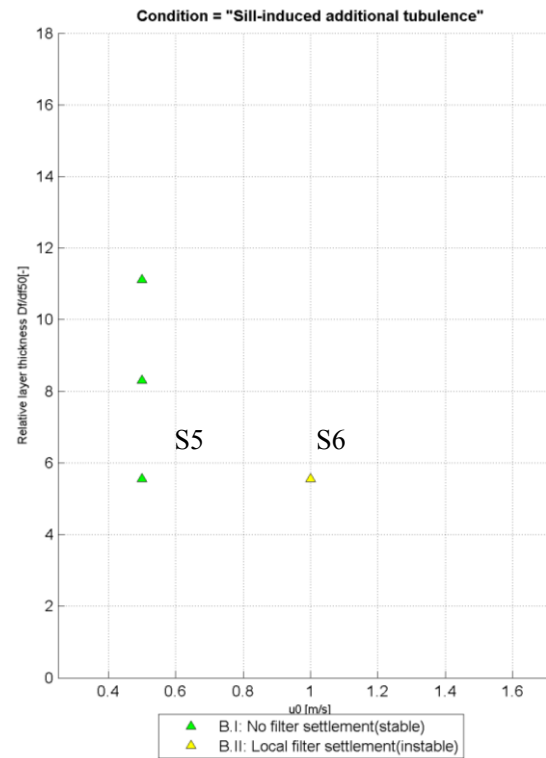


Figure 5-2: Visual observation of bed (in) stability for condition (2) sill-induced additional turbulence.

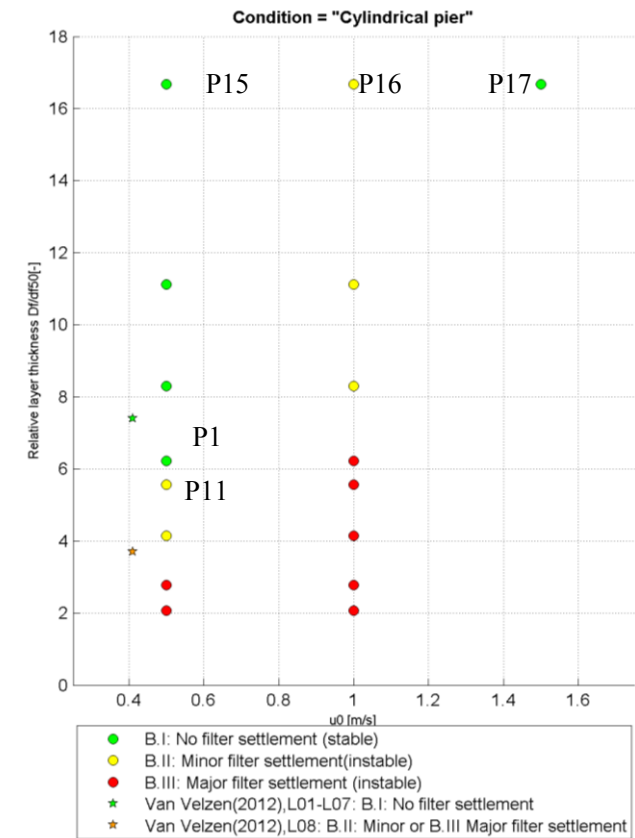


Figure 5-3: Visual observation for condition (3) with a cylindrical pier. Test P16 shows visual observed minor settlement where the subsequent test P17 shows 'No filter settlement'.

5.1.2 Verification of visual observed bed instability

This section describes the comparison between visual observed bed stability and measured bed stability for conditions of uniform flow and flows with sill-induced additional turbulence. The method of 3D Stereophotography (3DSP) for data processing is applied to convert raw-3DSP data to high resolution images of bathymetry (resolution 1 mm) and filter surface level difference Δz_f images. The filter surface level difference is defined as the height of the filter-outer flow interface before the test minus the height of the filter-outer flow interface after the test.

Raw 3DSP data are available for uniform flow coupled tests: T05 (U5-U6), T06 (U7-U8), and T08 (U9-U10). 3DSP data are also available for flows with sill-induced turbulence for coupled tests T08 (S5-S6). The raw 3DSP data are processed to filter-outer flow interface (bathymetry) before test U5, U7, U9, S5, processed to a filter-outer flow interface after test U6, U8, U10, and S6. Figure 5-4, 5-5 and 5-6 show respectively the filter-outer flow interface z before test U9, the filter-outer flow interface z after test U10 and filter surface level difference Δz_f . In addition, a cumulative distribution curve (figure 5-7) and the statistical parameters (table 5-4): median and standard deviation of filter surface difference Δz_f are determined and applied in the comparison with results of 5.1.1.

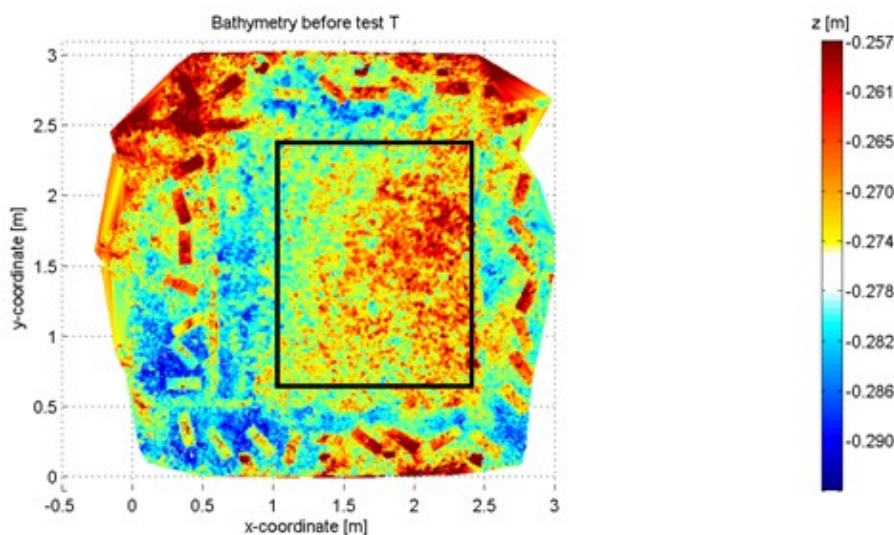


Figure 5-4: Example of filter-outer flow interface z [m] (before T08 (U9)). Red indicates higher regions relative to a reference level. Blue indicates lower regions relative to a reference level. The black outline is the polygon for which data is extracted for calculation of statistics. The reference level is fixed and constant for all tests.

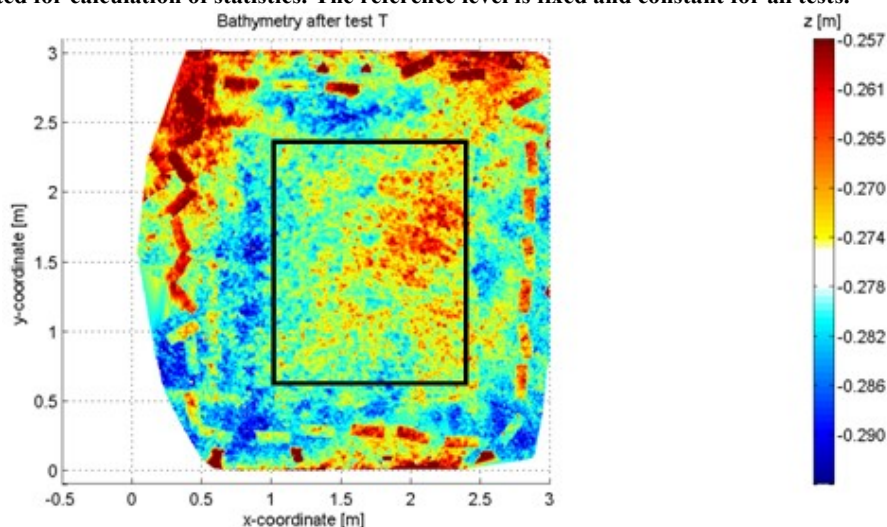


Figure 5-5: Example of filter-outer flow interface z [m] (after T08 (U10)). Red indicates higher regions relative to a reference level. Blue indicates lower regions relative to a reference level. The black outline is the polygon for which data is extracted for calculation of statistics.

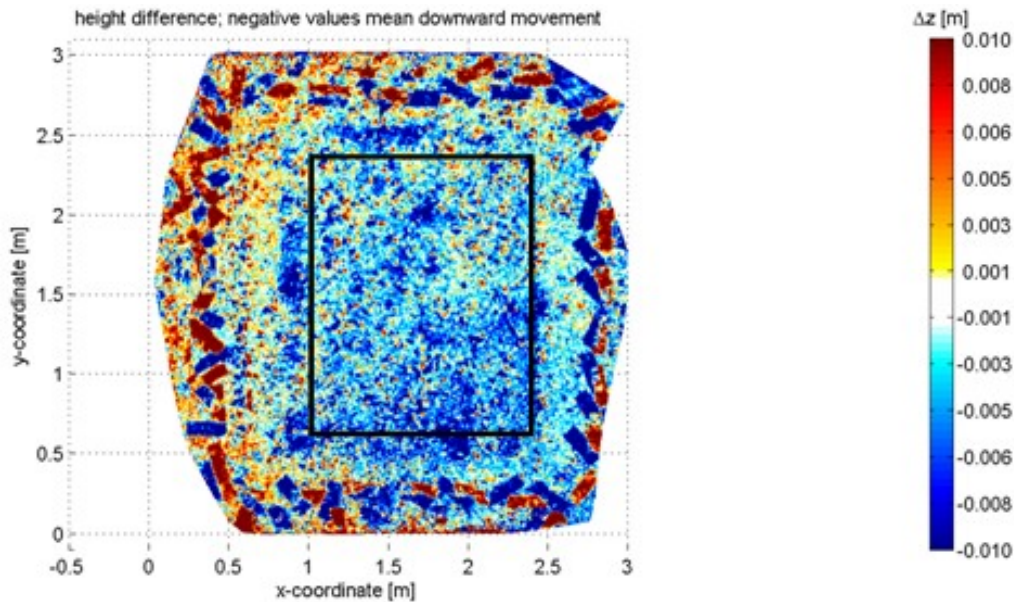


Figure 5-6: Example of filter surface level difference Δz_f [m] (between T08 (U9-U10)). Red indicates an increase in level (e.g. by filter grain displacement). Blue indicates a decrease in level. The black outline is the polygon for which data is extracted for calculation of statistics.

Appendix 6 describes the spatial variation of the filter surface level differences. The spatial variation filter surface level difference is quite uniform within the polygon for all uniform flow tests and tests of flow with sill-induced additional turbulence.

Results from section 5.1.1 show that for uniform flow and flows with sill-induced additional turbulence, the bed material is *unstable* during test U9 ($\bar{u} = 0.5$ m/s), U10 ($\bar{u} = 1.0$ m/s), U11 ($\bar{u} = 1.5$ m/s) and S6 ($\bar{u} = 1.0$ m/s). The bed material is *stable* during test U5 ($\bar{u} = 0.5$ m/s), U6 ($\bar{u} = 1.0$ m/s), U7 ($\bar{u} = 0.5$ m/s), U8 and S5 ($\bar{u} = 0.5$ m/s).

Median filter surface level difference is 0.28 mm and -0.25 mm for respectively tests T05 (U5-U6) and T06 (U7-U8). 50% of the area shows a decrease and 50% shows an increase in filter surface level. Local filter stone displacement could be a cause of increase or decrease of filter surface level. The median filter surface level difference is approximately zero, which confirms the visual observation of the bed stability for test U5-U6 and U7-U8 ('B.I No filter settlement').

Median filter surface difference is -3.44 mm for test T08 (U9-U10). The negative difference (median $\Delta z_f = -3.44$ mm) represents bed instability (filter settlement). The median value for filter surface level difference means that 50% of all calculated filter difference values are smaller than -3.44 mm. In addition, figure 5-7 shows that for approximately 80% of the filter surface area for test U9-U10, filter difference values smaller than zero (i.e. filter settlement) is measured. Therefore, bed instability can be classified as 'B.III Filter settlement at many locations'. Comparison of classification based on 3DSP with classification from section 5.1.1 confirms the visual observation of U10 (highest load condition). U10 is therefore the correct choice for validation.

The method of stereo-photography cannot distinguish filter settlement from filter stone erosion or deposition. Therefore, the visual observed filter settlement during test S6 could not be confirmed. The higher standard deviation for test with sill-induced additional turbulence S5-S6 compared with the standard deviation for uniform flow tests with stable filter stones (U5-U6, U7-U8, U9-U10), might represent the filter stone instability.

Table 5-4 shows that a uniform flow test with a relative layer thickness $D_f/d_{f50} = 2.8$ [-] results in a stable geometrical open filter, while a uniform flow test with a relative layer thickness of $D_f/d_{f50} = 1.4$ [-] results in instable geometrical open filter.

Table 5-4: The relative layer thickness, median filter settlement and variation in filter settlement in the polygon area for uniform flow conditions and flows with a sill. All tests have the same $d_{f50} = 18\text{mm}$. The general classification of combined filter and bed instability based on visual observation is also described. There is no stereo-photography data available for test U1-U4 and S1-S4).

Parameter	Description	Unit	Test U5-U6 (T05)	Test U7-U8 (T06)	Test U9-U10 (T08)	Test S5-S6 (T07)
-	Visual observation at $\bar{u} = 0.5$ m/s.	-	'Both filter and bed are stable'	'Both filter and bed are stable'	'Only bed instable'	'Both filter and bed are stable'
-	Visual observation at $\bar{u} = 1.0$ m/s.	-	'Both filter and bed are stable'	'Both filter and bed are stable'	'Only bed instable'	'Both filter and bed are instable'
D_f/d_{f50}	Relative layer thickness	[-]	2.8	5.6	1.4	5.6
μ	Median filter difference	[mm]	0.28	-0.25	-3.44	-3.57
σ	Standard deviation	[mm]	3.7	3.4	4.3	6.5

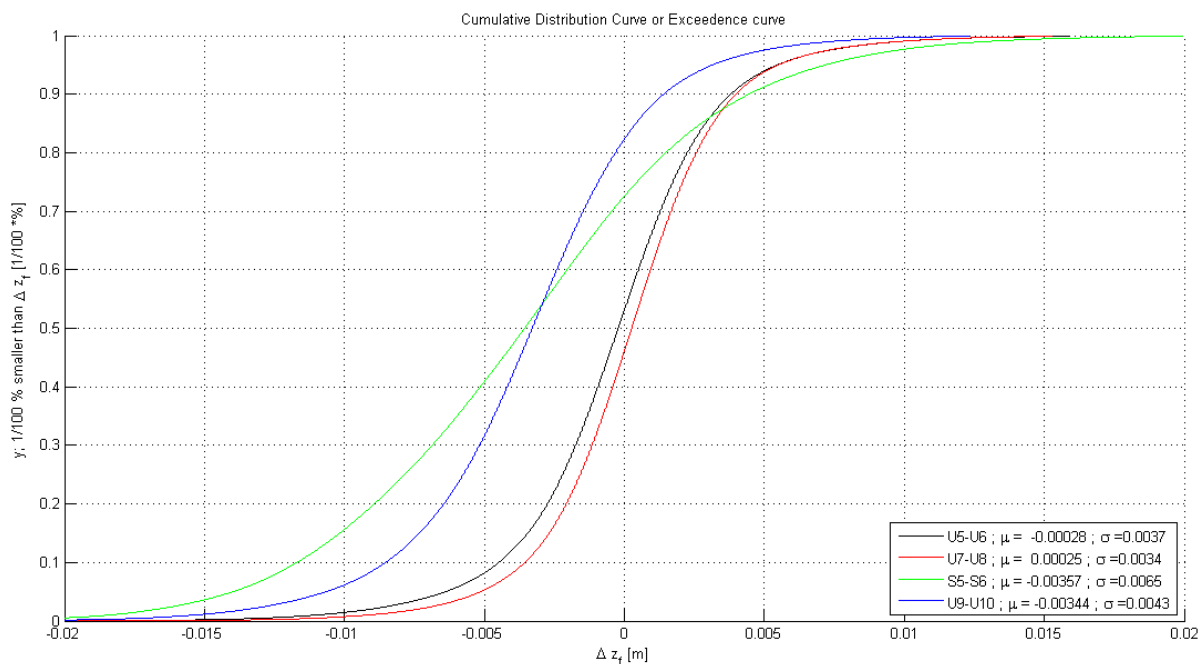


Figure 5-7: Exceedence curve or cumulative distribution curve of filter surface level difference (Δz_f). Negative surface level difference equals lowering of the filter surface level, where a positive value means an increase in filter surface level.

5.2 Hoffmans (2012) for uniform flows

This section describes the validation of the design formulas for the condition of uniform flow. Two figures are presented, i.e. the simplified version of the formula of Hoffmans (2012) (figure 5-8; equation 1.2) and the full version of Hoffmans (2012) (figure 5-9; equation 1.3). The logarithmic curves describe the design formula of Hoffmans (2012) with different values of α , i.e. $\alpha_{d,Hoffmans}$ (blue curve), $\alpha_{d,Sande}$ (green curve) and $\alpha_{d,Sande,lowerlimit}$ (red curve). The visually observed general classification (e.g. ‘Only bed is *instable*’) from section 5.1 is plotted as a markers in figures 5-8 and 5-9. In addition, experimental data of Van de Sande (2012), Van Huijstee and Verheij (1991) and Bakker (1960) are visualized in figure 5-8 and figure 5-9.

A, B, C, and D positioned next to the validation figures (e.g. figure 5.9). These letters describe regions relative the curves of the formula of Hoffmans (2012). The markers of the class: ‘G.I Only filter is *instable*’ (blue) should be located above the green curve in area A. The markers of class: G.II ‘Both filter and bed are *instable*’ (yellow) should be located between the green and red curve in area C. The markers of G.II ‘Only bed is *instable*’ (red) should be located below the red curve in area D. Area B illustrates the area of ‘G.I Only filter is *instable*’ above the curve as proposed by Hoffmans (2012).

Section 5.1 described that for tests U1-U8 both filter and bed material were *stable*. In order to test the formula of Hoffmans (2012), either filter material, bed material or both must be *instable*. This means that for 4 out of 5 markers (figure 5.8 and figure 5.9) the threshold condition was not exceeded and therefore could not be applied in the validation of the formula.

The fifth marker represents test U10 with general classification ‘G.III: Only bed material is *instable*’, so should be in area D. This classification is confirmed with measurements with 3DSP (section 5.1.2). Marker U10 is located below the curve with $\alpha_{d,Sande}$ in both the full and simplified versions of the formula. Hence, the marker is also located below the curve $\alpha_{d,Hoffmans}$ for both versions.

Moreover, the location of marker U10 in figures 5-8 and 5-9 is at the lower limit of the area of simultaneous instability ($\alpha_{d,Sande,lowerlimit}$ the red curve) for the simplified formula of Hoffmans (2012). The location of marker U9 for the full version of the formula is slightly above the lower limit the area of simultaneous mobility ($\alpha_{d,Sande,lowerlimit}$, the red curve). Classification of marker U10 is in agreement with nearby classification of the markers of Van Huijstee and Verheij (1991) and Van de Sande (2012).

In addition, the dataset does not include a test above the design curves with $\alpha_{d,Sande}$ or $\alpha_{d,Hoffmans}$; therefore it could strictly not be concluded that $\alpha_{d,Sande}$ or $\alpha_{d,Hoffmans}$ are incorrect for uniform flow conditions at the moment. However, although the tests U1-U8 are classified as ‘Both filter and bed *stable*’, it is expected that at least U8, U2 and U4 would be classified as ‘Only filter is *Instable*’ when the flow velocity is increased beyond $\bar{u} = 1.0$ m/s (section 5.1.1). Test U2, U8 and U4 are visualized in figure 5-10 and 5-11 and both confirm the $\alpha_{d,Sande}$ or $\alpha_{d,Hoffmans}$. $\alpha_{d,Sande}$ is therefore in agreement with the data of Joustra (2012), thus for uniform flows. The test data of Joustra (2012) did not prove otherwise.

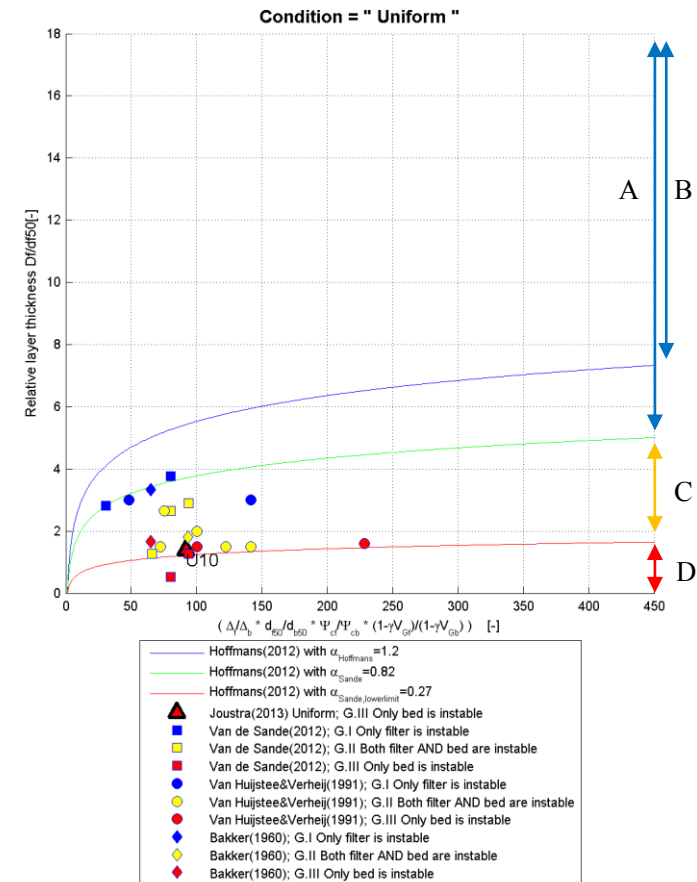
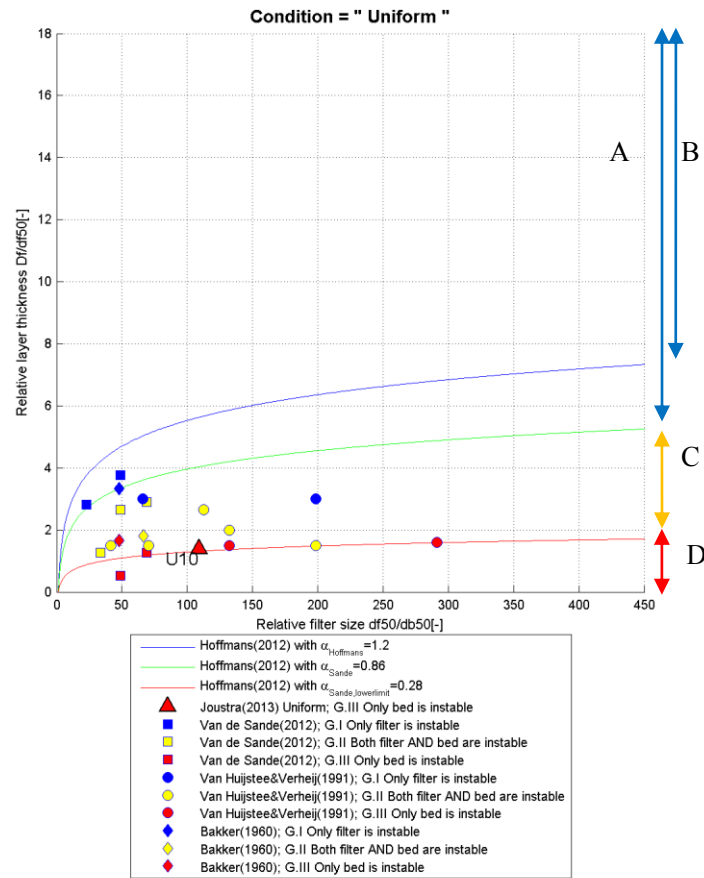


Figure 5-8: The marker U10 and general classification compared with the simplified formula. The green curve shows the $\alpha_{d,Sande}$ for the formula as proposed by Van de Sande (2012).

Figure 5-9: The markers and general classification compared with the full formula. The green curve shows the formula with the $\alpha_{d,Sande}$ as proposed by Van de Sande (2012).

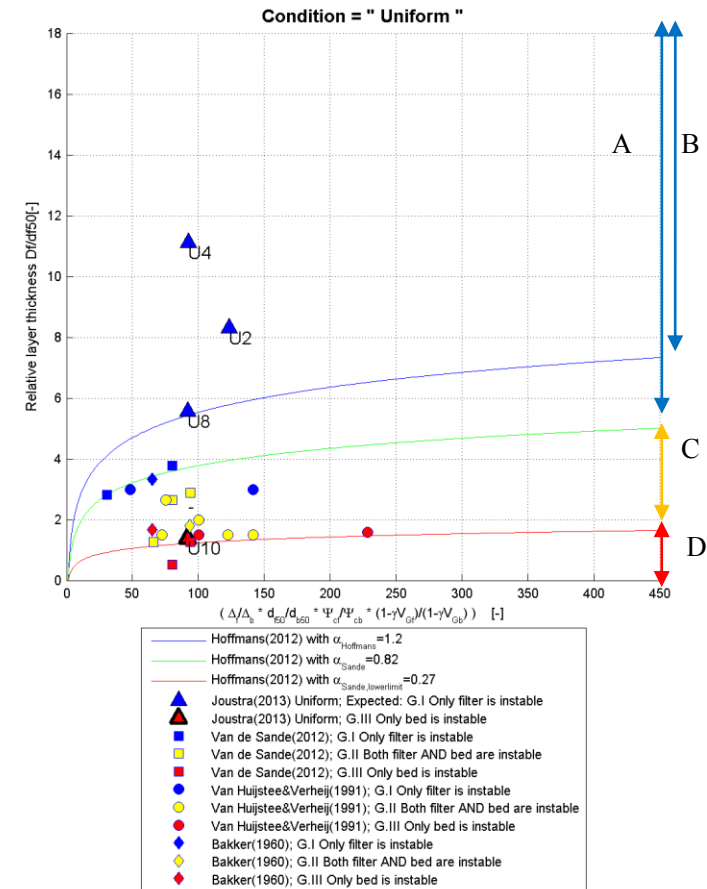
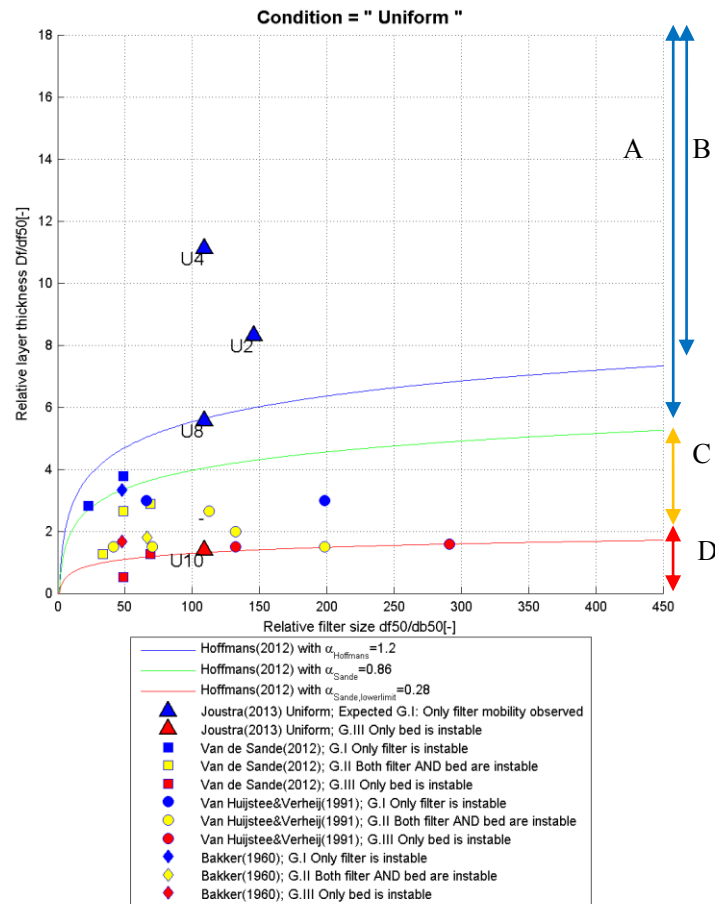


Figure 5-10: The markers and general classification compared with the simplified formula. Includes also ‘expected’ classification of U4, U2, and U8. The green curve shows the $\alpha_{d,Sande}$ for the formula as proposed by Van de Sande (2012).

Figure 5-11: The markers and general classification compared with the full formula. Includes also ‘expected’ classification of U4, U2, and U8. The green curve shows the $\alpha_{d,Sande}$ as proposed by Van de Sande (2012).

5.3 Hoffmans (2012) for flows with sill-induced additional turbulence

This section describes the validation for flows with sill-induced additional turbulence. Again, two figures are presented, i.e. the simplified version of the formula of Hoffmans (2012) (figure 5-12; equation 1.2) and the full version of Hoffmans (2012) (figure 5-13; equation 1.3). The logarithmic curves describe the design formula of Hoffmans (2012) with different values of α_d : $\alpha_{d,Hoffmans}$ (blue curve), $\alpha_{d,Sande}$ (green curve) and $\alpha_{d,Sande,lowerlimit}$ (red curve). For uniform flow, the (green) curve with the $\alpha_{d,Sande}$ is the threshold for bed instability. The visual observed general classifications from section 5.1.1 and data of Bakker (1960) are visualized as markers in figures 5-12 and 5-13. Results from section 5.1.1 shows that from the dataset of Joustra (2012) only test S6 is suitable for validation.

First, the general classification of marker S6 is ‘G.II Both filter and bed are *instable*’. Marker S6 is located above the formula of Hoffmans (2012) with $\alpha_{d,Sande,s.v.} = 0.86$ and $\alpha_{d,Sande, f.v.} = 0.82$ for respectively simplified version and full version of the formula with $\alpha_{d,Sande}$. In addition, marker S6 is also above and near the curve of the full version of the formula with $\alpha_{d,Hoffmans}$ and near and below the curve of the simplified version of the formula with $\alpha_{d,Hoffmans} = 1.2$. However, uncertainties in the filter or bed characteristics could shift the position of the marker S6 to below the full formula with $\alpha_{d,Hoffmans} = 1.2$ or to above the simplified version of the formula with $\alpha_{d,Hoffmans} = 1.2$. Conclusions should therefore be drawn with uncertainties in mind.

Second, although markers S1-S2 and S3-S4 could not be classified (high degree of filter mobility and turbidity), it is expected (but not proven) that the classification of at least S4 would be ‘B.I Only filter is *instable*’ if the degree of water turbidity decreased (section 5.1.1). The location of marker S4 is above the full and simplified formula with $\alpha_{d,Hoffmans}$ and $\alpha_{d,Sande}$ (figure 5-14 and figure 5-15).

Third, the marker of Bakker (1960) is classified as ‘G.I Only filter is *instable*’ and located above the full and simplified version of the formula with $\alpha_{d,Sande}$. In addition, the marker of the data of Bakker (1960) is located below the curve of the simplified and full version of the formula of Hoffmans (2012) with $\alpha_{d,Hoffmans}$. The marker of Bakker (1960) confirms the validity of the full and simplified version of the design formula with $\alpha_{d,Sande}$. In addition, it suggests that the formula of Hoffmans (2012) with $\alpha_{d,Hoffmans}$ is conservative, because the relative layer thickness is over-estimated. One should take into account two factors of uncertainty. Marker of Bakker (1960) (test M633-d) contains wide graded filter gradation, while test S6 contains narrow graded filter gradation. In addition, classification by Van de Sande (2012) (‘filter moves first’) was not directly seen during tests. Therefore, the marker is only included in this thesis as a reference and not applied in the validation for sill-induced additional turbulence.

In summary, the general classification of marker S6 and expected classification of marker S4 suggest that for flows with sill-induced additional turbulence, the curve of the full and simplified version of the design formula must increase (i.e. α_d must increase) The new curve of the of the formula of Hoffmans (2012) for flows with sill-induced turbulence lies between marker S6 and marker S4. The new α_d exceeds the value of $\alpha_{d,Sande}$. Furthermore, no conclusion can be made on the validity of the full and simplified design formula with $\alpha_{d,Hoffmans} = 1.2$ based on only a single marker S6. Although, $\alpha_{d,Hoffmans}$ appears to be better in line with marker S6 than $\alpha_{d,Sande}$. However, these conclusions are in contrast with the classification of the marker of Bakker (1960) and position of the marker relative to the full and simplified versions of the design formulas.

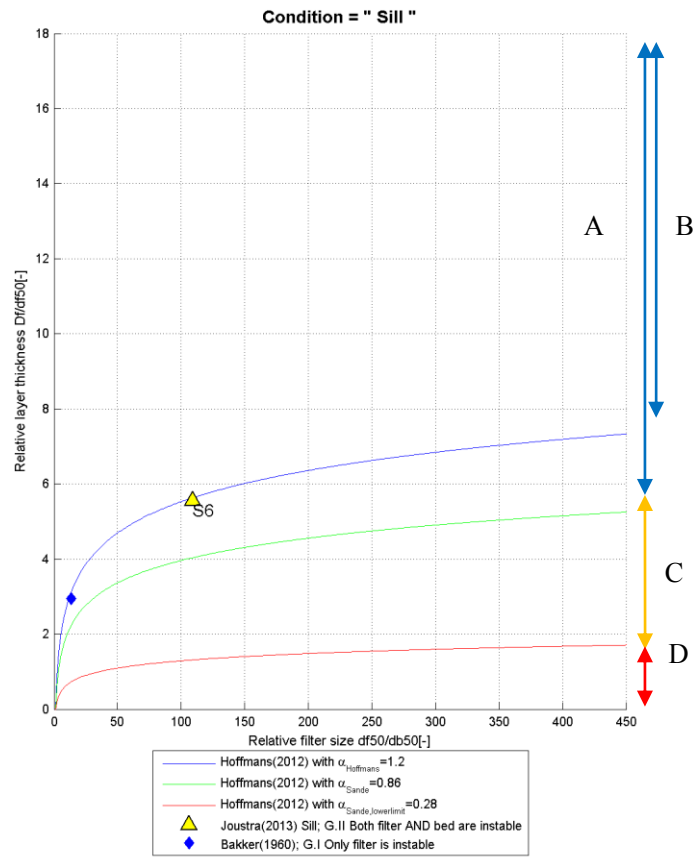


Figure 5-12: The markers and visual observed classification compared with the simplified formula. The green curve shows the $\alpha_{d,Sande}$ for the formula as proposed by Van de Sande (2012) for uniform flow.

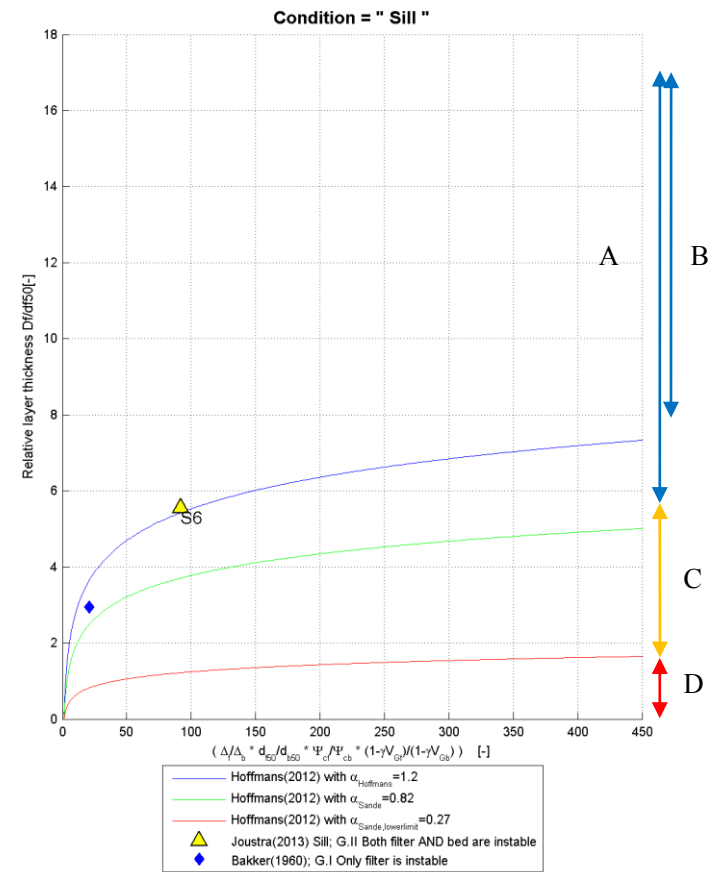


Figure 5-13: The markers and visual observed classification compared with the full formula. The green curve shows the formula with the $\alpha_{d,Sande}$ as proposed by Van de Sande (2012) for uniform flow.

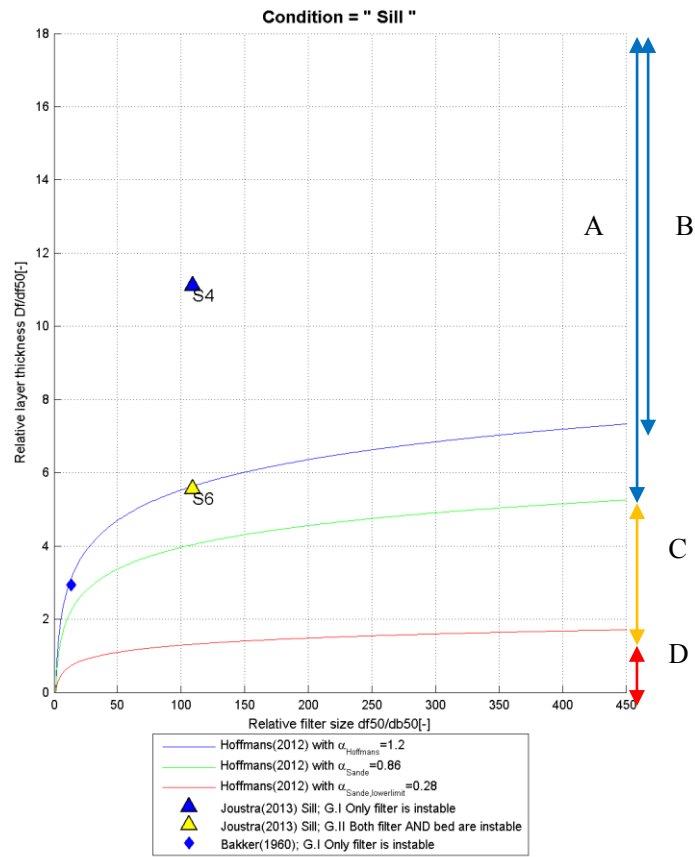


Figure 5-14: The markers and general classification compared with the simplified formula. Includes also 'expected' classification of S4. The green curve shows the $\alpha_{d,Sande}$ for the formula as proposed by Van de Sande (2012).

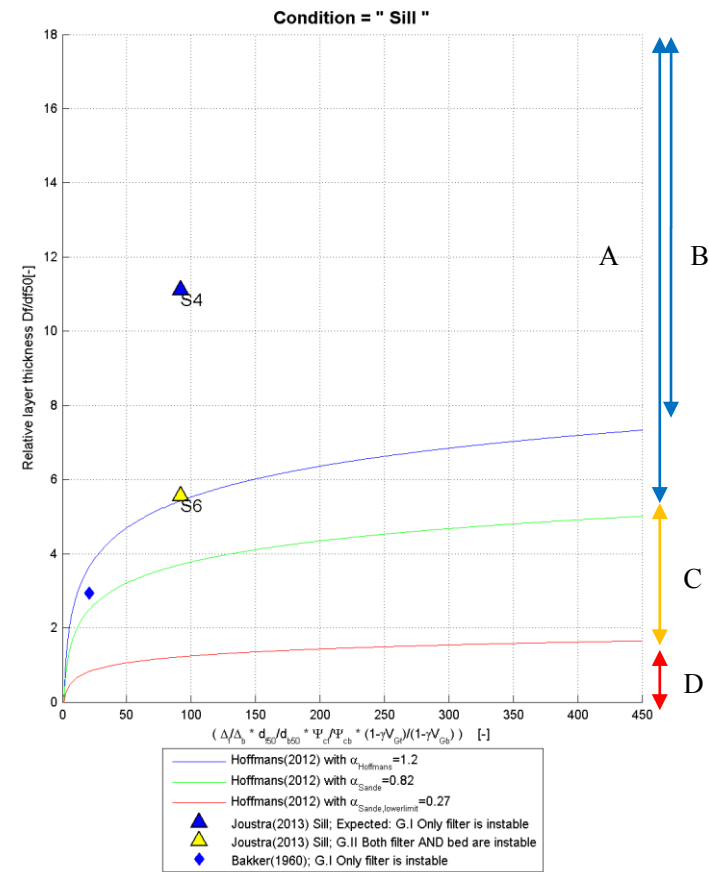


Figure 5-15: The markers and general classification compared with the full formula. Includes also 'expected' classification of S4. The green curve shows the $\alpha_{d,Sande}$ for the formula as proposed by Van de Sande (2012).

5.4 Hoffmans (2012) for flows with a cylindrical pier

This section describes the validation of the (full and simplified) formula of Hoffmans (2012) and Wörman (1989) for the flows with a cylindrical pier. Data of Van Velzen (2012) and Joustra (2013) are plotted as markers in figure 5-16 and 5-17. In addition, the curves of the simplified (equation 1.2) and full version (equation 1.3) of the formula of Hoffmans (2012) and the linear formula of Wörman (1989) (equation 1.4) are shown in figure 5-16 and 5-17. The logarithmic curves describe the design formula of Hoffmans (2012) with $\alpha_{d,Hoffmans}$ (blue curve), $\alpha_{d,Sande}$ (green curve) and $\alpha_{d,Sande,lowerlimit}$ (red curve).

Test P17 is classified as (section 5.1.1) ‘G.I Only filter is *instable*’. In addition, marker P2, P3, P6, P7, P10, P11, P13 and marker L08 from Van Velzen (2012) are classified as ‘G.III Only bed is *instable*’ (section 5.1.1). Section 5.6 describes remarks regarding the classification of marker of tests L01-L08.

Marker P17 indicates that ‘G.I Only filter is *instable*’ and is located above the curve of the full and simplified formula of Hoffmans (2012) with $\alpha_{d,Hoffmans}$ and $\alpha_{d,Sande}$ and confirms both formulas. However, markers P10, P6, P2 and P11 with ‘G.III Only bed is *instable*’ are located above the curves of the simplified formula of Hoffmans (2012) with $\alpha_{d,Sande} = 0.86$. In addition, P10, P6, P2, P11 and P7 are located above the full version of the formula of Hoffmans (2012) with $\alpha_{d,Sande} = 0.82$. Therefore, the bed stability as determined is underestimated by the full and simplified version of the formula of Hoffmans (2012) with $\alpha_{d,Sande}$. This conclusion is in agreement with the marker L08 and classification ‘G.III Only bed is *instable*’ of Van Velzen (2012). In addition, markers P10, P6, P2 are also located above the formula of Hoffmans (2012) in the simplified and full version with $\alpha_{d,Hoffmans} = 1.2$, and marker P11 is above the formula of Hoffmans (2012) in the full version of the formula with $\alpha_{d,Hoffmans} = 1.2$. Therefore, the formula of Hoffmans (2012) with $\alpha_{d,Hoffmans} = 1.2$ better in line with the test data compared to the formula of Hoffmans(2012) with $\alpha_{d,Sande}$, but still appears to be on the low side based on laboratory tests.

Therefore, in both simplified and full versions of the formula of Hoffmans (2012) either the $\alpha_{d,Hoffmans}$ or $\alpha_{d,Sande}$ underestimate the bed stability (required relative filter layer thickness) for application at flows with a cylindrical pier. The α_d should be increased to be better in agreement with the laboratory test data. Chapter 6 discusses a rough estimate range for a new value for α_d .

5.5 Wörman (1989) for flows with a cylindrical pier

Marker P17 (‘G.I Only filter is *instable*’) is located above the formula of Wörman (1989). In addition, marker P6, P2, P11, P7, P13 and P3 with visual observation ‘G.III Only bed is *instable*’ are located below the curve representing the formula of Wörman (1989). So most markers are in agreement with the formula of Wörman, and the formula performs quite reasonable. However, one marker P10 shows ‘G.III Only bed is *instable*’ and is located above the curve of Wörman. This single marker suggests that the design formula Wörman (1989) underestimates the required layer thickness for flow overs 0.5 m/s and filter layer thickness above 0.1 m. Therefore the gradient of the linear curve should be increased to better in agreement with marker P10. Chapter 6 discusses a new gradient for the formula of Wörman (1989).

5.6 Comparison between data of Van Velzen (2012) and Joustra (2012)

Van Velzen (2012) and Van de Sande (2012) both applied the data of Van Velzen (2012) in a validation of the design formula of Hoffmans (2012) and the design formula of Wörman (1989). First, Van Velzen (2012) classified the marker of test L01-L07 as ‘no winnowing’ (i.e. bed material is stable) and marker of test L08 as ‘winnowing’ (i.e. bed material is instable). Comparison between marker L01-L07 (above both design curves, i.e. filter should be instable), and L08 (below both design curves, i.e. bed should be instable), the simplified version of the formula of Hoffmans (2012) and the formula of Wörman (1989) resulted in a indication that both design formulas might be valid for flows with pier. Second, Van de Sande (2012) reclassified marker L01-L07 to ‘Filter moves first’ (i.e. should be located above both design formulas) and marker L08 to ‘Bed moves first’ (i.e. should be located below both design formulas). Van de Sande (2012) confirmed both design formulas with this classification. However, the philosophy of the

design formula of Hoffmans (2012) and Wörman (1989) requires that a marker with classification G.IV ‘Both filter and bed are *stable*’ cannot be applied in the validation, because it is yet unknown if the relative layer thickness is sufficient to prevent winnowing (i.e. the critical flow velocity, incorporated in the filter grain size, is not yet exceeded). In addition, Van Velzen (2012) did not observe filter instability, but designed the filter grain size sufficiently large to prevent shear failure (i.e. filter material is *stable*). Therefore, the marker of tests L01-L07 cannot be applied in a validation of the design formulas. The conclusions from section 5.4 and 5.5 cannot be compared based on L01-L07, because Van de Sande (2012) and Van Velzen (2012) did use (the only marker above the curves) L01-L07 in their validation. Test L08 (G.III ‘Only bed is unstable’) is in agreement with data of Joustra (2012) and is located below both design formulas, where it should be.

Furthermore, a test conducted by Van Velzen (2012) (Test L08, $D_f/d_{f50} = 3.7$ [-]) with a cylindrical pier showed *insufficient* relative layer thickness to prevent transport of bed material through the pores of the filter (winnowing). However, in a test conducted by Van de Sande (2012) in uniform flow and similar filter and bed characteristics, the relative layer thickness was *sufficient* to prevent transport of bed material through the pores of the filter (observed stable bed and instable filter). This was test T07 with $D_f/d_{f50} = 3.77$ [-] and similar relative grain size (d_{f50}/d_{b50}). Figure 0-6 and 0-7 in appendix 2 visualizes test T07 and L08. Hence, the value of $\alpha_{d,Sande}$ is based on test with simultaneous erosion of filter and bed material (G.II ‘Both filter and bed are *instable*’) classified for test L08 of Van Velzen (2012). Therefore, the actual curve (with new value for α_d) for the formula of Hoffmans (2012) for conditions with a cylindrical pier lies at least above marker L08. Thus an increase in α_d for flows with a cylindrical pier is likely, which is in agreement with the conclusion from section 5.4.

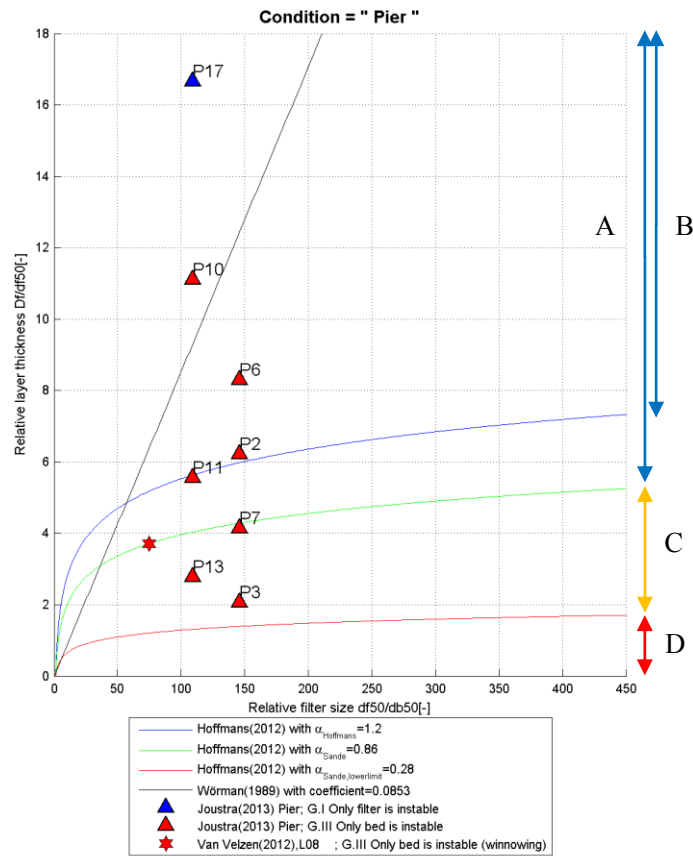


Figure 5-16: The markers and visual observed classification compared with the simplified formula of Hoffmans and formula of Wörman. The green and blue curve shows the formula of Hoffmans with respectively the $\alpha_{d,Sande}$ and $\alpha_{d,Hoffmans}$. The green curve is valid for uniform flow (Van de Sande, 2012). The dotted black line shows the linear formula of Wörman (1989).

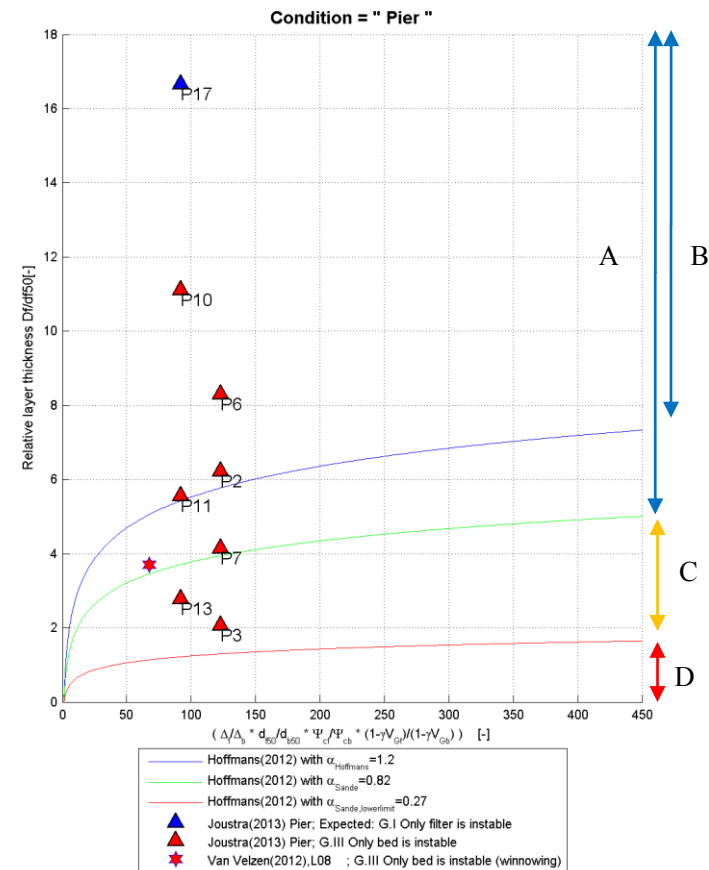


Figure 5-17: The markers and visual observed classification compared with the full version of the formula of Hoffmans. The green and blue curve shows the formula of Hoffmans with respectively the $\alpha_{d,Sande}$ and $\alpha_{d,Hoffmans}$. The green curve is valid for uniform flow (Van de Sande, 2012).

6 Discussion

6.1 Reflection on flow conditions and filter grain size

The depth average flow velocity is set at $\bar{u} = 0.5$ m/s, $\bar{u} = 1.0$ m/s or $\bar{u} = 1.5$ m/s within this thesis. These values are slightly higher (~5%) compared to the flow velocity measured at a height of 40% of the water depth above the bed for uniform flow. These differences are negligible, therefore they do not affect the classification of filter and bed stability for the condition of uniform flow. The filter grain size in the laboratory experiments were designed to be instable at approximately $\bar{u} = 1.0$ m/s, because investigation of winnowing failure and pressure measurements inside the filter were the main priority of the experiments of Joustra(2012). However, it turned out that the flow velocities in uniform flow did not exceed the critical threshold for instability (phase 3 of Breusers, 1977). In future tests the flow velocities should be further increased to the velocity where either the filter material or the bed material becomes instable. This instability is required to test the formula of Wörman (1989) and Hoffmans (2012) because of the applied philosophy of simultaneous erosion of filter and bed material. In addition, an incremental flow velocity during the test is preferred with smaller steps than 0.5 m/s in order to better distinguish simultaneous erosion from non-simultaneous erosion. Filter settlement is a process that takes time, thus one should take sufficient time per flow velocity step to assess the influence of flow velocity before increasing the velocity further.

6.2 Reflection on choice of classification of stability

This section describes six remarks about the general classification, filter stability classification and bed stability classification. The first remark describes the discussion of the general classification. The second, third and fourth remarks describe the discussion of the filter stability classification. Finally, the fifth and sixth's remark describe the discussion of the bed stability classification and expected classification of U2, U4, U8 and S2.

The first remark regards the general classification. Van de Sande (2012) applied the general classification of 'filter moves first', 'simultaneous erosion' and 'bed moves first'. In this thesis, the way the general classification is applied, is similar to the general classification as applied by Van de Sande (2012). The general classification could not be applied directly as you cannot 'see' in the movie that the filter moves first. That is because the movie itself is of a test with only one velocity (e.g. $\bar{u} = 1.0$ m/s; 'G.I Only filter is *instable*'). However, the test selected for validation is the test with the lowest flow velocity with the general classification where filter is instable (G.I), bed is instable (G.III) or both are instable (G.II). In addition, because it is known what was observed at the previous test (with lower average velocity, e.g. $\bar{u} = 0.5$ m/s; 'G.IV Both filter and bed are *stable*'), this method can be applied to validate the formula.

The second remark regards the type of analysis for the filter stability classification. First, the only method of classification that could be applied to all tests is the visual observation to determine the degree of filter instability. The classification for visual observation of filter instability as applied by Van Huijstee and Verheij (1991) is chosen to best fit the previous validation results and criteria for incipient motion. Van de Sande (2012) determined the critical average flow u_{cr} based on measured transport of filter material, which is a less subjective method than visual observation. However, this type of data was not available in the dataset by Joustra (2012) and therefore visual observation was chosen.

The third remark regards the choice for the phase describing the critical threshold for incipient of motion. Van Huijstee and Verheij (1991) clearly stated a critical threshold for the filter material of phase 3 of the classification presented in Breusers (1977) (figure 4-2). However, Van de Sande (2012) did not clearly describe the phase used as the critical threshold for incipient motion. Comparison between Van de Sandes

(2012) transport-velocity graphs and the defined $u_{cr,f}$ seem to suggest that it is more likely that he chose a critical threshold similar to phase 1 (occasional particle movement at some locations) or phase 3 (frequent particle movement at many locations), than phase 6 of Breusers (1977) (permanent particle movement at all locations). The criterion for filter instability within this thesis is based on phase 3 of Breusers (1977), equal to the phase applied by Van Huijstee & Verheij (1991). If the threshold phase is higher than 3 (for uniform flow: $0.035 < \Psi_{cf} < 0.055$), then that would have no effect on the general classification of the data of Joustra (2012) (from all tests with uniform flow, the filter mobility did not exceed phase 3, thus also not phase 6). It would however reduce the confidence in the interpretation of test U4, U2 and U8, because phase 6 requires a higher flow velocity than phase 3 and thus also a possible higher load on the bed material (i.e. bed instability). However, choosing a lower critical threshold phase for incipient motion does highly affect the results described in chapter 5, i.e. it affects the validation results for both versions of the formula of Hoffmans (2012) for uniform flow and flow with sill-induced additional turbulence. This does not affect the conclusion for the validity of the formula of Wörman (1989). For example, consider using classification F.II 'shaking stones, a single stone rolls' (between phase 1 and 3) instead of F.III (phase 3) as the critical threshold for incipient motion (uniform flow: $\Psi_{cf}=0.030$, instead $\Psi_{cf}=0.035$). Then for uniform flow, the data of Joustra (2012) would also confirm the design formula of Hoffmans (2012) with $\alpha_{d,Sande}$, but would suggest that the formula is conservative (figure 4-2, e.g. U5 would be classified G.I 'Only filter is *Instable*' ; blue coloured). In addition, for flows with a sill-induced additional turbulence, S5 (figure 4-2; in the new situation is classified as 'G.I Only filter is instable') would confirm the design formula of Hoffmans (2012) with $\alpha_{d,Sande}$, instead of suggesting an increase in α_d . Therefore, in practice one should take a lower phase for incipient of motion (i.e. uniform flow: $\Psi_{cf}=0.030$). For flows with a cylindrical pier, the conclusion for an increase of the gradient of the formula of Wörman (1989) and increase of α_d would still hold, when the threshold phase is lowered to F.II.

The fourth remark regards visual observation of filter instability from the images of the camera inside the cylindrical pier. The area covered is smaller than for the flow conditions 'uniform flow' and 'sill-induced additional turbulence'. If no filter instability is observed, there could still be some filter instability at a larger distance from the pier. It is assumed that if no instability is observed on the camera images, that no filter mobility occurred at all. This assumption is based on the fact that the highest degree of hydraulic load on the filter stones is expected at the sides of the pier, due to the relative high flow velocity as a result of flow contraction and the presence of turbulence due to the horse-shoe vortex. Therefore, filter instability outside the camera range is expected to have a negligible effect on the classifications of filter instability around the pier.

The fifth remark regards the different methods in classification of bed instability. For best comparison of data and with the formula of Hoffmans (2012), one could have chosen a similar method for determination of incipient of motion as applied by previous validations with data of Van de Sande (2012) and Van Huijstee & Verheij (1991). Bed material transport however was not measured by Joustra (2012) and no camera images at the filter-bed interface were available to classify horizontal transport and vertical transport. Instead the method of visual observation of filter settlement is applied to identify bed instability. All three methods have advantages and disadvantages. Observation inside the filter is probably the most accurate method for determination of the threshold for incipient motion. The method of visual observation of filter settlement could overestimate the critical flow velocity for incipient motion of the bed material, but it was the only method which could be applied to the dataset.

The sixth remark regards the expected classification of test U2, U4 and U8 which confirm the formula of Hoffmans (2012). Table 6-1 describes the filter and bed characteristics of test T4 of Van Huijstee & Verheij (1991), with approximately similar bed grain size ($d_{b50} = 0.165$ mm in all tests of Joustra (2012)). Test T4 confirms the expected classification of U2, U4 and U8. The filter grain size d_{f50} of test T4 is larger (i.e. requires a higher flow velocity than 1.0 m/s for instability) than the filter grain size of U2 ($d_{f50} = 24.1$

mm), U4 ($d_{f50} = 18.0$ mm) and U8 ($d_{f50} = 18.0$ mm). The layer thickness D_f/d_{f50} in test T4 is 3.0 [-], while the relative layer thickness is larger during test U4 ($D_f/d_{f50} = 11.1$ [-]), U2 ($D_f/d_{f50} = 8.3$ [-]), and U8 ($D_f/d_{f50} = 5.6$ [-]). In other words, under higher load conditions (T4) than applied at tests U2, U4, and U8, the layer thickness was still sufficient to prevent bed instability. Therefore, it is probable that U2, U4 and U8 are classified as F.I ‘Only filter is *instable*’ when the flow velocities exceed 1.0 m/s. The expected flow condition of S2 could not be confirmed due the limited amount of available tests with sill-induced additional turbulence.

Table 6-1: Test T4 of van Huijstee & Verheij (1991). General classificatino of Van de Sande (2012)

Test ID	d_{b50} [mm]	d_{f50} [mm]	D_f [mm]	D_f/d_{f50} [-]	d_{f50}/d_{b50} [-]	General classification
T4	0.151	30	90	3.0	198.7	'Filter moves first'

6.3 Design of D_f/d_{f50} for uniform flow

Van de Sande (2012) analyzed the incipient motion within multiple datasets (Bakker in 1960, Haverhoek in 1968, Wouters in 1982, Konter et al. 1990, Van Huijstee and Verheij in 1991, and Van Velzen (2012). Van de Sande (2012) then combined all data into one dataset which was used by Van de Sande (2012) for validation of the formula of Hoffmans (2012) (equation 1.2 and 1.3) and concluded that the formula is valid for uniform flow. The $\alpha_{d,Sande,s,v}$ and $\alpha_{d,Sande,f,v}$ could be optimized by reanalyzing the dataset of Van de Sande (2012) and only applying tests with uniform flow. The $\alpha_{d,Sande,s,v}$ (0.86) and $\alpha_{d,Sande,f,v}$ (0.82) are a safe upper limit for the area of simultaneous erosion, but $\alpha_{d,Sande}$ is based on a fit of full and simplified version of the formula of Hoffmans (2012) to the highest marker classified with simultaneous erosion. This highest marker is the data of Van Velzen (2012). Sections 5.3 and 5.4 show that flows with sill-induced turbulence and flows with cylindrical piers require a higher α_d than the $\alpha_{d,Sande}$. The test of Van Velzen (2012) contains flows with a cylindrical pier. Therefore, excluding the data of Van Velzen (2012) would optimize $\alpha_{d,Sande}$ (i.e. the α_d valid for non-uniform flow).

6.4 Design of D_f/d_{f50} for flows with sill-induced additional turbulence

Results in section 5.3, based on marker S6 suggest that $\alpha_{d,Sande}$ is not applicable in conditions with sill-induced additional turbulence and α_d should therefore be increased in both the full and the simplified versions of the formula of Hoffmans (2012) for the application for flows with sill-induced additional turbulence. However, no new α_d can be proposed with satisfying confidence based on the strict classifications applied in this thesis. The first reason is the scarcity of test markers. For example, there were no test markers with ‘Only bed is *Instable*’ (section 5.1). A second reason is the high uncertainty in the visual observed classification. This uncertainty is caused by the difficulty of visual observation of bed instability (as filter settlement) in highly turbulent conditions. It is therefore strongly recommended to perform additional tests with markers (just) above, at and just below the curve of the formula of Hoffmans (2012) with $\alpha_{d,Sande}$, to determine a safe α_d for flows with sill-induced additional turbulence.

A first remark is the effect of the uncertainty resulting from visual observation, on the conclusion that α_d should increase for conditions with sill-induced additional turbulence. The bed instability classification of marker S6 is ‘F.II Local filter settlement’, as only locally filter settlement was visually observed. Other locations within the test section were not suitable for visual observation, because of the high degree of filter mobility. If the filter settlement occurred at many locations (F.III), that would not make a difference on the conclusion of the increase of α_d . Incorrect classification of bed instability (e.g. actual bed stability classification is ‘Only filter is *instable*’) or the case that more than two of the filter layers are eroded at these locations, could prevent the conclusions that α_d must be increased. Erosion of more than two filter layers in not expected, based visual observation of the videos. However, incorrect classification of bed instability includes a high degree of uncertainty, because of the visual observed classification (6.2), which

lowers the confidence in the conclusion that α_d should increase for sill-induced additional turbulence (see also section 6.2; third remark).

A second remark is the effect of an increase of α_d on the physical meaning of the coefficient. This effect is discussed with preliminary results of analysis of the pressure measurements at multiple depths inside the filter as described by Van Velzen (2013). As described previously, marker S6 suggests that α_d should be increased, which would also suggest that the characteristic damping depth profile depends also on the additional turbulent intensity in the outer flow. The increase basically means that a geometrical open filter is less able to damp the fluctuations in the outer flow in additional turbulent conditions compared to uniform flow. However, preliminary results of an analysis of the pressure fluctuations inside the filter by Van Velzen (2013) suggest two conclusions. The first conclusion shows increased pressure fluctuations at all depths due to the presence of the sill. This is in line with the observation of Van de Sande (2012) that bed instability increases with increased turbulent intensities in the outer flow. The second preliminary result is that the damping profile of pressure fluctuations in the sill-induced additional turbulent conditions is quite similar to the damping profile of pressure fluctuations inside the filter in uniform flow. Although the pressure fluctuations cannot directly be related to flow velocities (and thus turbulent kinetic energy), it gives an indication that if α_d should be increased, the difference between the of $\alpha_{d,Sande}$ for uniform flow and the new α_d for flows with sill-induced additional turbulence is not that large.

A final remark is a rough estimate of the new α_d , based on the assumptions that S6 is correctly classified and S4 is expected to be classified as G.I 'Only filter is *instable*' as described in section 5.1.1. The expected classification would suggest that the bed is stable, therefore test S4 could be a reasonable upper limit for the full and simplified version of the formula of Hoffmans (2012). The new α_d is calculated with another presentation of the formula of Hoffmans (2012) (equation 1.2, equation 1.3), described by equation 6.1 and 6.2. Filling in equation 6.1 with test data of experiment S4 $D_f/d_{f50} = 11.1$ [-], the assumption $\Delta_f/\Delta_b = 1.00$ [-], $d_{f50}/d_{b50} = 109.1$ [-], $\Psi_{cf}/\Psi_{cb} = 0.79$ [-] and $(1 - \gamma V_{Gf})/(1 - \gamma V_{Gb}) = 1.07$ [-] results in a $\alpha_{d,f.v.} = 2.5$ and $\alpha_{d,s.v.} = 2.4$. This means that the new $\alpha_{d,f.v.}$ increases with a factor of 3.0 and the new $\alpha_{d,s.v.}$ increases with a factor of 2.8 compared with the $\alpha_{d,Sande}$. Marker S6 was also quite reasonable in line with $\alpha_{d,Hoffmans} = 1.2$. Therefore, a upper limit of α_d for flows with sill-induced additional turbulence might be within the range $1.2 < \alpha_{d,f.v.} < 2.5$ and $1.2 < \alpha_{d,s.v.} < 2.4$. Figure 6.1 visualizes the curves of Hoffmans with the α_d estimated.

$$\alpha_{d,f.v.} = \frac{D_f/d_{f50}}{\ln\left(\frac{\Delta_f}{\Delta_b} * \frac{d_{f50}}{d_{b50}} * \frac{\Psi_{cf}}{\Psi_{cb}} * \frac{(1 - \gamma V_{Gf})}{(1 - \gamma V_{Gb})}\right)} \quad (6.1)$$

$$\alpha_{d,s.v.} = \frac{D_f/d_{f50}}{\ln(d_{f50}/d_{b50})} \quad (6.2)$$

In summary, results (section 5.3) based on marker S6 suggests that $\alpha_{d,Sande}$ is not applicable in conditions with sill-induced additional turbulence and α_d should therefore increase. This section discussed the minimal degree of confidence in the classification marker S6 and rough estimates are calculated for a new value of α_d for sill-induced additional turbulence ($1.2 < \alpha_d < 2.5$). However, preliminary results of the pressure fluctuations analysis by Van Velzen (2013) show a similar damping profile of pressure fluctuations within the filter as in uniform flow, which suggests no or only a minor increase in α_d for sill-induced additional turbulence. Therefore, it is highly recommended to either conduct additional tests to confirm the rough estimates of the new α_d for sills with markers near the curves of Hoffmans (2012) with $\alpha_{d,Sande}$ or relate pressure signals inside the filter to turbulent kinetic energy and apply a similar method of Hoffmans (2012) (based on tests of Klar (2005)) to determine the new α_d for flows with sill-induced additional turbulence.

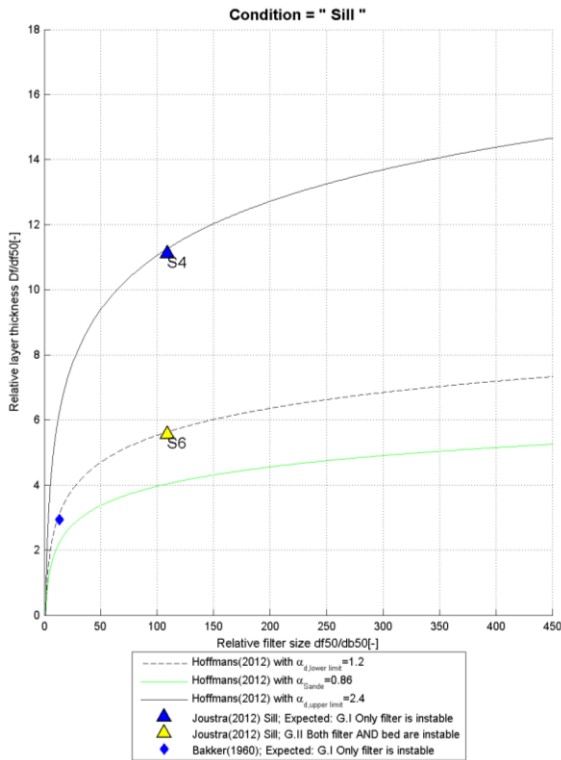


Figure 6-1: Simplified version of the formula. In addition, a rough estimate of the upper and lower limit of a range for α_d for flows with sill.

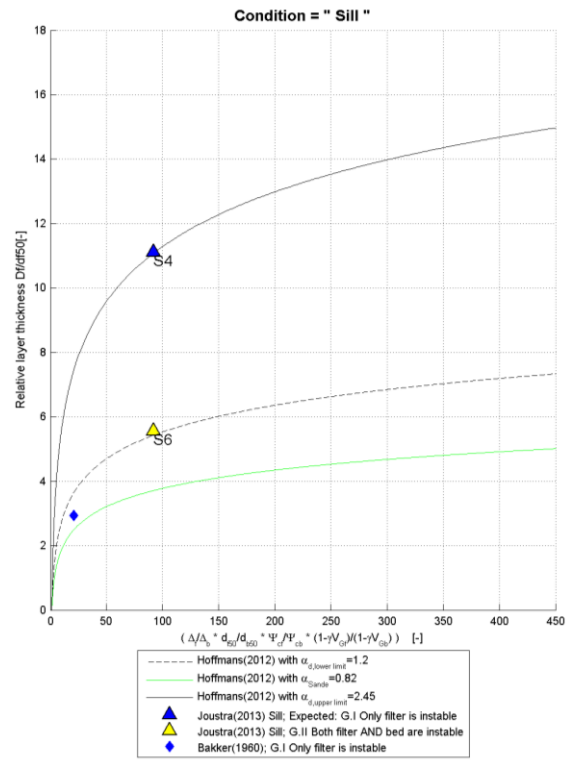


Figure 6-2: Full version of the formula. In addition, a rough estimate of the upper and lower limit of a range for α_d for flows with sill.

6.5 Design of D_f/d_{f50} for flows with a cylindrical pier

Hoffmans (2012)

Results in section 5.4 show that the minimum required layer thickness calculated with both full and simplified versions of the formula, are insufficient for stable bed material in front of the cylindrical pier. This means that the new α_d for cylindrical piers is higher than the $\alpha_{d,Sande}$.

Test P17 is a safe upper limit for a new α_d , as G.I ‘Only filter instability’ is observed, i.e. no bed instability. In addition, the classification of test P10 is ‘G.III Only bed material is *instable*’. Thus the curve with the α_d for cylindrical piers is probably located between test P17 and P10. An α_d which is in agreement with the test data of Van Velzen (2012) and data of Joustra(2012) can be determined with equation 6.3, equation 6.4, marker P10 (lower limit) and P17 (upper limit). Equations 6.3 and 6.4 are another presentation of the full version and simplified version of the formula as described with equation 1.2 (equation 6.3) and equation 1.3 (equation 6.4).

$$\alpha_{d,f.v.} = \frac{D_f/d_{f50}}{\ln\left(\frac{\Delta_f}{\Delta_b} * \frac{d_{f50}}{d_{b50}} * \frac{\Psi_{cf}}{\Psi_{cb}} * \frac{(1 - \gamma V_{Gf})}{(1 - \gamma V_{Gb})}\right)} \quad (6.3)$$

$$\alpha_{d,s.v.} = \frac{D_f/d_{f50}}{\ln(d_{f50}/d_{b50})} \quad (6.4)$$

Filling in equation 6.3 and 6.4 for test P17 with $D_f/d_{f50} = 16.7$ [-], the assumption $\Delta_f/\Delta_b = 1.0$ [-], $d_{f50}/d_{b50} = 109.1$ [-], $\Psi_{cf}/\Psi_{cb} = 0.79$ [-] and $(1 - \gamma V_{Gf})/(1 - \gamma V_{Gb}) = 1.07$ [-] results in a $\alpha_{d,f.v.} = 3.7$ and $\alpha_{d,s.v.} = 3.6$. This means the new upper limit with $\alpha_{d,f.v.}$ increases with a factor of 3.5 and the new $\alpha_{d,s.v.}$ increases with a factor of 3.1 compared with the $\alpha_{d,Sande}$.

Furthermore, filling in equation 6.3 and 6.4 for test P10 with $D_f/d_{f50} = 11.1$ [-], the assumption $\Delta_f/\Delta_b = 1.00$ [-], $d_{f50}/d_{b50} = 109.1$ [-], $\Psi_{cf}/\Psi_{cb} = 0.79$ [-] and $(1 - \gamma V_{Gf})/(1 - \gamma V_{Gb}) = 1.07$ [-] results in a $\alpha_{d,f.v.} = 2.5$ and $\alpha_{d,s.v.} = 2.4$. A upper limit would therefore be within the range $2.5 < \alpha_{d,f.v.} < 3.7$ and $2.4 < \alpha_{d,s.v.} < 3.6$. Figure 6.3 and figure 6.4 visualize the design formula of Hoffmans (2012) with the estimated α_d for cylindrical piers.

Wörman (1989)

Results in section 5.5 show that the formula of Wörman (1989) estimates the required layer thickness reasonably well for flows over 0.5 m/s and a layer thickness over 0.1 m, with the exception of test P10. Test P10 is not in line with the formula and indicates that the linear relation of Wörman (1989) of the formula should have a higher gradient to be in line with the test data of Joustra (2012).

First, the formula of Wörman (1989) is, according to the author, valid for the range of $0 < d_{b85}/d_{f85} < 0.1$ [-]. The smallest d_{f85} in this thesis gives a $d_{b85}/d_{f85} = 0.233/20.7 = 0.011$ [-], which is in agreement with this validity range. The largest d_{f85} in the data of Joustra (2012) is $d_{b85}/d_{f85} = 0.233/29.7 = 0.0079$ [-], which is also within the validity range. In addition, Wörman (1989) specified an additional restriction for applying the theoretical derived formula on which equation 6.5 is based. The restriction is that bed material grain size should be equal to or larger than the bed material grain size applied in the tests of Wörman (1989). The smallest d_{b85} in the tests of Wörman (1989) is 0.20 mm, where the d_{b85} in the tests of Joustra (2012) is 0.233 mm, which is in accordance to the first restriction.

Second, the formula of Wörman (1989) (equation 6.5) is rewritten with assumptions to equation 1.4 (Hoffmans, 2012; see also section 1.1). The conclusion for an increase in the gradient of the formula of Hoffmans, 2012; equation 1.4) followed from test P10 (G.III ‘Only bed is *instable*’), which was located above the curve. Therefore, the original formula (equation 6.5) is validated with test P10 to verify that the assumptions did not affect the conclusion for the increase in gradient of the linear relation. For test P10, the relative layer thickness is $D_f/d_{f15} = 200/15.5 = 12.9$ [-]. The minimum required relative layer thickness $D_f/d_{f15} = 9.5$ [-], according to equation 6.5, with $n_f = 0.4$ [-], $\Delta_f/\Delta_b = 1.00$ [-] and $d_{f85}/d_{b85} = 20.7/0.233 = 88.8$ [-]. Test P10 is clearly above the original design curve of Wörman (1989) (equation 6.5), thus the rewritten form with assumptions does not affect the conclusions.

$$\frac{D_f}{d_{f15}} = 0.16 * \left(\frac{n_f}{(1 - n_f)} * \frac{\Delta_f}{\Delta_b} * \frac{d_{f85}}{d_{b85}} \right) \quad (6.5)$$

Third, the tests of Joustra (2012) satisfy the criterion for the avoidance of ‘water depth effects’ in physical modelling of piers (Whitehouse, 1998). The tests of Wörman (1989) did not satisfy this criterion. Whitehouse (1998) described the criterion as a minimal water depth-pier diameter ratio of $h_w > 4 * D_{pier}$. The tests of Joustra (2012) contain water depths h_w of 6.7 times D_{pier} ($\bar{u} = 0.5$ m/s and $\bar{u} = 1.0$ m/s) and h_w of 4.44 times D_{pier} ($\bar{u} = 1.5$ m/s). The tests of Wörman (1989) contain water depths h_w which are 27% and 36% of $h_w = 4 * D_{pier}$ (large pier) and water depths of 50% and 67% of $h_w = 4 * D_{pier}$ (small pier). A water depth to pier size ratio below the criterion indirectly decreases the forward bound vortex, which probably governs the loads in the filter (Nielsen et al., 2010). It is thus likely that the forward bound vortex is affected in tests of Wörman (1989) and the loads at the filter-bed interface are lower compared with experiments of Joustra (2012). Therefore, for water depth to pier ratios higher than the criterion as described by Whitehouse (1998), flow velocities over 0.5 m/s and layer thicknesses over 0.1 m, it is recommended increase the gradient of the formula of Wörman (1989).

A new gradient of the formula of Wörman (1989) can be calculated, to be in line with the data of Joustra (2012). The new curve of Wörman (1989) is probably located between test P10 (G.III ‘Only bed is *instable*’) and P17 (G.III ‘Only filter is *instable*’). Using filter and bed characteristics of P10 and P17, assumptions $n_f = 0.40$ [-] and $\Delta_f/\Delta_b = 1.00$, results for equation 6.5 from the gradient 0.16 to a new

gradient between 0.22 [-] (P10) and 0.33 [-] (P17). For equation 1.4 this results in a gradient from 0.085 to a new gradient between 0.10 (P10) and 0.153 (P17).

Finally, the formula of Wörman (1989) did not include a safety factor explicitly, but did incorporate the local flow velocity u [m/s] as 2 times the non-disturbed depth average flow velocity \bar{u} (based on Breusers, 1977). This already incorporates additional safety. However, the additional safety is not sufficient to be in total agreement with the validation results. Figure 6.3 and 6.4 visualize the new upper and lower limit of the gradients for the formula of Wörman (1989) and the new range α_d for flows with a cylindrical pier.

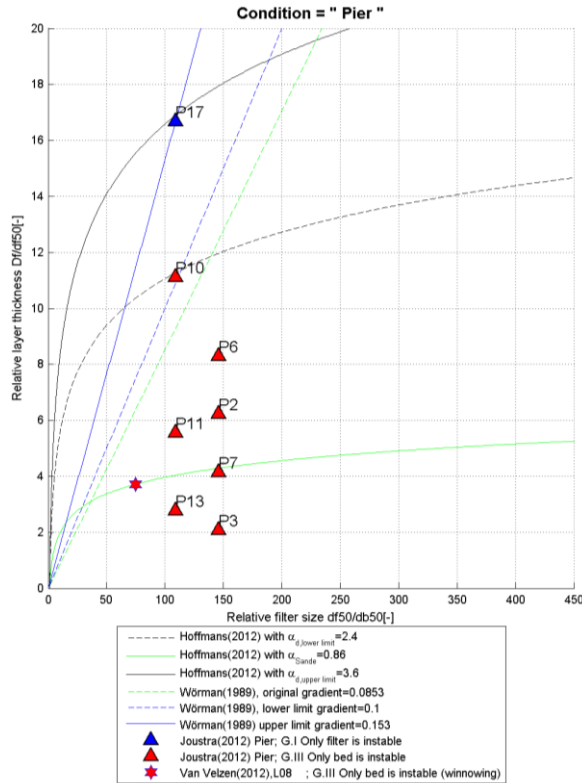


Figure 6-3: Simplified version of the formula of Hoffmans (2012) and the formula of Wörman (1989). In addition, a rough estimate of the upper and lower limit of a range for α_d for flows with a cylindrical pier. Also, the upper and lower limit of the new range for the gradient of the formula of Wörman (1989).

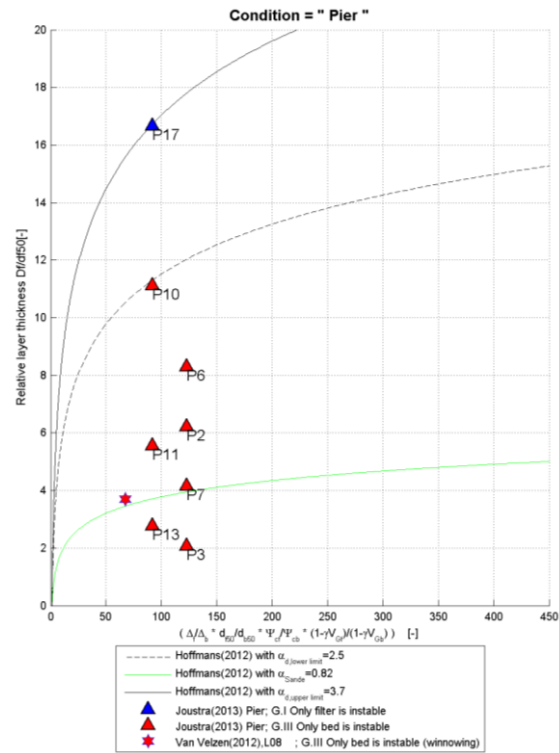


Figure 6-4: Full version of the formula of Hoffmans (2012) and the formula of Wörman (1989). In addition, a rough estimate of the upper and lower limit of a range for α_d for flows with a cylindrical pier.

6.6 Implications of results and physical mechanisms

The results for the formula of Hoffmans (2012) for flows with sill-induced additional turbulence and flows around a cylindrical pier (section 5.3 and 5.4) suggest to increase the value α_d to a new value of α_d for flows with sill-induced turbulence and to a new value of α_d for flows with cylindrical piers. Before the start of this thesis, it was expected based on theory that the formula is valid for non-uniform flows (i.e. sill-induced additional turbulence and cylindrical piers). The higher turbulent intensity in the outer flow compared to uniform flow (Hoffmans, 2012), affects both filter stability and bed stability (Van de Sande, 2012). Although the higher turbulence intensity is corrected for in the calculation of the stable filter grain size (equation 1.1), and results in a higher relative layer thickness (equation 1.2, equation 1.3), apparently according to the results of 5.3 and 5.4 α_d might be increased for sill-induced turbulence and should be increased for flows with a cylindrical pier.

$$\eta_{load}(z) = \frac{kf(z)}{kb} \approx e^{\frac{z}{\alpha_d * d_{f15}}} \quad (6.6)$$

The data suggests changing the α_d for the two cases of non-uniform flow. Thus the data indirectly suggests that the characteristic load damping profile $\eta_{\text{load}} [-]$ (equation 6.6; figure 2-5) is dependent on the degree of turbulence in the outer flow. This is not expected. In equation 6.6, K_b is the bed turbulent kinetic energy (i.e. the turbulence at the filter-outer flow interface; $z = 0$) and $k_f(z)$ is the turbulent kinetic energy at location z in the filter (z is negative). Hoffmans (2012) stated: ‘if k_b increases, the k_f also increases which is in agreement with observations’ (equation 6.6), i.e. the load damping profile (exponential decreasing with depth) should be the same in additional turbulent conditions.

However, the results from data of Joustra (2012) for conditions with a cylindrical pier suggest that exponential load damping (equation 6.6) is only valid, when the gradient of the load damping profile increases (figure 2-5) as a result of the increase in load damping coefficient α_d (equation 6.6). In other words, the loads penetrate deeper into the filter than in conditions of uniform flow. In conditions with a cylindrical pier, Nielsen et al. (2010) found that the horse shoe vortex (governing mechanism in unprotected piers (Breusers et al. 1977)) also penetrates into the filter. In addition, within this thesis a vertical down flow is measured above the filter surface interface and in front of the pier. Both the down flow and forward bound vortex flow mechanisms are therefore not sufficiently taken into account in the characteristic load.

Although surrounded with more uncertainty (because of uncertainty in visual observed classification of test S6), for sill-induced additional turbulence the gradient of the load damping profile should also be increased. This is not further discussed as this conclusion is contrast with pressure fluctuation damping profile from the preliminary results of Van Velzen (2013) (section 6.5). Further research into the research in the characteristic damping of loads under sill-induced additional turbulence is therefore recommended, e.g. validation of the range of α_d for flows with sill-induced additional turbulence.

Wörman (1989) or the formula of Hoffmans (2012) for piers?

For flows with a cylindrical pier, the formula of Wörman is preferred above the formula of Hoffmans (2012), because the formula of Wörman is more in agreement with test data than the formula of Hoffmans (2012) and indirectly takes into account the horse shoe vortex penetration into the filter as found by Nielsen et al. (2010). Although the formula of Hoffmans (2012) is less empirical derived than the formula of Wörman (1989) (thus theoretically applicable or a wider range of non-uniform conditions) the change of α_d with a factor of approximately 3 does lower the confidence in the validity of an exponential decrease of characteristic load (based on tests with uniform flow velocity of Klar (2005)). Wörman (1989) found the linear relation with tests with a cylindrical pier, where Hoffmans (2012) determined the load damping coefficient α_d on test under uniform flow conditions (Klar, 2005). Uniform flows do not include the additional turbulence around a pier such as horse-shoe vortices. Therefore, to test the validity of the exponential load damping as applied in the derivation of the formula of Hoffmans (2012); either the average flow velocity and flow velocity fluctuations inside the filter around the cylindrical pier should be measured and analysed, or additional tests for flows with a cylindrical pier and tests in the region with relative grain size of d_{150}/d_{b50} between 1 and 50 should be conducted. Until more tests can be performed to improve the formula of Hoffmans (2012) for piers, the formula of Wörman is preferred.

7 Conclusion and recommendation

A design formula for the computation of the minimum relative layer thickness of geometrical open filters is the formula Hoffmans (2012), which is valid for uniform flow (Van de Sande, 2012) and theoretically valid for non-uniform flow. In addition, the formula of Wörman (1989) is valid for the non-uniform flow condition of flows with a cylindrical pier and layer thicknesses below 0.1 m flow velocity of 0.5 m/s. The main objective of this thesis is to test the validity of the design formula of Hoffmans (2012) for flows of sill-induced additional turbulence and flows with a cylindrical pier. The formula of Wörman (1989) is included in this thesis to investigate performance for cylindrical piers for flows over 0.5 m/s and to compare the performance with the performance of the formula of Hoffmans (2012) for cylindrical piers. The performance of the both design formulas is tested with data from experiments conducted by Joustra (2012). This dataset contains the test conditions: uniform flow, flows with sill-induced additional turbulence and flows with a cylindrical pier.

7.1 Conclusions

1) *How do the data compare to previous validation of the load damping coefficient α_d (Van de Sande, 2012) for uniform flow?*

The data of Joustra (2012) with condition of uniform flow are in agreement with the formula of Hoffmans (2012) with the load damping coefficient $\alpha_d = 0.82$ for the full version and $\alpha_d = 0.86$ for the simplified version. This conclusion is based on: (A) the combined filter and bed stability classification of one single test below both the curves of the formula and (B) the expected classification of 3 tests when the flow velocity was further increased. The visually observed classification and expected classification of these four tests are in agreement with the combined filter and bed stability classification of tests with approximately similar filter, bed grain sizes and layer thickness of data of Van Huijstee & Verheij (1991). In addition, the visually observed classification of the single test (i.e. A) is in agreement with a measured filter surface level decrease (i.e. filter settlement) using the method of 3D Stereo-photography. Only, one single test could be classified and selected for validation, because the flow velocities did not exceed the critical threshold for incipient motion of either filter or bed material.

2) *What is the effect of sill-induced additional turbulence on the load damping coefficient α_d ?*

The data of Joustra (2012) with flows with sill-induced additional turbulence suggest to increase the load damping coefficient $\alpha_d = 0.82$ for the full version and the $\alpha_d = 0.86$ for the simplified version of the formula of Hoffmans (2012). This conclusion is based on (C) the classification of a single test. A rough estimate of the new α_d is proposed based on (C) the classification of the single marker and (D) an expected (but not proven) classification of another test (i.e. G.I 'Only filter is *instable*'). A rough estimate of the new load damping coefficient for the full version of the formula of Hoffmans (2012) and flows with sill-induced additional turbulence is within the range $1.2 < \alpha_{d, f.v.} < 2.5 [-]$ and for the simplified version of the formula of Hoffmans (2012) is within the range $1.2 < \alpha_{d, s.v.} < 2.4 [-]$.

The classification of the single test (C) is determined using visually observation of bed instability (i.e. filter settlement) from underwater camera images, while the filter grains were highly mobile. In addition, the upper limit of the range is based on an expected classification. The remaining tests with sill-induced additional turbulence in the dataset of Joustra (2012) were not suitable for validation. The high degree of filter mobility and turbidity prevented classification of these remaining tests. The limited number of tests that were suitable for validation and the uncertainty in the classification of bed instability of the single test (C), suggest that this increase in load damping coefficient to a new α_d is not solidly proven and further research with tests near and above the curve of Hoffmans (2012) is highly recommended.

3) What is the effect of flows with a cylindrical pier on the load damping coefficient α_d ?

The data of Joustra (2012) for flows with a cylindrical pier suggest to increase the load damping coefficient $\alpha_d = 0.82$ for the full version and the $\alpha_d = 0.86$ for the simplified version of the formula of Hoffmans (2012). The conclusion to increase the α_d for the simplified and full version is based on the underestimation of the bed stability by the formula of Hoffmans (2012) for respectively 4 and 5 tests. A new estimate of α_d for flows with cylindrical piers is probably within the range $2.5 < \alpha_{d,f.v.} < 3.7$ for the simplified version and $2.4 < \alpha_{d,s.v.} < 3.6$ for the full version of the formula of Hoffmans (2012).

4) How do the data of flows with a cylindrical pier and flow velocities over 0.5 m/s compare to the design formula of Wörman (1989)?

Data of Joustra (2012) for flows with a cylindrical pier suggest that the formula of Wörman estimates the minimum required layer thickness reasonably well for average flow velocities over 0.5 m/s and layer thicknesses over 0.1 m. Although the gradient (or coefficient) of the linear formula of Wörman (1989) should be increased, because this formula underestimated the bed stability for 1 test. Therefore, the gradient of 0.085[-] in equation 1.4 should be changed to a gradient probably within the range between 0.10 and 0.153. The gradient of 0.16 [-] within the original formula of Wörman (1989) should be changed to a gradient probably in the range between 0.22 [-] and 0.33 [-]. These changes to the formula yield for filter material, bed material and flow characteristics (e.g. water depth to pier diameter ratios) similar to the tests of Joustra (2012).

5) How do the data compare to the previous validation of the formula of Hoffmans (2012) and the formula of Wörman (1989) based on data of Van Velzen (2012) for flows with a cylindrical pier?

Results based on data of Joustra (2012) suggested that for flows with a cylindrical pier the load damping coefficient α_d in the formula of Hoffmans (2012) should be increased (answer to research question 3). Also the gradient in the formula of Wörman (1989) should be increased (answer to research question 4). These results are not in agreement with the conclusions from the previous validation by Van Velzen (2012) and Van de Sande (2012). Van Velzen (2012) and Van de Sande (2012) suggested that data of Van Velzen (2012) are in line with both (unchanged) design formulas.

A probable cause for the dissimilar conclusions is the difference in classification of the single marker above curves of both design formulas. First, this single marker is classified as ‘no winnowing’ by Van Velzen (2012). Second, Van de Sande (2012) classified this marker as ‘filter moves first’. But Van Velzen (2012) did only classify the bed instability (‘winnowing’) and did not determine the filter instability. Moreover, the filter grains were designed to prevent filter instability, thus filter instability did probably not occur. The filter material, bed material or both materials should be instable before the test can be compared with the formula of Hoffmans (2012) (section 4.2). In addition, it is probable that both filter material and bed material were stable during the single marker of Van Velzen (2012) above the curves, thus the test is not applicable in the validation of both formulas. The remaining test markers are in agreement with the results based on data of Joustra (2012).

7.2 Recommendations

7.2.1 Recommendations for further investigation

- *Optimize the load damping coefficient α_d for uniform flows.*
The dataset of Van de Sande (2012) includes tests of non-uniform flow (e.g. data of Van Velzen (2012)). Results in this thesis suggested that the load damping inside the filter in non-uniform flow (i.e. flows with a cylindrical pier) probably differs from the load damping profile inside the filter in uniform flow. Excluding non-uniform flow data from the dataset and select only uniform flow data could optimize the value for α_d .
- *Test the validity of the roughly estimated and uncertain range of the load damping coefficient α_d for flows with sill-induced additional turbulence.*
Results suggested an increase in α_d for sill-induced additional turbulence. However, the scarce number of tests, the associated uncertainty in test classification and the preliminary seemingly contradicting results from the analysis of the pressure fluctuations profile by Van Velzen (2012) question the confidence in the conclusion for an increase of α_d . The pressure fluctuation measurements by Van Velzen (2012) could be further analyzed and related to α_d and compare with the range suggested in this thesis. Or additional tests could be conducted with markers above and near the curve of the formula of Hoffmans (2012) (figure 6-1, figure 6-2).
- *Determine the characteristic load damping in the filter for flows with a cylindrical pier.*
Tests of flows with a cylindrical pier suggest that the load damping coefficient α_d should increase with approximately a factor 3 relative to the α_d valid for uniform flows. Changing the α_d for the cylindrical pier suggests that the characteristic load damping profile might not describe the flow processes near a cylindrical pier very well, e.g. the horse shoe vortex penetration (Nielsen et al., 2010). In addition, the characteristic load damping profile is exponential which causes the logarithmic relation between filter and bed material characteristics and the relative layer thickness. While Wörman (1989) found a linear relation between the filter and bed characteristics and the relative layer thickness based on tests with cylindrical piers and an empirical fitted gradient. Therefore it is recommended to further investigate the characteristic load damping in the filter at flows with cylindrical piers. Tests in the area of d_{f50}/d_{b50} larger than 200 and the area d_{f50}/d_{b50} smaller than 50 should be conducted to determine if the relation should either be linear or logarithmic.

7.2.2 Recommendations for the design practice

The following recommendations are based on results of the research, described in this thesis.

- Apply the safe upper limit of the load damping coefficient as proposed by Van de Sande (2012): $\alpha_d = 0.86$.
- For sill-induced additional turbulence no safe upper limit can be proposed. An upper limit could be $\alpha_d = 2.5$, but validation is highly recommended before applied in practice.
- Apply for flows with a cylindrical and test conditions similar to this thesis the original formula of Wörman with a gradient of 0.33 (equation 6.5). When the rewritten form of equation 6.5 is applied (equation 1.4), a gradient of 0.153 should be used. The formula of Wörman is preferred above the formula of Hoffmans (2012).
- If the formula of Hoffmans (2012) is applied at flows with a cylindrical piers, than at least an $\alpha_d = 3.7$ should be applied.

References

- Bakker, K.J., Verheij, H.J., de Groot, M.B. (1994). *Design relationship for filters in Bed protection*. Journal of Hydraulic engineering. 12: 1082-1088.
- Breusers, H. N. C., Nicollet, G., & Shen, H. W. (1977). *Local Scour Around Cylindrical Piers*. Journal of Hydraulic Research, 15(3), 211-252. doi: 10.1080/00221687709499645.
- Briaud, J. L., Ting, F. C. K., Chen, H. C., Gudavalli, R., Perugu, S., & Wei, G. S. (1999). *SRICOS: Prediction of scour rate in cohesive soils at bridge piers*. Journal of Geotechnical and Geoenvironmental Engineering, 125(4), 237-246
- Chiew, Y. M. (1995). *Mechanics of riprap failure at bridge piers*. Journal of Hydraulic Engineering-Asce, 121(9), 635-643. doi: 10.1061/(asce)0733-9429(1995)121:9(635).
- Chiew, Y. M. (2000). Failure behavior of riprap layer at bridge piers under live-bed conditions. *Journal of Hydraulic Engineering* 126(1).
- Chiew, Y. M. (2004). Local scour and riprap stability at bridge piers in a degrading channel. *Journal of hydraulic Engineering*, 130(3).
- Chiew, Y. M. (2006). *Thoughts on Riprap Protection around Bridge Piers*. Paper presented at the ICSE 3, Amsterdam.
- CIRIA, CUR, CETMEF (2007). *The Rock Manual. The use of rock in hydraulic engineering (2nd edition)*. C683, CIRIA, London.
- Franken, A., Ariëns, E., Klatter L. (1995). *Handleiding voor het ontwerpen van granulaire bodemverdedigen achter tweedimensionale uitstroombouwwerken*. Utrecht: Bouwdienst Rijkswaterstaat, Hoofdafdeling Waterbouw.
- de Graauw, A.F., van der Meulen, T. van der Does de Bye, M.R. (1983). *Granular filters: Design criteria*. Journal of Waterway, Port, Coastal and Ocean Engineering. ASCE. 110(1). Paper no.:18602.
- Hoffmans, G. J.C.M. (2012). *The Influence of Turbulence on Soil Erosion*. Delft: Eburon Academic publishers.
- Hofland, B. (2005). *Rock & Roll. Turbulence-induced damage to granular bed protections*. Communications on Hydraulic and Geotechnical Engineering. Report No. 05-4. Department of Civil Engineering and geosciences, Delft University of Technology. Delft.
- Joustra, R. (2012). *Interface stability in granular open filter: Laboratory test report*. Report. University of Twente & Deltares: Enschede.
- Klar, M. (2005). *Design of an endoscopic 3-D Particle-Tracking Velocimetry system and its application in flow measurements within a gravel layer*. Phd thesis, Ruperto-Carola University, Heidelberg, Germany.
- Melville, B. W. (2008). *The physics of local scour at bridge piers*. Paper presented at the International conference on scour and erosion, Amsterdam.
- Nielsen, A. W., Sumer, B. M., Fredsoe, J., & Christensen, E. D. (2010). *Scour Protection Around Offshore Wind Turbines. Monopiles*. Paper presented at the Scour and erosion, San Fransisco, California, USA.
- Schiereck, G. J. (1995). *Introduction to Bed, bank and shore protection*. Delft: Delft University Press.
- Sumer, B. M., & Fredsoe, J. (2002). *The mechanics of scour in the marine environment* (Vol. 17). Singapore: World Scientific Publishing Co. Pte.
- Van de Sande, S. A. H. (2012). *Stability of open filter structures*. Master of Science, Delft University of Technology, Delft, The Netherlands.
- Van Velzen (2013). Memo: KPP rekenregels ontgroning 2012 – Drukmetingen. Preliminary result report. Not yet published as paper.
- Van Velzen, G. (2012). *Flexible scour protection around cylindrical piers*. Master of Science, Delft University of Technology, Delft.
- Verheij, H. J., & Hoffmans, G. J. C. M. (1997). *Scour manual*. Rotterdam, The Netherlands: A. A. Balkema.
- Verheij, H. J., Hoffmans, G. J. C. M., den Adel, H., Akkerman, G. J., & Giri, S. (2010). *Interface stability of granular filter structures*. Delft: Deltares.
- Whitehouse, R. (1998). *Scour at marine structures*. London: Thomas Telford Ltd.
- Wörman, A. (1989). *Riprap protection without filter layers*. Journal of Hydraulic Engineering, 115(12), 15.
- Yang, C.T. (2003). *Sediment transport: Theory and practice*. Malabar, Florida: Krieger Publishing Company.

Appendices

1. Five failure mechanisms

The result of the design process is design of a geometrical open filter with a certain filter diameter d_f , filter gradation (degree of non-uniformity) and (relative) layer thickness D_f . However, a failure mechanism might not be incorporated sufficiently in the design process and might cause failure to sustain the main function of the geometrical open filter.

Failure mechanisms are important to take into account in the design of any hydraulic structure (Chiew, 1995, 2000, 2006):

1. Shear failure (figure 0-1)
2. Winning (figure 0-2)
3. Edge failure (figure 0-3)
4. Bed form induced failure (figure 0-4)
5. Bed degradation induced failure (figure 0-5)

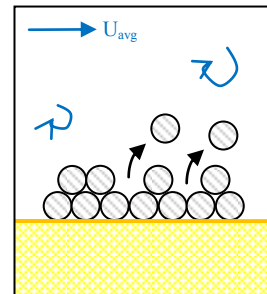


Figure 0-1: Shear failure.

The filter grain induced resistance is insufficient to withstand the hydraulic load. The top layer material is eroded by the flow.

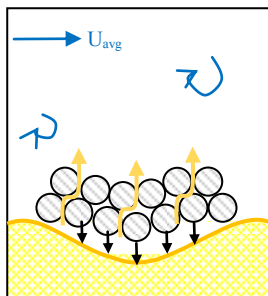


Figure 0-2: Winnowing induced failure

The filter layer thickness is insufficient to damp the hydraulic load on the bed material. The underlying bed material is transported through the filter layer pores. This transport of bed material causes layer settlement.

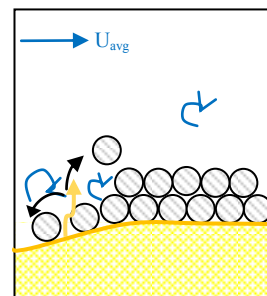


Figure 0-3: Edge failure.

The flow pattern at the edge of the top layer causes a local increase in hydraulic load. The top layer material at the edge is eroded. This result in local settlement of the layer.

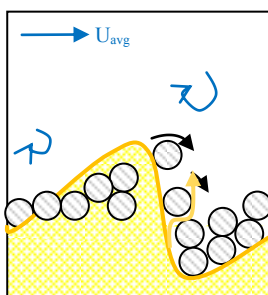


Figure 0-4: Bed form induced failure.

Bed forms like ripples and sand waves might destabilize the top layer. Cracks in the top layer increase the hydraulic load on the sub-layers and bed material and sediment can be transported.

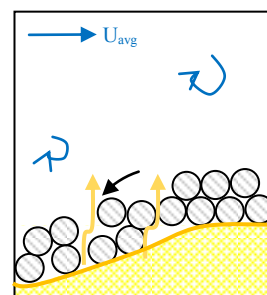


Figure 0-5: Bed degradation induced failure.

General scour or general riverbed lowering can cause lowering of the bed surrounding the scour protection. Again cracks in the top layer increase the hydraulic load on the other layers and bed material transport can be the result.



2. Previous validation results

This section describes the previous validation results of Van de Sande (2012) and Van Velzen (2012). Figure 0-6 and figure 0-7 describe the validation results of respectively the simplified and the full version of the formula. The validation results of van Velzen (2012) are described by figure 0-8.

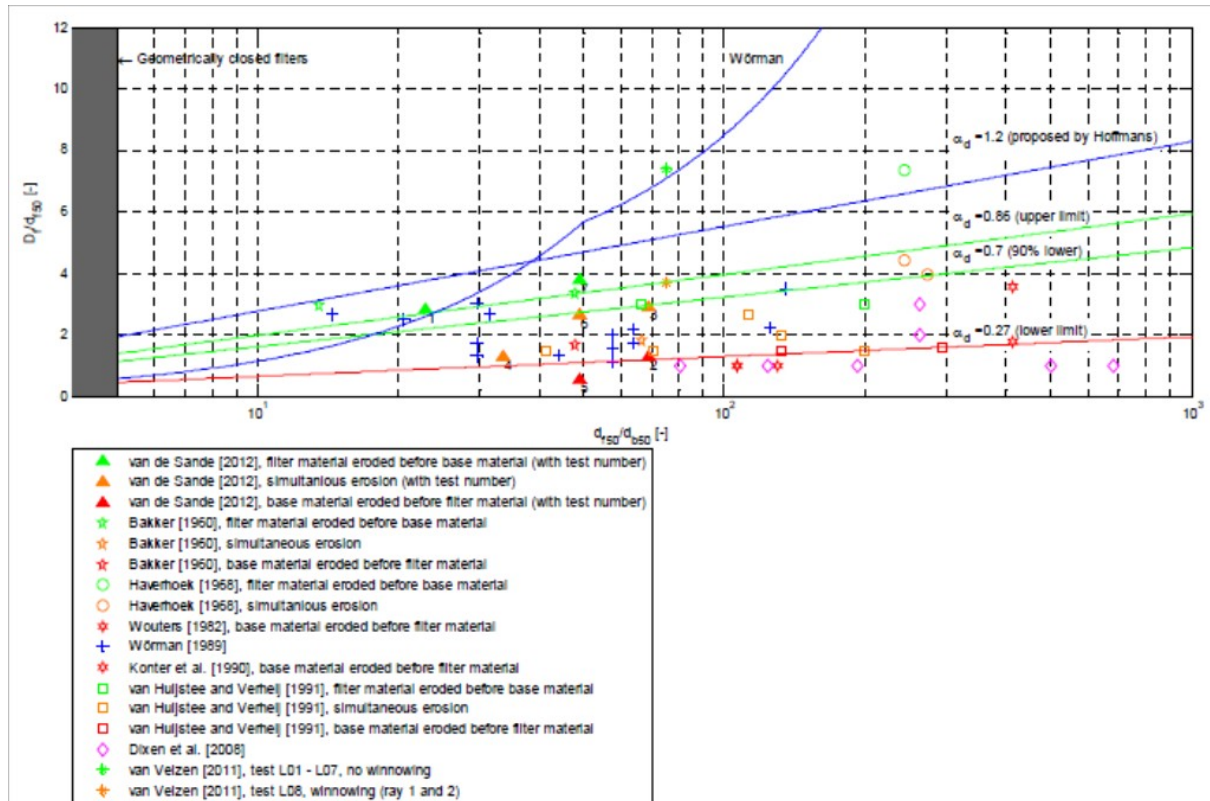


Figure 0-6: Validation results of the simplified version of the formula (Van de Sande, 2012)

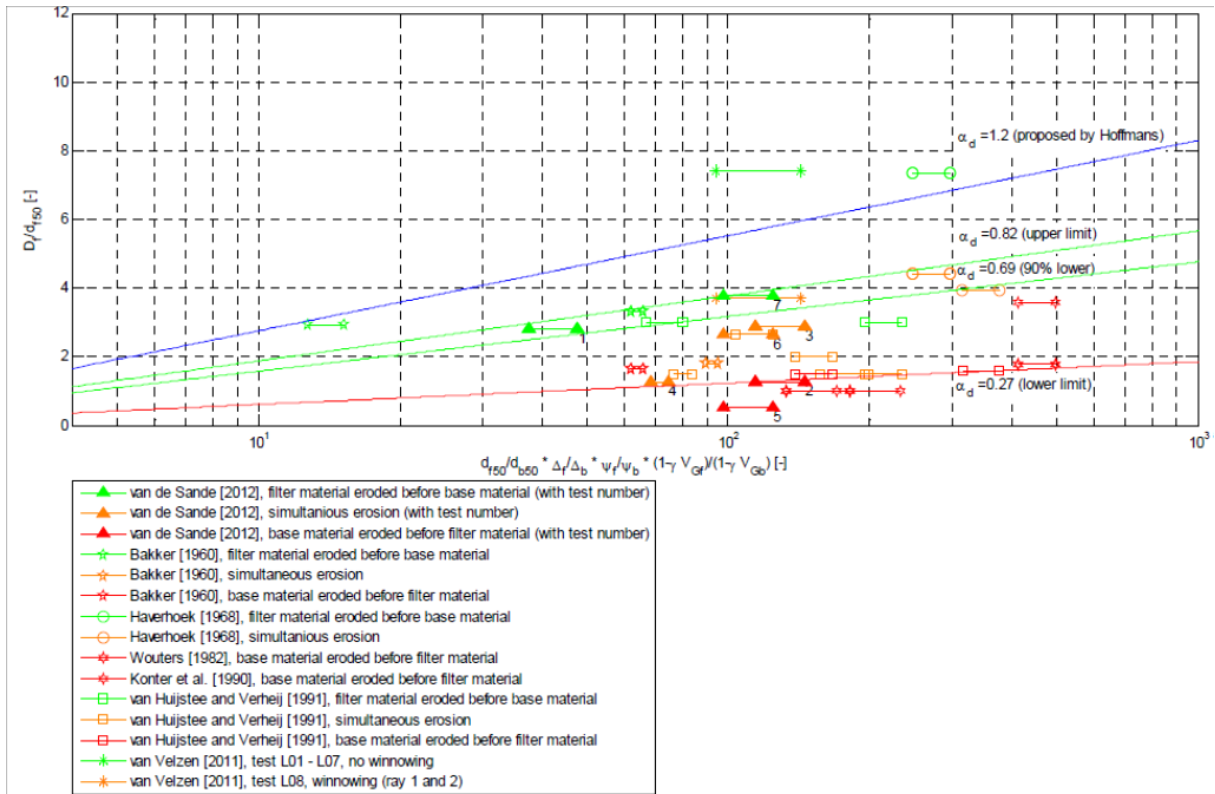


Figure 0-7: Validation results of the full version of the formula by Van de Sande (2012).

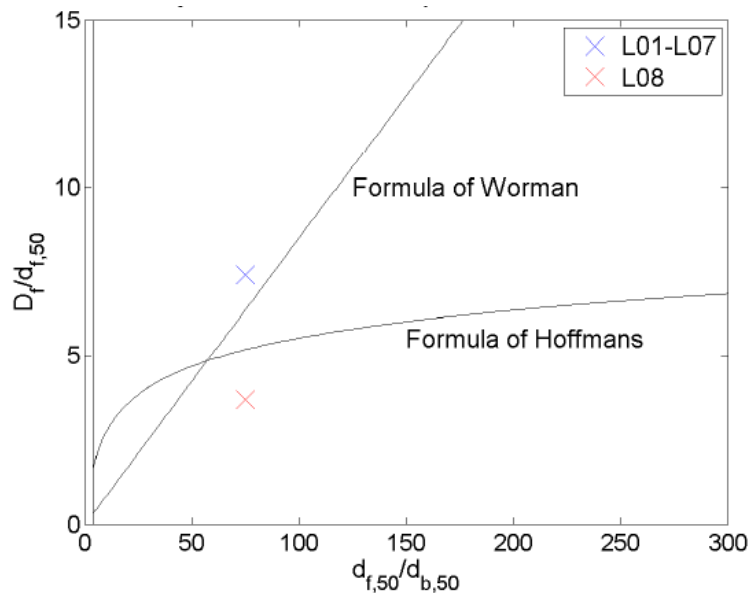


Figure 0-8: Validation results of the formula of Hoffmans (simplified version) and the formula of Worman (Van Velzen, 2012) for cylindrical pier conditions.

3. Sieve curves of filter material

The stone gradations were weighted and counted per weight class interval of 0.5 gram. The density ρ_{filter} is assumed on 2650 kg/m^3 . The resulting sieve curve is visualized by Figure 0-9.

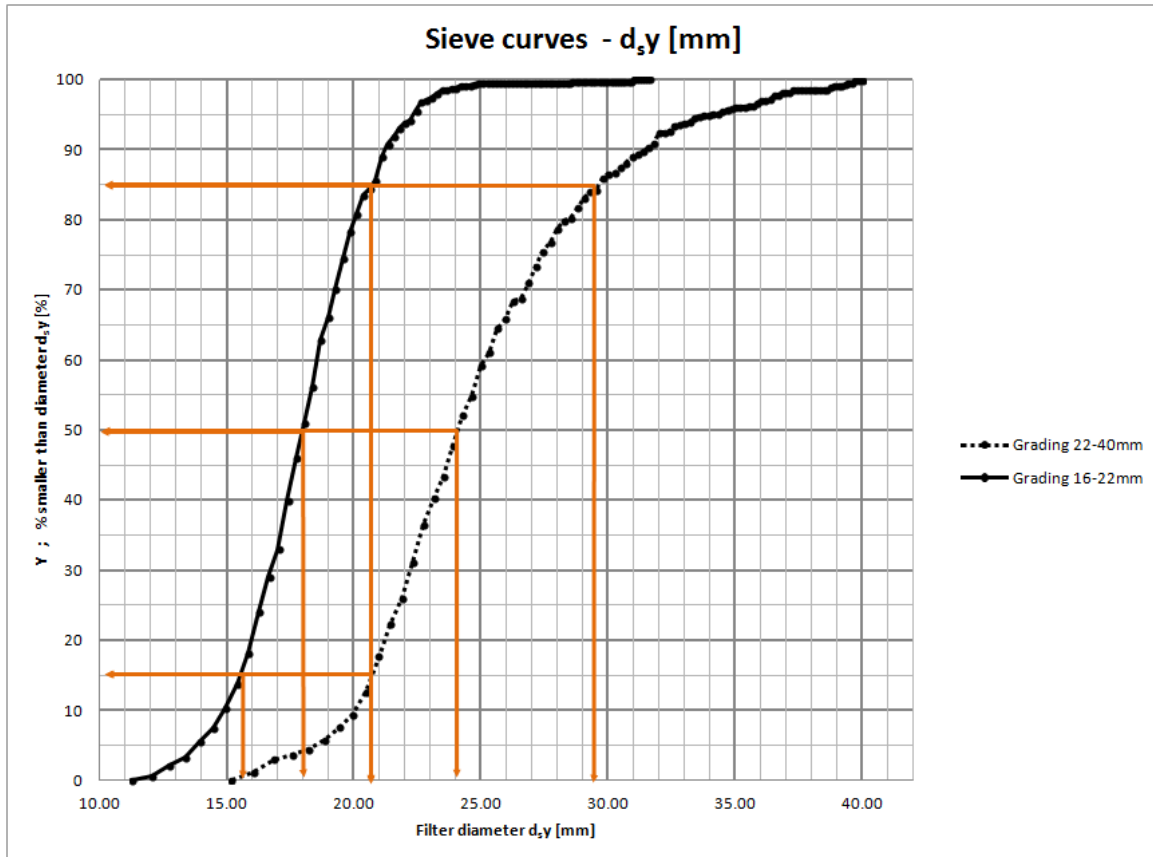


Figure 0-9: Sieve curve of filter grading. Orange lines indicate the representative filter diameter sizes.

Table 0-1: Calculated grain diameters from sieve curves. V_g is a parameter representing the grading by $V_g = 1 - d_{15}/d_{50}$.

	d15 [mm]	d50 [mm]	d85 [mm]	d85/d15 [-]	V_g [-]	d50/d15 [-]	d85/d50 [-]
Grading 1 (16-22)	15.5	18.0	20.7	1.33	0.14	1.16	1.15
Grading 2 (22-40)	20.7	24.1	29.7	1.43	0.14	1.16	1.23

The ratio d_{85}/d_{15} are in both gradations smaller than 1.5 [-], so both gradations are classified as ‘narrow’. Both gradations are defined as ‘well graded’ as no gap grading is observed (missing diameters in the distribution), therefore the d_{85}/d_{50} , d_{50}/d_{15} values give a representation of the type of grading. The ratio d_{50}/d_{15} and d_{85}/d_{50} are relevant for the validity for the assumptions for the formula of Hoffmans (2012). d_{50} & V_g are input for the validation of the full formula.

4. Sieve curve of bed material

In contrary with the filter stone grading, the bed material was sieved and weighted per diameter interval. In total 7 samples are taken from the bed. The density ρ_{bed} is assumed on 2650 kg/m^3 . The resulting sieve curves are visualized by Figure 0-10.

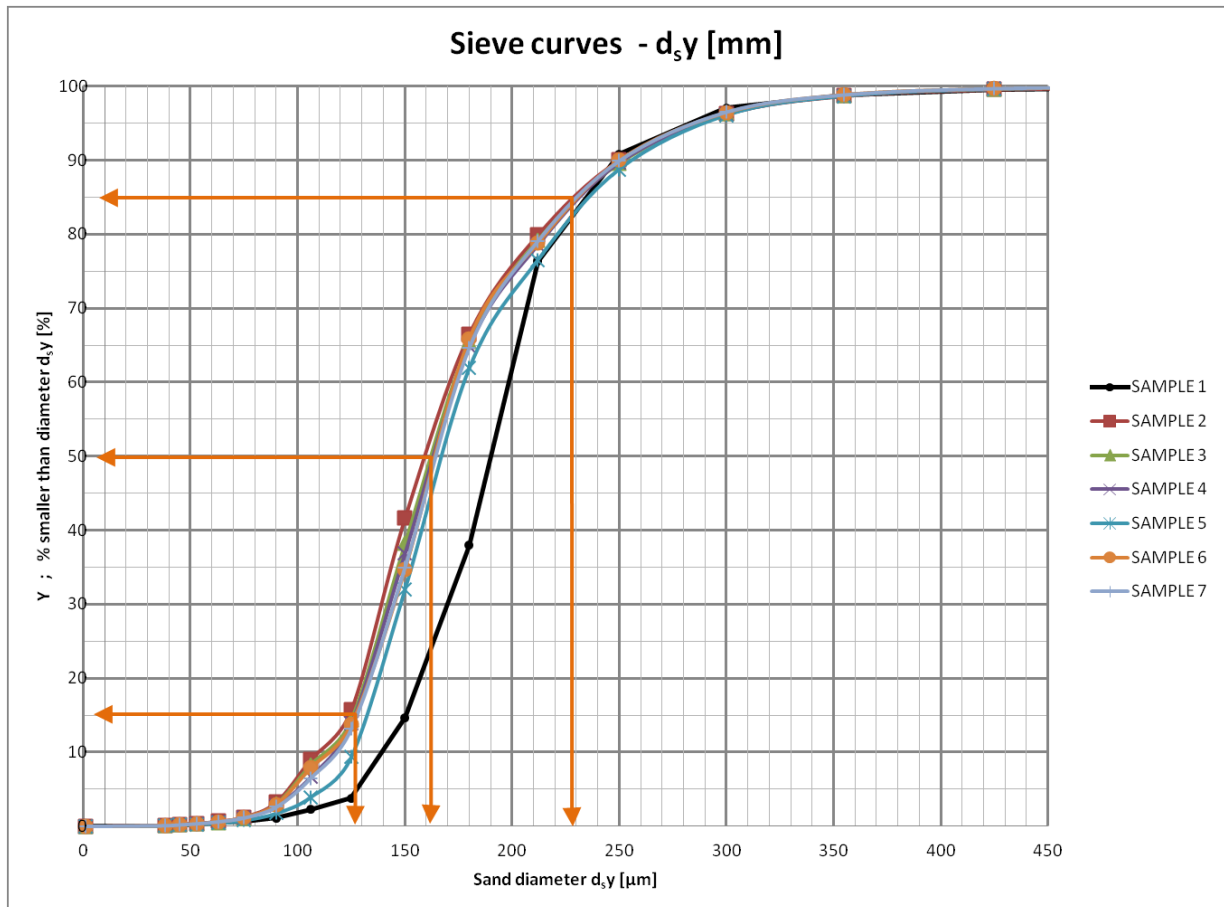


Figure 0-10: Sieve curves of 7 samples of bed material. Orange lines indicate the representative filter diameter sizes.

The first remark is that most samples are approximately equal, with exception of the sieve curve of sample 1. It is unknown where this sample is taken; therefore the median statistics of the grain sizes is applied as the representation of the bed material in the basin. Table 0-2 describes the calculated and derived grain diameters of the bed material, relevant for the validation.

Table 0-2: Calculated absolute and relative grain diameters from sieve curves. V_g is a parameter representing the grading by $V_g = 1-d_{15}/d_{50}$ [-]. The bold values are applied as representative values for the bed material.

	d15 [mm]	d50 [mm]	d85 [mm]	d85/d15 [-]	V_g [-]	d50/d15 [-]	d85/d50 [-]
Sample 1	0.150	0.190	0.235	1.56	0.21	1.26	1.23
Sample 2	0.123	0.160	0.231	1.88	0.23	1.30	1.44
Sample 3	0.126	0.163	0.233	1.86	0.23	1.30	1.43
Sample 4	0.126	0.164	0.234	1.85	0.23	1.30	1.43
Sample 5	0.131	0.168	0.238	1.82	0.22	1.28	1.42
Sample 6	0.126	0.165	0.233	1.84	0.23	1.30	1.41
Sample 7	0.127	0.165	0.233	1.83	0.23	1.30	1.41
Average	0.130	0.168	0.234	1.81	0.23	1.29	1.40
Median	0.126	0.165	0.233	1.84	0.23	1.30	1.42

5. Flow condition in front of pier

Figure 0-11 describes the velocity measurements in horizontal (downstream direction) and vertical direction in front of the cylindrical pier. Figure 0-12 and figure 0-13 describe the zoomed in plots of the velocity signals.

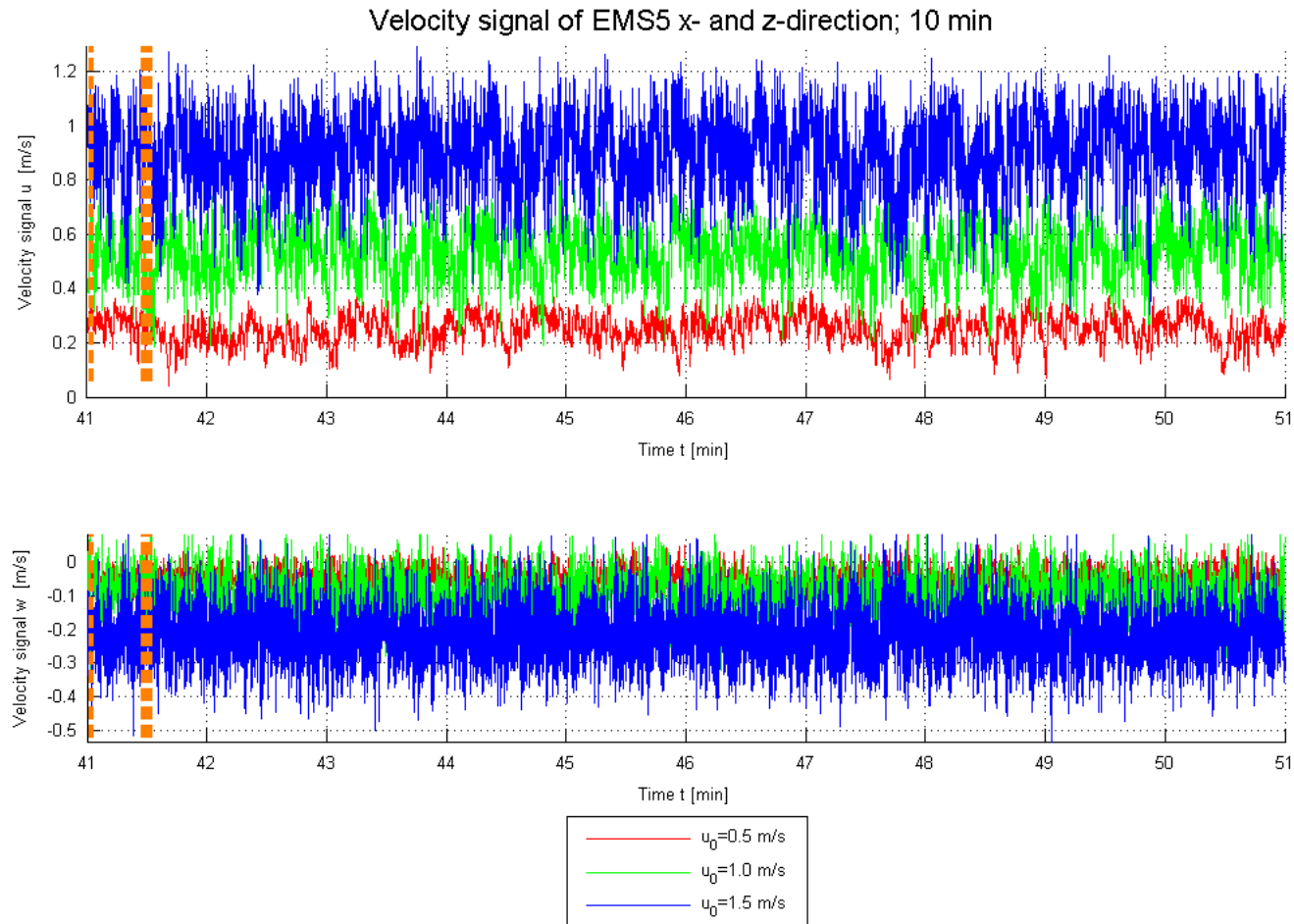


Figure 0-11: EMS signal sensor 5 during test T08a, T08b, and T08c. The orange vertical lines show the zoomed in on signal (figure 0-5)

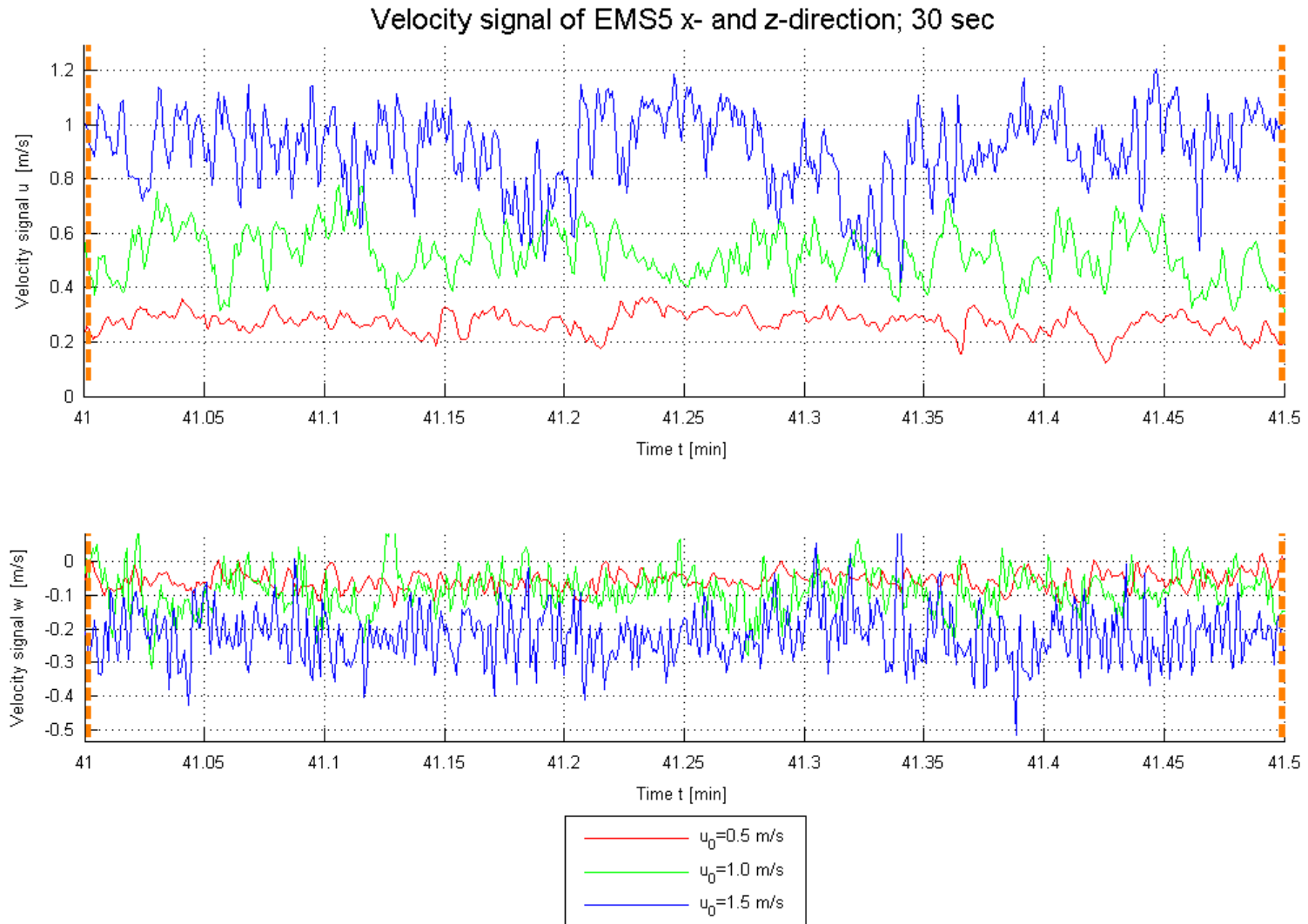


Figure 0-12: Zoomed in version of EMS signal 5 in front of the pier. 5 cm distance from the pier and ~13cm above the outer flow-filter interface.

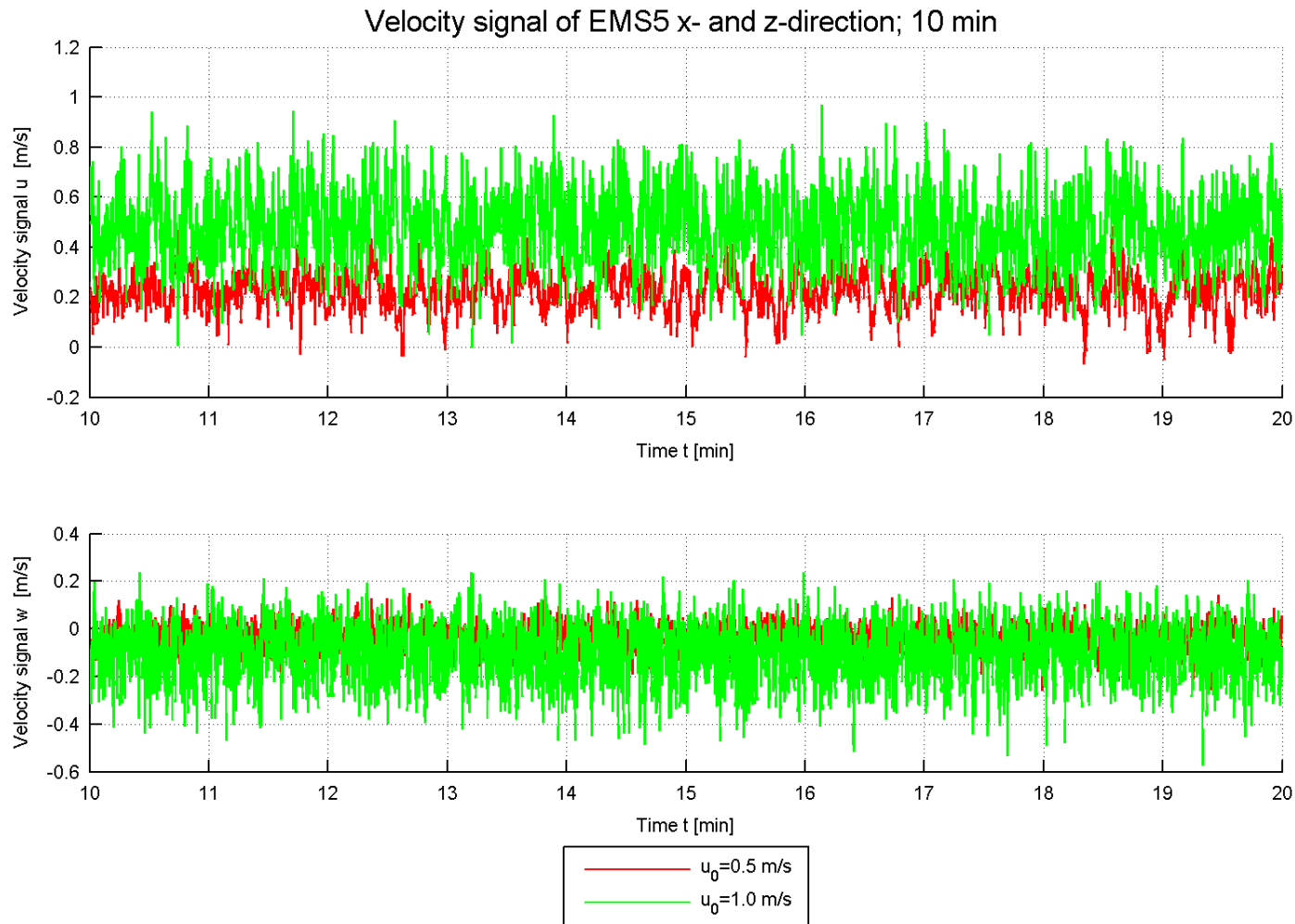


Figure 0-13: Velocity signal from $t = 10$ minutes to $t = 20$ minutes in front of the pier. Test P13-P14. A sill was constructed in the upstream test section.



6. Spatial variation in measured bed stability

The spatial variability in bathymetry before, after and difference for test U5-U6, U7-U8 and U9-U10 are described by figure 0-14, 0-15, 0-16 and 0-17. Test S5-S6 and U9-U10 show more filter surface level lowering than test U5-U6 and U7-U8. The difference plots of U9-U10 and S5-S6 show quite uniform a distribution of filter surface level decrease within the polygon area. The difference plots of U5-U6 and U7-U8 have also a uniform distribution of the filter surface level difference within the polygon.

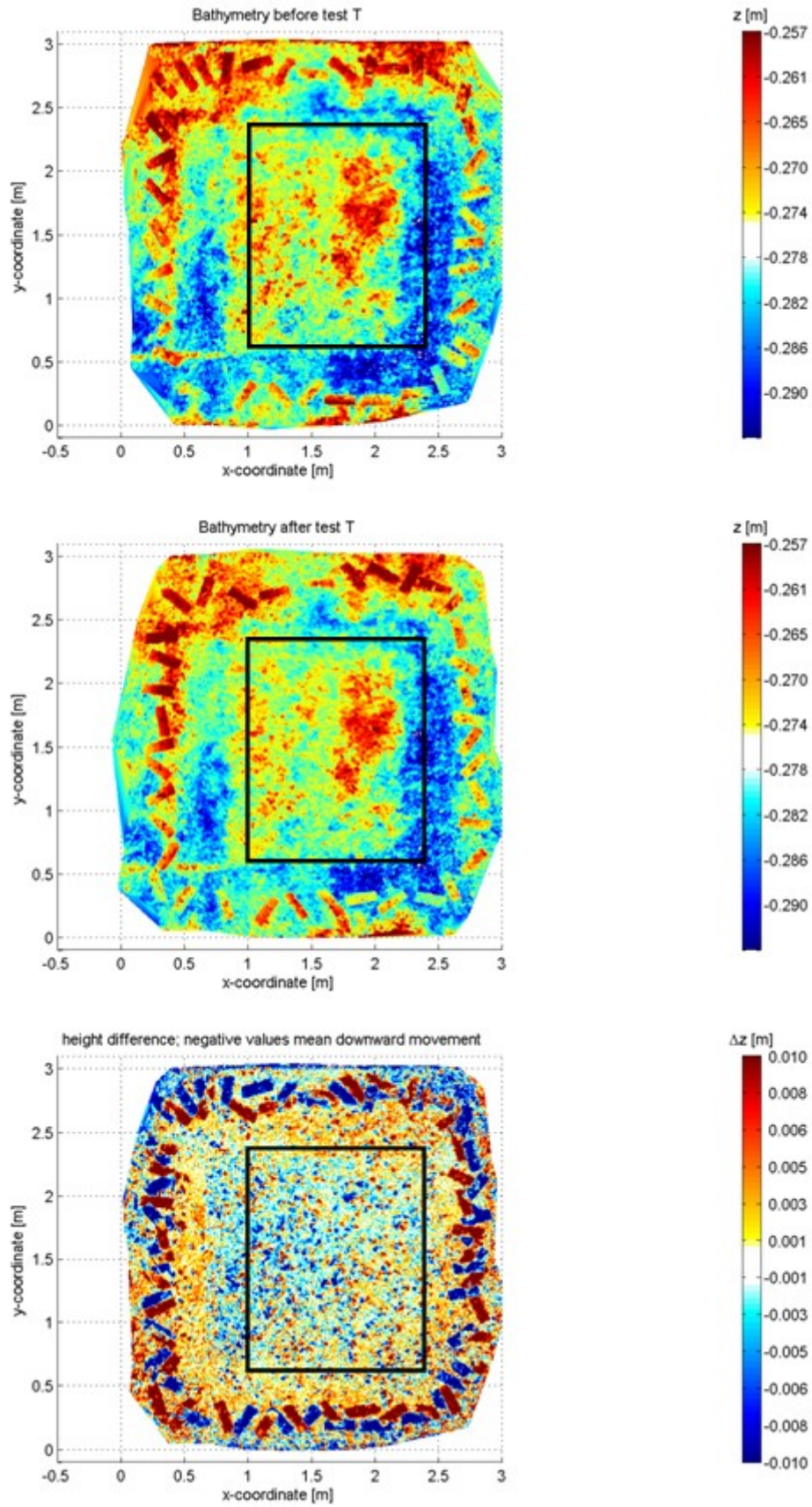


Figure 0-14: Test U5-U6 (T05). The plot above shows the filter level before U5, the plot in the middle shows the filter level after U6 and the plot below shows the filter surface level difference.

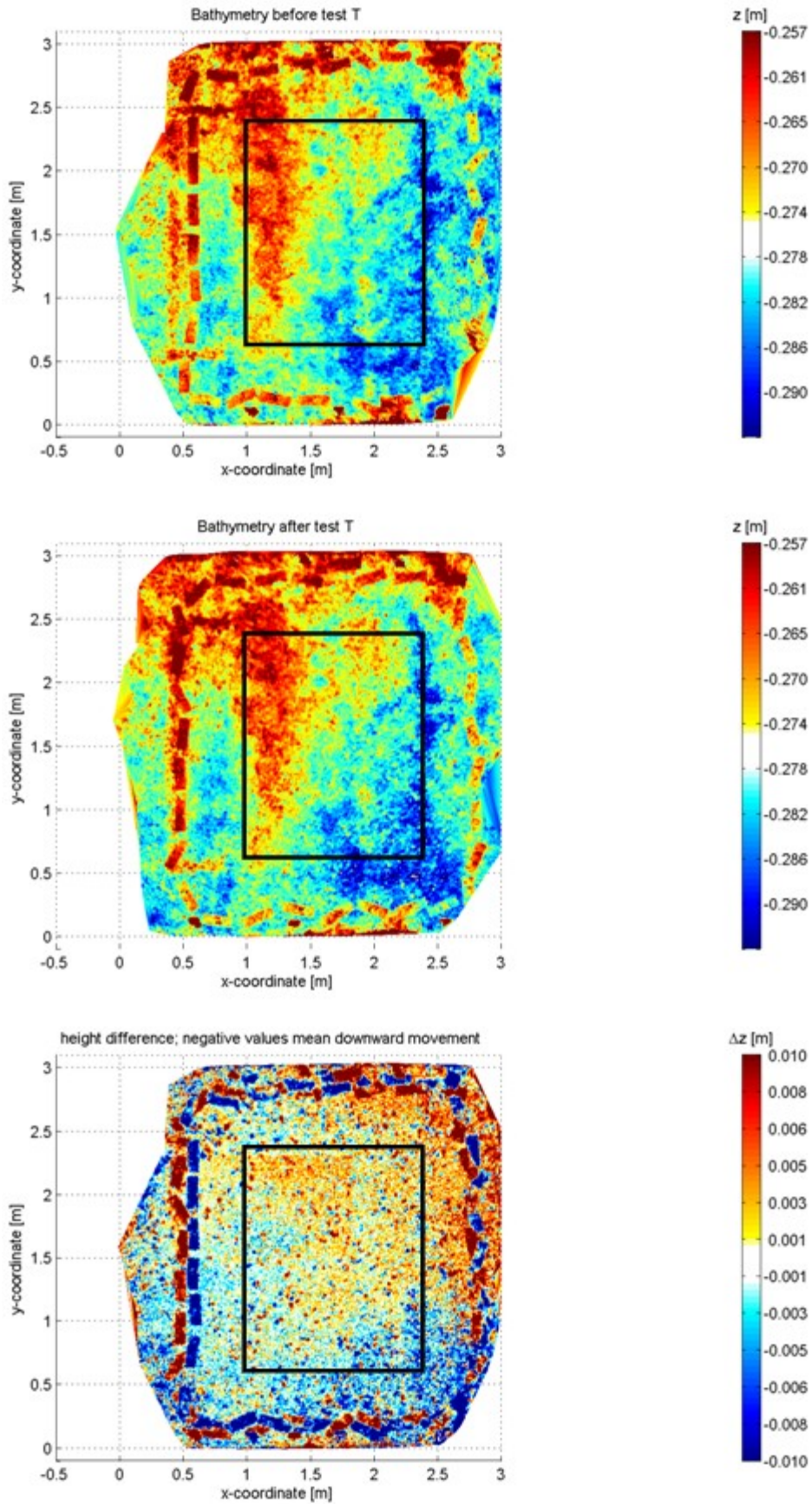


Figure 0-15: Test U7-U8 (T06). The plot above shows the filter level before U7, the plot in the middle shows the filter level after U8 and the plot below shows the filter surface level difference.

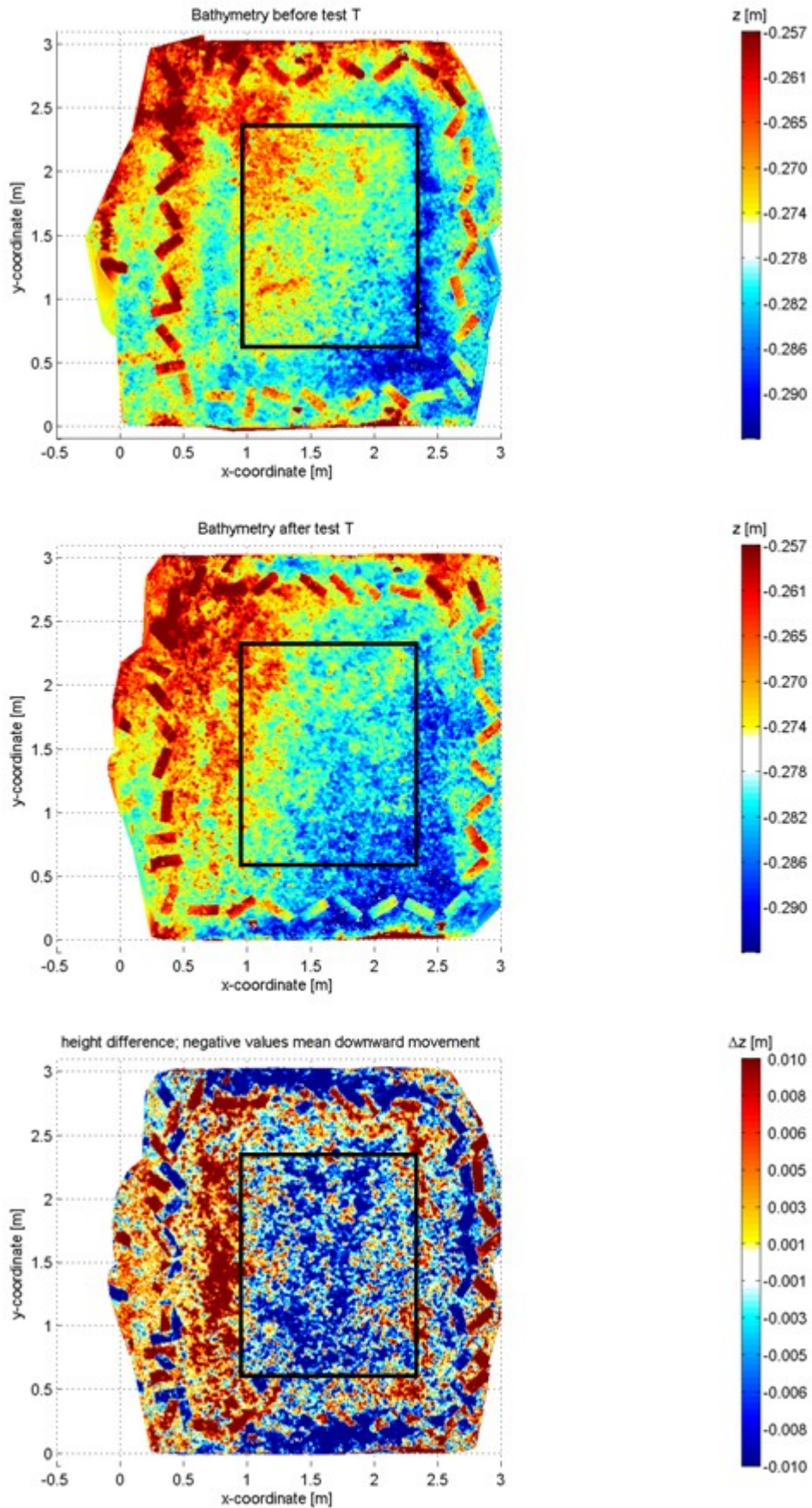


Figure 0-16: Test S5-S6 (T07). The plot above shows the filter level before S5, the plot in the middle shows the filter level after S6 and the plot below shows the filter surface level difference.

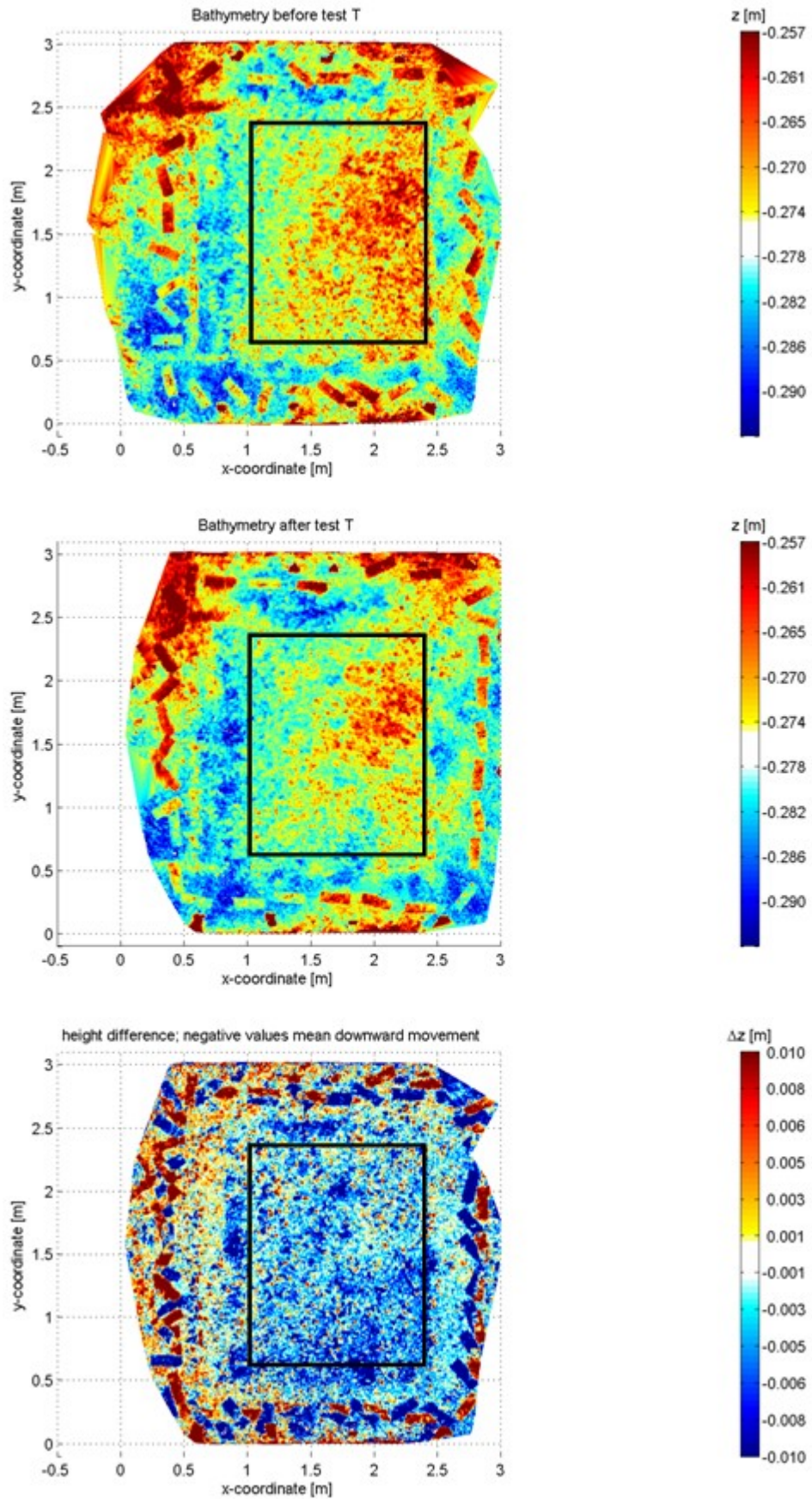


Figure 0-17: Test U9-U10 (T08). The plot above shows the filter level before U9, the plot in the middle shows the filter level after U10 and the plot below shows the filter surface level difference.